DOI:10.15774/PPKE.ITK.2010.005

Dynamical modelling and model analysis in neuroendocrinology

Theses of the Ph.D. Dissertation

Dávid Csercsik

Supervisor:
Gábor Szederkényi, Ph.D.

Scientific advisor:
Katalin Hangos, D.Sc.

Péter Pázmány Catholic University
Faculty of Information Technology

Budapest, 2010

DOI:10.15774/PPKE.ITK.2010.005

DOI:10.15774/PPKE.ITK.2010.005

Tartalmi kivonat

Dinamikus modellezés és modellanalízis a neuroendokrinológiában

Ezen disszertáció elsődleges célja hogy az utóbbi évtized biológiai kutatásai során elért néhány fontos eredményt állapottér modellek segítségével a biológiai rendszerelmélet keretei közé helyezzen. További cél, hogy egy, a biológiai modellezésben széleskörben elterjedt modellosztály identifikálhatósági tulajdonságaival kapcsolatban eredményeket fogalmazzon meg. A tézisben részletezett és felhasznált matematikai modellek a közönséges differenciálegyenletek (ODE) körébe tartoznak, a modellek paraméterei optimalizációs eljárásokkal kerülnek meghatározásra.

Elsőként egy, a gyors (G protein csatolt), és lassú (β-arresztin csatolt) jelátvitelhez kapcsolódó modell kerül bemutatásra. A javasolt modell alkalmas a két konvergens, de kvalitative különböző jelátviteli útvonal kölcsönhatásának, emellett a jelátvitel RGS és ERKP függő szabályozási módjainak leírására. A modell szimulációs eredményei az eredő G-protein függő és független ERK dinamika tekintetében jó egyezést mutatnak a kísérleti megfigyelésekkel.

Másodsorban, míg a Hodgkin-Huxley típusú modellek osztálya széles körben elterjedt, és domináns az elméleti idegtudomány irodalmában, közismertek az olyan tanulmányok, melyek ezen fontos modellosztály identifikálhatósági tulajdonságainak analízisét tűznék ki célul. Ebből kifolyólag egy Hodgkin-Huxley típusú feszültségfüggő ioncsatorna identifikálhatósági tulajdonságait vizsgáltam voltage clamp mérési módszert feltételezve. Az identifikálhatósági eredmények tükrében egy új identifikációs eljárást javaslok, mely a paraméterbecslési probléma dekompozícióján alapul. A vizsgálat eredményei közvetlenül alkalmasak új kritériumok megfogalmazására a voltage clamp mérési eljárások tervezésének tekintetében.

Harmadrészt, a dolgozat a GnRH neuronok modellezésének és paraméterbecslésének kérdéseit vizsgálja egy egyszerű, egy komparttmentel rendelkező Hodgkin-Huxley típusú elektrofiziológiai modell segítségével, mely hypothalamikus szeletben található GnRH neuronok voltage clamp görbéinek és a current clamp görbék legfontosabb tulajdonságainak (nyugalmi potenciál, depolarizációs amplitúdó, akciós potenciál utáni hiperpolarizáció, átlagos tüzelési frekvencia ingerlő áram hatására) reprodukciójára képes. A modell paramétereinek változtatásával, ami a nyugalmi potenciál emelkedéséhez vezet, a modell képessé válik a burst-ölésre. Vizsgálatra kerül a különféle paraméterek hatása a burst hosszára.

DOI:10.15774/PPKE.ITK.2010.005

Abstract

Dynamical modelling and model analysis in neuroendocrinolgy

The primary goal of this dissertation is to put certain importanat recent biological results of neuroendocrinology into the framework of systems biology by constructing and using dynamic state-space models. A further aim is to provide results corresponding to the identifiability properties of a system class widely used in biological modelling. The models detailed in this thesis are ordinary differential equation (ODE) models, the parameters of which are determined via optimization methods.

At first, a model is provided for the description of convergent signaling pathways corresponding to rapid (G protein coupled) and slow (β-arrestin coupled) transmission. The proposed model is able to describe the interaction of the two convergent, but qualitatively different signaling mechanisms, as well as the RGS and ERKP mediated regulation of signaling. The simulation results show that the model gives rise to an acceptable qualitative approximation of the G protein dependent and independent ERK activation dynamics that are in good agreement with the experimentally observed behavior.

At second, while the application of the Hodgkin-Huxley model class is widespread and dominant in the literature of computational neuroscience, there is a lack of articles, which aim at the analysis of the identifiability properties of this important system class. Motivated by this issue, the identifiability properties of a single Hodgkin-Huxley type voltage dependent ion channel model under voltage clamp circumstances are analyzed. Based on the results of identifiability analysis, a novel identification method is proposed, which is based on the decomposition of the parameter estimation problem in two parts. The results of the analysis are used to formulate explicit criteria for the design of voltage clamp protocols.

Thirdly, problems related to the modelling and parameter estimation of GnRH neurons were investigated. A simple, one compartment Hodgkin-Huxley type electrophysiological model of GnRH neurons is presented, that is able to reasonably reproduce the voltage clamp traces, and the most important qualitative features in the current clamp traces, such as baseline potential, depolarization amplitudes, subbaseline hyperpolarization phenomenon and average firing frequency in response to excitatory current observed in GnRH neurons originating from hypothalamic slices. Applying parametric changes, which lead to the increase of baseline potential and enhance cell excitability, the model becomes capable of bursting. The effects of various parameters to burst length are analyzed.

DOI:10.15774/PPKE.ITK.2010.005

Contents

DOI:10.15774/PPKE.ITK.2010.005

DOI:10.15774/PPKE.ITK.2010.005

DOI:10.15774/PPKE.ITK.2010.005

Notation and Acronyms

Notation of the variables and currents of the GnRH neuronal model

V	membrane potential
I_A	A-type potassium current
I_K	delayed rectifier potassium current
I_M	non-inactivating potassium current
I_T	low voltage activated Ca^{2+} current
I_R	R type high voltage activated Ca^{2+} current
I_L	L type (slowly inactivating) high voltage activated Ca^{2+} current
I_{leakNa}	sodium leak current
I_{leakK}	potassium leak current

DOI:10.15774/PPKE.ITK.2010.005

Acronyms

AP	Action potential
APPS	Asynchronous parallel pattern search
CC	Current clamp
DAP	Depolarizing afterpotential
E_2	Estradiol
ERK	Extracellular regulated kinase
FSH	Follicle-stimulating hormone
GDP	Guanosine-diphosphate
GFP	Green fluorescent protein
GnRH	Gonadotropin releasing hormone
GPCR	G protein-coupled receptor
GRK	G protein-coupled receptor kinase
GTP	Guanosine-triphosphate
HH	Hodgkin-Huxley
HVA	High voltage activated
LH	Luteinizing hormone
LVA	Low voltage activated
MAPK	Mitogen activated protein kinase
MAPKP	Mitogen activated protein kinase phosphatase
ODE	Ordinary differential equation
P_4	Progesterone (P_4)
RGS	Regulators of G protein signaling
VC	Voltage clamp

DOI:10.15774/PPKE.ITK.2010.005

Chapter 1

Introduction

Systems biology is an emerging interdisciplinary branch of science that aims at studying and computationally describing the interactions and interaction networks in biological systems [14, 17]. The models resulting from this approach can be used to explain dynamical mechanisms and phenomena, and for gaining predictions corresponding to the behavior of the system of interest.

To increase the clinical relevance of such models, one has to use sub-models based on as up-to-date biological information as available, and reduce the role of empirical and phenomenological approaches everywhere where the biological knowledge makes it possible.

The work reported in this thesis presents contributions to systems biology in the above sense: two chapters (2. and 4.) focus on systems biology models corresponding to neuroendocrinology [106], and one chapter (3.) focuses on methodological issues, especially mathematical (identifiability) properties of a model class (Hodgkin-Huxley type models) widely used in systems biology.

Motivation: Complex nonlinear elements in the female reproductive neuroendocrine system. Probably one of the most important known complex biological systems is the female reproductive neuroendocrine system. Here the buzzword *complex* [161, 42] corresponds not only to the high number of interacting elements and the high number of interactions (see Appendix A), but also to the special highly nonlinear nature of the observed dynamics.

The neuroendocrine cells in the hypothalamus secrete Gonadotropin releasing hormone (GnRH) in a pulsatile way [166], with GnRH pulse frequency varying on the scale of 8-240 minutes. The anterior pituitary, in response to GnRH, secretes hormones as well in a pulsatile way to stimulate the growth and development of ovarian follicles: Follicle-stimulating hormone (FSH) and luteinizing hormone (LH). In addition to some other regulation mechanisms, the ovarian hormones feed back to the hypothalamus and also to the pituitary.

Via the multiple feedback loops connecting these endocrine and neuroendocrine tissues, the system of hypothalamic, ovarian and pituitary hormones together with morpological changes in the ovary regulate and maintain the menstrual cycle in adult women. Although cycles are usually between 25 and 30 days apart, but a woman's normal cycle can range anywhere from 22-40 days long.

DOI:10.15774/PPKE.ITK.2010.005

One of the most exciting challenge of the reproductive neuroendocrinology is to map the connections between these time scales of weeks and minutes (milliseconds, if considering neuronal activity). Many results point to the assumption, that the understanding of this complex dynamics can not be done without the help of computational models [16, 21, 57, 62, 61, 129].

The aim of this work, however, is not to describe the whole reproductive neuroendocrine system, but to focus on some important interactions and elements, and create mathematical descriptions (computational models) for them, which include the paradigms of recent biological findings of the field, and try to analyse and estimate them by using methods and tools of modern systems and control theory.

Especially the issues of key elements in the GnRH system are addressed: the G protein signaling, which is the mechanism via the hormone acts on the gonadotropin cells in the pituitary, and the GnRH neuron, which is responsible for the synthesis and secretion of this important neuropeptide.

β-arrestins and slow transmission: New aspects of signaling. Signaling through G protein-coupled receptors (**GPCR**s) is a well known mechanism of information transmission in intercellular communication (see later section 2.1). However, the operation of the intracellular pathways, which are connected to these receptors, are not yet fully understood, and in the recent decade significant new biological mechanisms related to these pathways have been identified.

The most widely accepted classic paradigm of signaling until the 2000s has been that the significantly important elements which contribute to information transfer into the internal system of the cell are the α and $\beta\gamma$ subunits of G proteins (see the review [104]). This paradigm was in good agreement with the classical concept of drug efficacy in the context of receptor-occupancy theory where the efficacy is considered as an intrinsic property of the ligand-receptor pair [52].

One of the most important main targets of the intracellular pathways affected by G protein related signaling is the family of MAPK/ERK cascades [73, 90, 177], which play a central role in the intracellular signaling network. Proteins called G protein-coupled receptor kinases (GRKs) are able to rapidly terminate this signaling response via phosphorylating the receptor, typically on its cytoplasmic tail [128]. Following phosphorylation, β-Arrestins bind the receptor, which blocks further G protein-initiated signaling.

In recent years it has been shown that β-Arrestins not only take part in receptor desensitization [50], but form an endocyctic protein complex, which initiates a G protein independent regulation of ERK [36, 113, 127, 8, 10]. The recognition, that a single receptor acts as multiple source of signaling pathways and various drugs binding to this receptor might differentially influence each of this pathways (in contrast to pathway-specific drugs), led to the reassessment of the efficacy concept [52].

These biological findings opened a way for dynamical models [106], which are able to describe the interaction of the two convergent, but qualitatively different signaling mechanisms. Section 2.2 is addressing this issue.

DOI:10.15774/PPKE.ITK.2010.005

Identifiability properties of the Hodgkin-Huxley model class The HH (Hodgkin-Huxley) modelling formalism [71] of membrane currents and cell electrophysiology is the most widely used framework for the purpose of modelling excitable cells. The dynamical descriptions of neuronal behavior, ranging from the fundamental theoretical principles [76, 77, 78] to the wide range of applications with special focus [136, 93, 133, 18, 46], are predominantly based on this model class.

Although several articles have been published which are focusing on parameter estimation problem in the case of HH based models under various assumptions (see [145, 144, 165, 148, 102, 74]), there is a lack of literature data which address the identifiability properties of such models.

Furthermore, there is a lack of a well grounded parameter estimation method that relies on the results of the identifiability analysis, and that can handle the possibly appearing identifiability problems.

Therefore, the aim of my work reported in this thesis was to provide a rigorous formal identifiability analysis of a simple Hodgkin-Huxley type ion channel model, interpret the results, and to provide a parameter estimation method which takes into account the arising possible identifiability issues.

Electrophysiological properties of GnRH neurons revealed through transgenics and GFP tagging. As mentioned before, GnRH neurons govern important central role in the control of the reproductive neuroendocrine system. With the application of cell marking based on the green fluorescent protein (GFP) and transgenic mice, the targeted measurements and electrophysiological experiments on GnRH neurons became available [67, 142]. Another possibility for gaining measured data is the application of "immortalized" GnRH neurons [119, 162], so called GT1 cells. Since these methods became widespread, the electrophysiological features of this important neuroendocrine cell have been studied extensively both experimentally and also several mathematical models have been constructed to explain the underlying mechanisms of their properties.

Until now, the mathematical models corresponding to GnRH neurophysiology were based mainly on data collected from immortalized GT1 cells. The behavior of these cells (eg. firing frequency, depolarization magnitudes) is significantly different compared to GnRH neurons in hypothalamic slices, which exhibit probably more common properties compared to in-vivo GnRH neurons.

However, in recent years, based mainly on the GFP tagging method, significant amount of experimental data has been published on the electrophysiology of GnRH neurons [67, 138, 35, 80]. These articles, together with the possibility of targeted measurements can serve as a good basis for the synthesis of an electrophysiological model of the GnRH neuron, which is able to take into account as much as possible from the up-to-date biological knowledge corresponding to the ion channels and dynamics of this unique neuroendocrine cell.

The above motivating facts let us try to construct a simple Hodgkin-Huxley type dynamical model of GnRH cell electrophysiology based on literature data published on its various ionic currents, and estimate its parameters based on GFP based whole cell patch clamp recordings.

DOI:10.15774/PPKE.ITK.2010.005

The structure of the thesis is as follows. In chapter 2 the biological background of G protein and β-Arresitn coupled signaling is summarized, and the corresponding dynamical reaction kinetic model is described. Chapter 3.1 introduces the class of Hodgkin-Huxley type models of ionic currents and neuronal electrophysiology, analyses the identifiability properties of one such channel under voltage clamp conditions, and provides a parameter estimation method based on the results of identifiability analysis. Chapter 4 describes the dynamical neuronal model of GnRH electrophysiology. The possible applications and future perspectives are described in chapter 6. Appendix A gives a summary about the biology and interactions of the female reproductive neuroendocrine system. Appendix B descibes simulation results corresponding to a subsystem of the model described in 2. Appendix C details the procedure of electrophysiological recordings of the GnRH neurons. The mathematical details of parameter estimation, and estimated parameters of the GnRH neuronal model can be found in Appendix D.

DOI:10.15774/PPKE.ITK.2010.005

Chapter 2

Dynamic models of intracellular signaling pathways: rapid and slow transmission

In this chapter, a dynamic computational model is presented in the form of ordinary differential equations (ODEs), which describe the interplay of rapid (G protein coupled) and slow (β-arrestin coupled) transmission in the signaling process of ERK activation. At first, in section 2.1, the biological background is detailed, then the model concepts, model development (section 2.2), model simulation results (section 2.3) and conclusions (section 2.4) are presented.

2.1 Rapid (G protein dependent) and slow (β-arrestin dependent) transmission

Diverse signaling molecules, including neurotransmitters, hormones, phospholipids, photons, odorants, taste ligands and mitogens, bind to their specific G protein-coupled receptors (**GPCR**s), also known as seven-transmembrane receptors (7TMRs), in the membrane of the target cells, which subsequently interact with their respective G proteins to induce a cascade of downstream i.e. intracellular signaling.

The G proteins are heterotrimeric signaling molecules composed of three subunits, α, β and γ, which dissociate upon receptor-induced exchange of GDP for GTP on the α subunit (Gα) to form a free Gα and a dimer of G$\beta\gamma$ subunits [60, 59, 114]. Many isoforms of these subunits have been cloned in the past years and have been classified into four groups according to the subtype of their α subunit: Gαs, Gαi, Gαq and Gα12. All these Gα subunits, as well as the dissociated $\beta\gamma$ subunits, and other receptor-interacting proteins are capable of initiating diverse downstream signaling pathways via second messenger molecules, such as cyclic AMP, cyclic GMP, inositol triphosphate, diacylglycerol, and calcium.

Activation of the signal induced by the GPCR depends on the rate at which ligand-bound receptor catalyzes exchange of GDP for GTP on the Gα subunit. Following exchange, GTP-bound $G\alpha$ dissociates, at least partially, from both the receptor and $G\beta\gamma$ complex. The length of time that $G\alpha$GTP and $G\beta\gamma$ can interact

DOI:10.15774/PPKE.ITK.2010.005

with effectors is determined by the rate at which $G\alpha$ hydrolyzes GTP to GDP. Following hydrolysis, inactive GαGDP binds $G\beta\gamma$ with high affinity, and terminates $G\beta\gamma$ signaling. GTPase-activating proteins (GAPs) speed up the hydrolysis of GTP by $G\alpha$ [174]. In this work $G\beta\gamma$ signaling events are not examined.

The novel concept of slow transmission via β-arrestins has already been mentioned in section 1. Following GPCR activation, the ligand-bind receptor can be phosphorylated by GPCR kinases (GRKs). As described for eg. in [9, 8, 7] in the case of dopamine receptors, β-Arrestins bind to the receptors after phosphorylation to uncouple them from G proteins and participate in the recruitment of the endocytic protein complex, thus leading to an attenuation of GPCR signaling.

On the other hand, the signaling complex composed of the ligand, the receptor, β-Arrestin2, and PP2A can dephosphorylate the protein Akt on the site Thr308, and initiate a G protein independent signaling cascade. Furthermore, an another signaling complex binding to the phosphorylated receptor composed of β-Arrestin, ERK1/2, Raf-1 and MEK can initiate ERK activation [37]. The later case, leading to the β-Arrestin dependent activation of ERK, will be in the focus of this study.

Together, the G-protein and β-arrestin coupled pathways form a signaling network convergent to the central target kinase ERK.

Another important mechanism contributing to the dynamics of signaling is the **feedback regulation**, about which there are only a few models available in the literature [94, 176]. At the same time, efforts to take into account the β-Arrestin dependent slow transmission as a second pathway convergent to G protein signaling is also not prevalent either in literature. The mechanisms of the regulation of G protein signaling are described in section 2.2.4 in detail.

2.2 Model developement

Much effort has been made nowadays to find plausible mathematical models for the description of the general dynamics of GPCR activation [1, 168, 169, 167], ligand efficiency [107, 25, 85] and receptor desensitization [143] in order to analyze signaling dynamics, and lay down the fundamentals of dynamical pharmacology [3].

To join the above mentioned efforts, the aim of this chapter is to propose a simple (in a sense minimal) reaction kinetic model and the implied equations for G protein signaling, based on biochemical and physiological observations collected about cell signaling pathways corresponding to a simplified model of fast-, and slow-transmission as well as the regulation of G protein signaling that is able to reproduce the downstream activation pattern (like ERK or Akt) recently described qualitatively in [37]. Our modeling effort is directed towards describing the dynamics, i.e. the time evolution of the key components participating in G protein dependent and independent signaling. This may enable us to analyze cellular activation in the case of parallelly or competitively acting agonists and apply control theoretic methods for finding optimal drug dosing strategies in the future.

Three model variants will be developed. The basic model described in 2.2.1 is able to describe ligand binding, and the cycle of $G\alpha$ GTP activation, deactivation and reactivation by the ligand-bound receptor. Thereafter, in section 2.2.3, we will

DOI:10.15774/PPKE.ITK.2010.005

Table 2.1: Notations of species in the basic model

Specie	Notation
$R(G\alpha - GDP)$	A
L	B
$R(G\alpha - GTP)L$	C_1
RL	D
$(G\alpha - GTP)$	E
$(G\alpha - GDP)$	F
R	G

extend our model with the reactions describing receptor phosphorylation by GRKs (G protein coupled receptor kinases), which is a key issue of the slow transmission process. Afterwards, in 2.2.4 we extend the model with the reactions describing the two convergent pathways of ERK activation, and the RGS and ERKP-mediated negative regulation of G protein signaling.

We aim at constructing a model in strict reaction kinetic form (governed by the mass action law), in order to stay in a model class for which the deficiency-based multistability-related results of Feinberg et al. [44, 31, 32] can be applied in the future. These results provide very strong theorems about qualitative behavior of reaction kinetic systems, based only on the structure of the reaction network, independently of its parameters. Furthermore, these and other [151, 152] multistability-related results offer the possibility to explain interesting physiological phenomena related to typical dynamic, pulsatile intercellular signals, for example, in the case of GnRH-affected gonadotropine cells [164], or dopamine-affected prolactin cells [12].

2.2.1 The basic reaction structure of the G protein signaling mechanism

The most simple reaction kinetic model of G protein signaling is constructed in this subsection, which is able to describe ligand binding, Gα activation, deactivation and reactivation. Furthermore, the model contains the Gα uncoupled ligand bound receptor that enables to extend the model with slow transmission related reactions in the following sections.

In order to simplify the form of the equations, the notations in Table 2.1 for species is introduced, with the notation C_i used for complexes.

For the development of a simple mathematical model of basic G protein signaling, the reaction scheme depicted in Fig. 2.1 is used. In the reaction schemes, the notation is the following: Arrows between components define transformations, and arrows pointing to arrows denote enzymatic catalysis (see the later reaction schemes).

It can be clearly seen from the reaction scheme in Figure 2.1 that the model does not describe active and inactive receptor forms, as for example the models detailed in [25, 143]. The reason for this lays in the fact that in this study the properties

DOI:10.15774/PPKE.ITK.2010.005

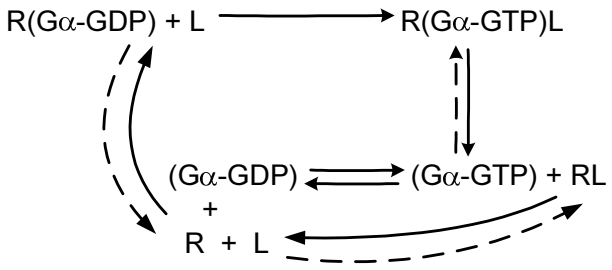

Figure 2.1: The basic reaction scheme of G protein signaling: The receptor (R) binds the ligand (L), and induces GDP -> GTP exchange. Thereafter the Gα GTP subunit dissociates, and after a while the GTP is hydrolyzed to GDP. After this, the Gα GDP subunit can reassociate with the ligand bound receptor.

of the ligand corresponding to achieve conformational changes in the receptor are not of primary interest, but the qualitative features of the two (G protein dependent and independent slow transmission) signaling pathways, and the feedback regulation of signaling will be in the focus. According to this aim, it can be assumed that conformation change of the receptor always appears after ligand binding, and is always followed by GDP/GTP exchange on the α subunit.

It is important to note that the primary input of the model is the ligand concentration on the cell surface. Processes affecting the concentration profile of the ligand such as degradation and reuptake, may be taken into account via the term L_{env} in eq. 2.5. The $G\alpha - GTP$, and later, in the case of the extended model, the ERK activation corresponds to the output of the system.

2.2.2 The basic model

The basic model describes a cell together with the cell surface, and the only component for which the system is open, is the ligand. This can be understood as the effect of the cell's environment that influences the ligand concentration on the cell surface (if the ligand concentration in the environment rises, the ligand concentration on the cell surface will rise too).

For all other components, the system is closed. This can be described by the following conservation equations (see notations in Table 1):

- The conservation of G protein: $[G\alpha^{tot}] = [A] + [C] + [E] + [F]$
- The conservation of receptors: $[R^{tot}] = [A] + [C] + [D] + [G]$
- The conservation of the ligand: $[L^{tot}] = [B] + [C] + [D]$

The dynamic time-dependent or state variables of the system are the concentrations of the complexes, and the reactions in the system obey the mass action law.

DOI:10.15774/PPKE.ITK.2010.005

Modeling assumptions

For the reactions, the following assumptions are made:

1. One molecule of ligand can activate one $G\alpha - GDP$-bound receptor, and phosphorylate the $G\alpha - GDP$ to $G\alpha - GTP$.
2. The $G\alpha - GTP$ subunit can dissociate from the ligand-bound receptor.
3. The recombination of the α and $\beta\gamma$ subunits of the G protein is considered to be fast, and so the deactivation of the G protein is described by one reaction corresponding to the hydrolysis of GTP to GDP (as in [143]). Thus the G$\beta\gamma$ signaling, and $\beta\gamma$ subunits are neglected.
4. The deactivated free $G\alpha - GDP$ can associate with a free receptor and form a $G\alpha - GDP$-bound receptor complex, which can be activated again by one molecule of the ligand.
5. Phosphate required for phosphorylation reactions is present in a great excess.
6. We do not take receptor internalization into account. Results show that receptor internalization does not appear in many cases, for example in the case of prolactin cells [51].

State equations

The state or differential equations in the model will be derived from the reaction equations related to the reaction kinetic model formed by the chemical reactions. The explicit derivation of the state equations is presented only in the case of the basic model structure of the G protein signaling mechanism. The method for deriving the equations from the reactions via the mass action law is the same in the case of the later models extended with slow transmission and the regulation of signaling.

The considered reactions (using the notation in Table 2.1) are as follows.

The binding of the ligand (L) by the ($G\alpha - GDP$)-bound receptor ($R(G\alpha - GDP)$), and receptor induced exchange of GDP for GTP on the Gα and the dissociation of Gα is described by the following reactions:

$$A + B \underset{k_1^-}{\overset{k_1^+}{\rightleftharpoons}} C_1 \underset{k_2^-}{\overset{k_2^+}{\rightleftharpoons}} D + E \tag{2.1}$$

The hydrolysis of $G\alpha - GTP$ to $G\alpha - GDP$ is described as

$$E \underset{k_3^-}{\overset{k_3^+}{\rightleftharpoons}} F \tag{2.2}$$

Following hydrolysis, inactive GαGDP binds $G\beta\gamma$ and the free receptor

$$G + F \underset{k_5^-}{\overset{k_5^+}{\rightleftharpoons}} A \tag{2.3}$$

DOI:10.15774/PPKE.ITK.2010.005

The dissociation of the ligand from the receptor is described in the form

$$D \underset{k_4^-}{\overset{k_4^+}{\rightleftharpoons}} G + B \tag{2.4}$$

The dissociation of the receptor and the ligand before reactivation of G protein is included to secure the ability of the ligand to escape from the cycle. Because the first ligand binding reaction is assumed to be irreversible, and only the concentration of the free ligand is affected by the input (the environment's ligand concentration), there is no other way to describe the fall of the ligand concentration on the cell surface.

The above reactions imply the following differential equations by the mass-action law:

$$\begin{aligned}
\frac{d[A]}{dt} &= -k_1^+[A][B] + k_1^-[C_1] + k_5^+[G][F] - k_5^-[A] \\
\frac{d[B]}{dt} &= -k_1^+[A][B] + k_1^-[C_1] + k_4^+[D] - k_4^-[G][B] + k_s([L_{env}] - [B]) \\
\frac{d[C_1]}{dt} &= k_1^+[A][B] - k_1^-[C_1] - k_2^+[C_1] + k_2^-[D][E] \\
\frac{d[D]}{dt} &= k_2^+[C_1] - k_2^-[D][E] - k_4^+[D] + k_4^-[G][B] \\
\frac{d[E]}{dt} &= k_2^+[C_1] - k_2^-[D][E] - k_3^+[E] + k_3^-[F] \\
\frac{d[F]}{dt} &= k_3^+[E] - k_3^-[F] - k_5^+[G][F] + k_5^-[A] \\
\frac{d[G]}{dt} &= k_4^+[D] - k_4^-[G][B] - k_5^+[G][F] + k_5^-[A]
\end{aligned} \tag{2.5}$$

The term $k_s([L_{env}] - [B])$ corresponds to the input (u) of the system, in which $u = L_{env}$ denotes the concentration of the ligand in the cell's environment. Note that L_{env} is a function of time in general.

Simulation results of the basic model can be found in Appendix B (10.1).

2.2.3 The extended model I: Receptor phosphorylation

If we want to take the concentration of phosphorylated receptor-ligand complex into account, which initiates the G protein independent slow transmission signaling, we have to extend our model with three more state-variables:

- The concentration of GPCR kinase - $[GRK]$
- The concentration of activated GPCR kinase and ligand bind receptor complex - $[GRK - RL]$

DOI:10.15774/PPKE.ITK.2010.005

- The concentration of phosphorylated ligand bind receptor - $[RL_p]$

We assume that the concentration of phosphorylated receptors depends only on the concentration of GRK and on the concentration of ligand-bound receptors, which can be phosphorylated by GRK-s.

For the development of a simple mathematical model of receptor phosphorylation, the reaction scheme shown in Fig. 2.2 is used.

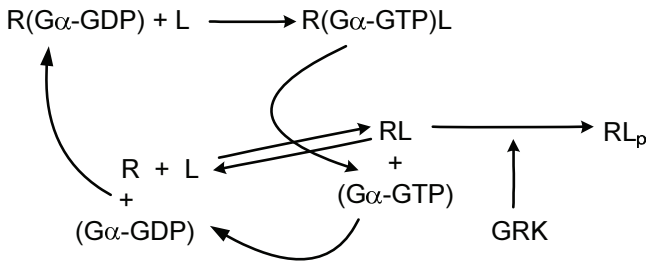

Figure 2.2: The reaction scheme of G protein signaling extended with receptor phosphorylation

2.2.4 The extended model II: Slow transmission and Regulation of signaling

In this section the further extended model is described, which includes the above detailed G-protein signaling model, the mechanism of receptor phosphorylation, slow transmission and the regulation of signaling.

As described in [37], β-Arrestins that bind the receptor after phosphorylation, can serve as scaffolding molecules that facilitate cell signaling to ERK (and also to other subgroups of MAPK proteins through MEK and Raf, as described in [90]). The activation of MAPK cascades can be furthermore initiated by a small GTP-binding protein (smGP; RAS-family protein), which transmits the signal either directly or through a mediator kinase to the MAPK kinase (MAP3K or MAPK^3) level of the MAPK cascades (MAPK-s are activated by MAP kinase kinases - MAPKKs -, which are in turn actiated by MAP kinase kinase kinases - MAP3Ks or MAPK^{3}s). As DeWire describes in [37], with si-RNA methods and the application of mutant receptors, it can be shown, that the resulting ERK phosphorylation (activation) is composed as a result of the activation induced by G proteins and the activation originated from β-Arrestin mediated slow transmission.

Experimental investigations show that the G protein-mediated ERK activity is maximal at 2 min after stimulation, and the β-arrestin2 mediated ERK activity is minimal until 10 min post-stimulation, but is responsible for nearly 100% of ERK signaling at times beyond 30 min [37].

It has also been shown [81, 89] that the regulators of G protein signaling (**RGS**) are basically the guanosine triphosphatase (GTPase)-accelerating proteins that specifically interact with G protein α subunits. RGS proteins enhance the intrinsic rate at which certain heterotrimeric G protein α-subunits hydrolyze GTP to GDP, thereby

DOI:10.15774/PPKE.ITK.2010.005

limiting the duration that α-subunits activate downstream effectors. This activity defines them as GTPase activating proteins (GAPs).

These regulator proteins display remarkable selectivity and specificity in their regulation of receptors, ion channels, and other G protein-mediated physiological events [171]. Recent findings show that RGS proteins selectively regulate signaling by certain G protein-coupled receptors (GPCRs) in cells, irrespective of the coupled G protein [122].

Furthermore, RGS proteins can change the nature of the start and end of a signaling event, while leaving the intensity of the signal unchanged [174]. Results of the investigation of RGS protein functioning and regulation of G protein signaling in yeast can be found in [69, 40].

There are multiple RGS subfamilies consisting of over 20 different RGS proteins. RGS2 blocks Gqα-mediated signaling, a finding consistent with its potent Gqα GAP activity.

MAPKs (including ERK) are feed-back regulated through map kinase phosphatases (MAPKP or **ERKP**), which are able to dephosphorylate MAPK-s [15, 94].

If RGS proteins were active unrestrictedly, they would completely suppress various G protein mediated cell signaling, as it has been shown in the over-expression experiments of various RGS proteins. Thus, physiologically the modes of RGS-action should be under some regulation. The regulation can be achieved through the control of either the protein function and/or the subcellular localization [75]. It can be assumed that RGS proteins (RGS2 and RGS3) are up-regulated via the phosphorylation of mitogen-activated protein kinases (MAPK or ERK) [94].

Extension of the reaction scheme

The further step in model development is to extend the model with the reactions describing the MAPK/ERK activation, and to take into account the RGS-mediated G protein feedback regulation, and ERKP mediated ERK auto-regulation. To make our model able to describe the signaling regulation process, we extend again the set of state variables (species) to obtain the set in Table 2.2.

DOI:10.15774/PPKE.ITK.2010.005

Table 2.2: Notations for the final model

Specie	Notation	Specie	Notation
$R-(G\alpha-GDP)$	A	$(G\alpha-GTP)-ERK$	C_3
L	B	ERK_p	K
$R-(G\alpha-GTP)-L$	C_1	RL_p-ERK	C_4
RL	D	RGS	L
$(G\alpha-GTP)$	E	ERK_p-RGS	C_5
$(G\alpha-GDP)$	F	RGS_p	M
R	G	$RGS_p-(G\alpha-GTP)$	C_6
GRK	H	$ERKP$	N
$RL-GRK$	C_2	ERK_p-ERKP	C_7
RL_p	I	$ERKP_p$	O
ERK	J	$ERKP_p-ERK_p$	C_8

Modelling assumptions

1. We assume that β-Arrestin, PP2A and Akt is in great excess, and they bind rapidly to the receptor forming the signaling complex, which immediately activates the second messenger cascade leading to the induction of ERK signaling.

2. The ERK signaling cascade (MAP3K, MAPKK, MAPK) is neglected in the case of G protein based signaling.

3. Furthermore, we suppose, that RGS proteins are activated by the active form of ERK [94].

The phosphorylation of the ligand-bound receptor by GRK is described by the following reaction:

$$H+D \underset{k_6^-}{\overset{k_6^+}{\rightleftharpoons}} C_2 \underset{k_7^-}{\overset{k_7^+}{\rightleftharpoons}} H+I \tag{2.6}$$

The dephosphorylation of the phosphorylated receptor is represented by the reaction

$$I \underset{k_8^-}{\overset{k_8^+}{\rightleftharpoons}} D \tag{2.7}$$

We describe the signaling process and regulation by the reactions described in Eqs. (2.1) - (2.7) extended by the following reactions.

- The ERK activation by $(G\alpha-GTP)$ and RL_P through β-Arrestin is described by the reactions:

$$E+J \underset{k_9^-}{\overset{k_9^+}{\rightleftharpoons}} C_3 \underset{k_{10}^-}{\overset{k_{10}^+}{\rightleftharpoons}} E+K \qquad I+J \underset{k_{11}^-}{\overset{k_{11}^+}{\rightleftharpoons}} C_4 \underset{k_{12}^-}{\overset{k_{12}^+}{\rightleftharpoons}} I+K$$

DOI:10.15774/PPKE.ITK.2010.005

- The ERK-mediated RGS activation and the regulation of G protein signaling by the GAP-activity of RGS is represented by

$$K + L \underset{k_{13}^-}{\overset{k_{13}^+}{\rightleftharpoons}} C_5 \underset{k_{14}^-}{\overset{k_{14}^+}{\rightleftharpoons}} K + M \qquad M + E \underset{k_{15}^-}{\overset{k_{15}^+}{\rightleftharpoons}} C_6 \underset{k_{16}^-}{\overset{k_{16}^+}{\rightleftharpoons}} M + F$$

- Finally, the following reactions are related to the deactivation of ERK and RGS:

$$K \underset{k_{17}^-}{\overset{k_{17}^+}{\rightleftharpoons}} J \qquad M \underset{k_{18}^-}{\overset{k_{18}^+}{\rightleftharpoons}} L$$

- If we also want to take into account the ERKP-mediated ERK feedback autoregulation shown in Fig. 2.3, we have to extend our system with the following reactions:

$$K + N \underset{k_{19}^-}{\overset{k_{19}^+}{\rightleftharpoons}} C_7 \underset{k_{20}^-}{\overset{k_{20}^+}{\rightleftharpoons}} K + O \underset{k_{21}^-}{\overset{k_{21}^+}{\rightleftharpoons}} C_8 \underset{k_{22}^-}{\overset{k_{22}^+}{\rightleftharpoons}} J + O$$

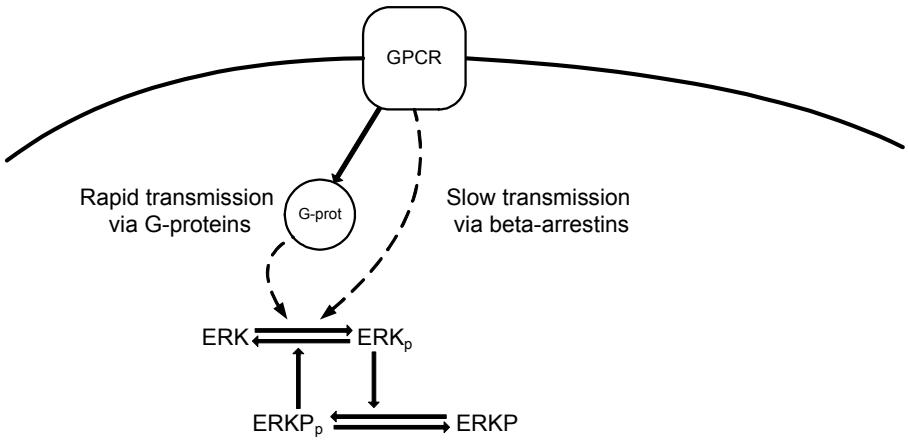

Figure 2.3: The reaction scheme of ERK feedback autoregulation by ERKP: The ERK proteins can be activated either by the conventional G-protein coupled pathways or via slow transmission. In both cases the activation of ERK triggers the activation of the ERKP regulatory protein, which enhances the activation of ERK. The subscript $_p$ denotes the active (phosphorylated) form of the proteins, the continual arrows indicate direct effect, and the dotted arrows indicate indirect effect through other molecules

- The deactivation of ERKP is described by the reaction

$$O \underset{k_{23}^-}{\overset{k_{23}^+}{\rightleftharpoons}} N$$

DOI:10.15774/PPKE.ITK.2010.005

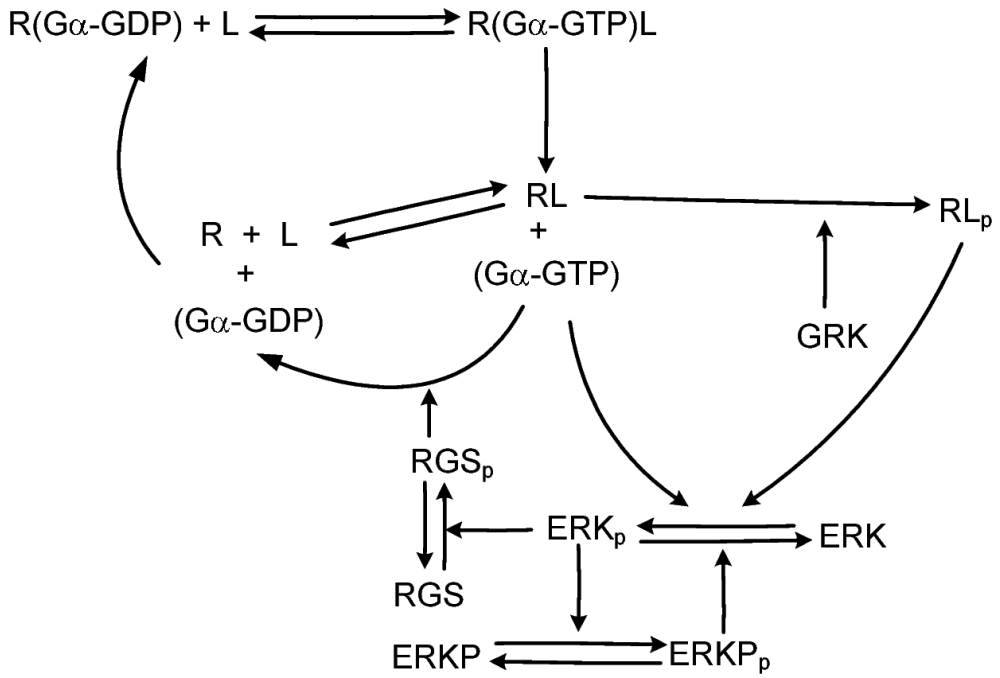

Figure 2.4: The reaction scheme of G protein signaling, ERK activation and regulation of signaling

The subscript p in Figure 2.3 corresponds to the activated forms of the enzymes. This mechanism is included in the resulting reaction scheme in Fig. 2.4.

Finally, the resulting reaction scheme in Fig. 2.4 summarizes the structure of all the above reactions. It is important to observe a large, RGS mediated and a small $ERKP$ feedback loop, which implies a cascade structure.

2.3 Model verification

The models described in the above sections were verified by simulation. During the verification process, the simulation results of the models were tested against theoretical expectations, and the simulation results of the extended model II were compared to published experimental data regarding the time evolution of ERK activation. This section describes and discusses these results.

2.3.1 Simulation results

For the simulation of the extended model II, the parameters collected in Table 2.3 were used. The parameters were obtained via parameter estimation with MATLAB using the Nelder-Mead simplex algorithm for the best fit of experimental data of DeWire et al. [37, 105]. The right sub-figure of Figure 2.5 and both sub-figures of Figure 2.6 show averaged experimental values [105], and their empirical variances denoted by circles. For a good fit we expect the model to provide trajectories which remain in the intervals defined by the experimental deviations.

DOI:10.15774/PPKE.ITK.2010.005

Table 2.3: Parameter set for the final, extended model's simulation

Param.	Value	Param.	Value	Param.	Value
k_1^+	100	k_9^+	5.3019	k_{17}^+	6.2324
k_1^-	100	k_9^-	5.3019	k_{17}^-	0
k_2^+	120	k_{10}^+	2.5539	k_{18}^+	0
k_2^-	0	k_{10}^-	0	k_{18}^-	0
k_3^+	0.3170	k_{11}^+	8.9418	k_{19}^+	0.3791
k_3^-	0	k_{11}^-	8.9418	k_{19}^-	0.3791
k_4^+	1	k_{12}^+	9.3924	k_{20}^+	0.2354
k_4^-	1	k_{12}^-	0	k_{20}^-	0
k_5^+	1	k_{13}^+	1.2696	k_{21}^+	0.4
k_5^-	1	k_{13}^-	1.2696	k_{21}^-	0.4
k_6^+	0.6827	k_{14}^+	1.2316	k_{22}^+	0.4325
k_6^-	0.6827	k_{14}^-	0	k_{22}^-	0
k_7^+	0.3584	k_{15}^+	5.9983	k_{23}^+	0.015
k_7^-	0	k_{15}^-	5.9983	k_{23}^-	0
k_8^+	0.5	k_{16}^+	6.6509		
k_8^-	0	k_{16}^-	0		

Note that the spontaneous deactivation of RGS protein was neglected in these final simulation experiments, and so the parameters k_{18}^+ and k_{18}^- were set to 0. The time interval of the simulations was 60 minutes in this case. The initial conditions were set to describe a fully deactivated cell with all signaling activations on the basal level.

We have to note that the sensitivity of the results with respect to certain parameters (eg. k_1^+, k_1^-, k_2^+) was not high enough to obtain an accurate estimated value. A simple sensitivity analysis of the model is described in Appendix C.

It is important to note that if we wish to compare the resulting parameter values to the values found in the literature, we have to denormalize every concentration (which is hardly feasible due to imperfect information about intracellular protein concentrations), and modify the corresponding rate constants to achieve the same time patterns. This is why a simulation method with normalized concentrations has been used in our study to analyze only the qualitative features of the model structure.

The results of the simulations, i.e. the system responses are depicted in Figs. 2.5 and 2.6. In the left sub-figure of Fig. 2.5 the simulated $G\alpha$, RGS and ERKP -activation pattern can bee seen. Here again, the total activated ERK concentration is taken into account, which includes also the complexes, where the activated ERK acts as an enzyme (ERKP and RGS activation). In the case of other components, the concentration of the free element is depicted. In the case of ERKP the total active concentration is depicted (the sum of the free active enzyme and the complex with ERK). The reason for this is that the free active ERKP concentration is not very informative, as the enzyme immediately forms complexes with ERK.

DOI:10.15774/PPKE.ITK.2010.005

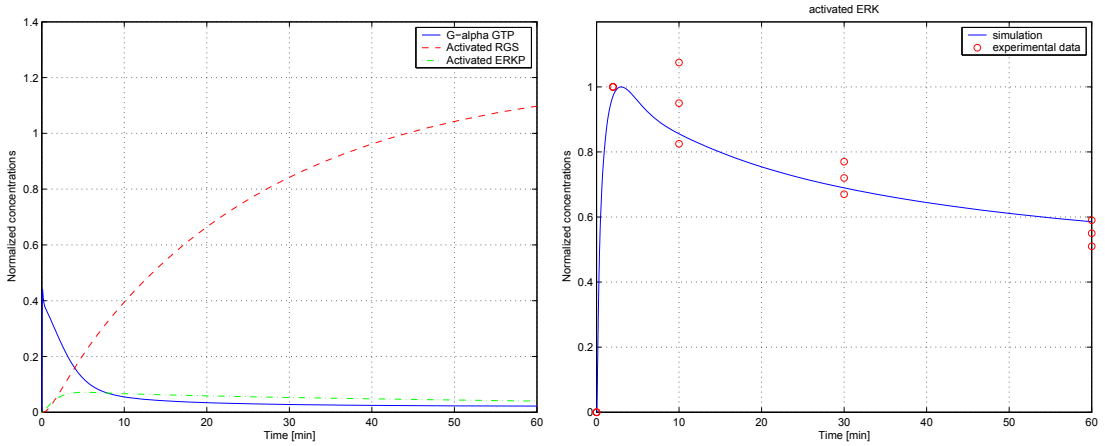

Figure 2.5: Activation pattern of $G\alpha - GTP$, the corresponding regulators and ERK in the case of both transmission mechanism active. The circles on the second plot correspond to experimental results.

The $G\alpha$-activation pattern is strongly affected by receptor phosphorylation and ERK-induced activation of RGS-proteins, which rapidly dephosphorylate the $G\alpha - GTP$ to $G\alpha - GDP$.

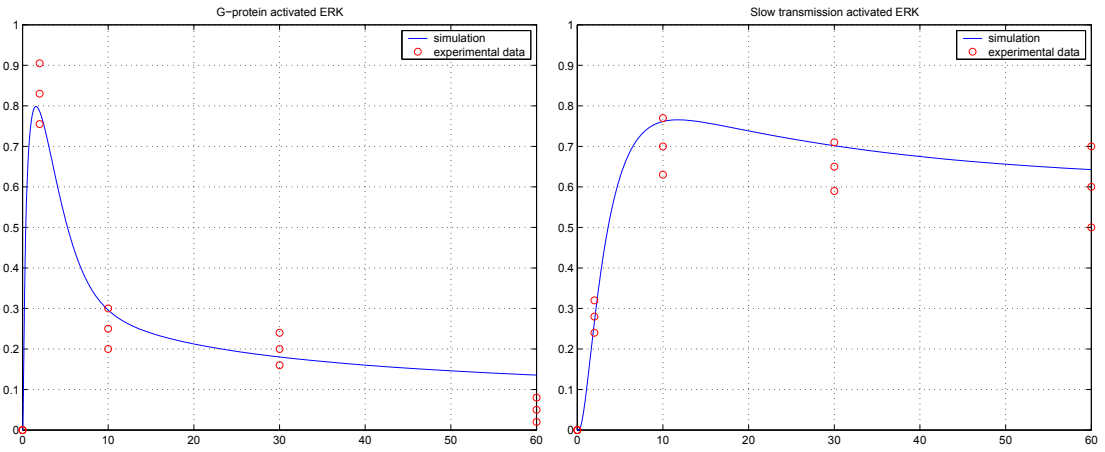

Figure 2.6: G protein versus β-Arrestin mediated signaling. The circles correspond to experimental results

In Fig. 2.6 we can see the ERK activation pattern corresponding to pure G protein dependent and G protein independent, RL_p (β-Arrestin) mediated signaling. The left sub-figure of Fig. 2.6 depicts the ERK activation in the case, when no slow transmission is taken into account. In the right sub-figure the G protein independent signaling is illustrated.

DOI:10.15774/PPKE.ITK.2010.005

2.3.2 Discussion

If one wants to compare our simulation results with the experimental curves found in the literature, an important observation should be made. In several articles that reports on experiments (eg. [37]), the curves are normalized with the maximum concentration observed during the measurement. The reason behind this is, that in the case of many western-blot measurements, no information is available of the remaining inactive protein pool. These "actual maximum-normalized" curves can be easily derived from the data of our simulation results by re-normalizing the data with the actual maximum value of the concentration-curve. Unfortunately, a "total quantity-normalized" curve can not be obtained from an "actual maximum-normalized" curve, if we do not have any information about the remaining, inactive protein pool.

The **basic model** described in 2.2.1 is able to describe the ligand-induced G protein activation in the cell, but is unable to describe receptor phosphorylation, the regulation of signaling. Furthermore, as described in Appendix B 10.1, the fast return of G protein activation to basal level after the stimulus also can not be described by this model, except if we suppose very fast spontaneous dephosphorylation of the $G\alpha - GTP$ to $G\alpha - GDP$. However, in this case a smaller part of the total G protein pool becomes activated, and a less significant but non-zero steady-state is still present.

In the case of the **extended model II**, it can be seen in both Fig. 2.6 and 2.5 that the G protein activation and the G protein induced ERK activation has a pulsative maximum around 2 min, and is eliminated via the feedback of RGS activation. The G protein independent ERK activation, which can be related to the RL_p concentration, has a slower rising period, and remains more stable during the simulation period.

As it can be seen in the second plot of Figure 2.5, the resulting activation pattern, which is in good agreement with experimental data, inherits the qualitative features of both pathways: The rapid maxima of ERK activation at 2-3 minutes can be related to the G protein dependent pathway, and the remaining tonic activation originates from the slow transmission pathway. Both the theoretical considerations and simulation results show that the resulting activation pattern of the second plot of Figure 2.5 is not the simple sum of the activation patterns depicted in Figure 2.6, because of the feedback mechanisms and other effects.

We have to note again, normalized concentrations were used because of the lack of information about intracellular protein concentrations and in vivo reaction rate constants. This implies that the identified parameters can not be directly compared to literature data related to measurements with known concentrations. But the model fulfills its main aim, and shows the required qualitative dynamic behavior and complexity for the description of the two-pathway regulated signaling system.

2.4 Conclusions

A simple, in a sense (regarding the number of reactions) minimal dynamic model of G protein dependent and independent signaling is proposed in this chapter. The

DOI:10.15774/PPKE.ITK.2010.005

model focuses on the characteristic qualitative pattern of the time evolution of the key components this way enabling experimental verification.

We have shown that if we take both ERK-mediated RGS and MAPKP feedback regulations into account, a qualitatively acceptable downstream behavior can be obtained in total ERK activation as well as in particular cases of G protein dependent and/or independent signaling.

Based on the simulation results presented here, we can conclude that modeling of slow transmission, RGS and MAPK-mediated regulation of signaling can be efficiently described using the framework of reaction kinetic systems, that may be essential when analyzing the dynamic behavior for physiological cell signaling. This type of model enables us to use the deficiency-based stability and multistability-related results of Feinberg et al. [44, 31, 32]. In addition, the determination of optimal time-dependent drug dosing may also be possible using control theoretic methods.

The proposed mathematical model could be an effective tool to analyze the qualitative effect of pathway selective drugs on signaling dynamics, for example Lithium in the case of dopamine-signaling [9], and to underline the importance of such medicines.

If the measurement or estimation of intracellular protein concentrations and rate constants were available, the model parameters could be re-estimated to quantitatively fit experimental data, and be comparable to other literature results. Such an improvement of the model would be of great importance, since the relative concentrations of the proteins corresponding to the signaling system may vary with cell type and thus can give rise to qualitatively different signaling dynamics. This extension could open the way to study how the variation of cell stoichiometry of reactants can affect signaling kinetics.

DOI:10.15774/PPKE.ITK.2010.005

Chapter 3

Identifiability and parameter estimation of a single Hodgkin-Huxley type ion channel under voltage clamp measurement conditions

In this chapter some theoretical issues of Hodgkin-Huxley (HH) type models (the model class used later in Chapter 4) are addressed. in particular, the identifiability properties of a single HH type voltage dependent ion channel model under voltage clamp circumstances are analyzed. The elimination of the differential variables is performed, and the identifiability of various parameters is analyzed. As we will see, the formal identifiability analysis shows that even in the simplest case when only the conductance and the steady state activation and inactivation parameters are to be estimated, no identifiable pair from the three can be chosen.

In addition, a possible novel identification method is proposed, which is able to handle the arising identifiability problems. The proposed method is based on prior assumptions and on the decomposition of the parameter estimation problem in two parts. The first part includes the estimation of the maximal conductance value and the activation/inactivation parameters from the values of steady state currents obtained from multiple voltage step traces, utilizing the prior assumptions corresponding to the mathematical form of steady state functions. The use of steady state currents allows the estimation of the first parameter group independently of the other parameters. This parameter estimation problem results in a system of nonlinear algebraic equations, which is solved as an optimization problem.

The second part of the parameter estimation problem focuses on the parameters of the voltage dependent time constants, and is also formulated as an optimization problem. The parameter estimation method is demonstrated on in silico data, and the optimization process is carried out using the Nelder-Mead simplex algorithm in both cases.

The results of the chapter are used to formulate explicit criteria for the design of voltage clamp protocols.

DOI:10.15774/PPKE.ITK.2010.005

3.1 The concept of identifiability

Once the model structure is fixed (see later Eqs. (3.1)-(3.3) in our case), the next key step of the modelling process is parameter estimation the quality of which is crucial in later usability of the obtained model (see [109] and for e.g. the parameter estimation procedure detailed in chapter 4).

The identifiability properties of the system describe whether there is a theoretical possibility for the unique determination of system parameters from appropriate input-output measurements or not. Basic early references for studying identifiability of dynamical systems are the books [157, 158]. The study and development of differential algebra methods, that are used for identifiability analysis, contributed to the better understanding of important system theoretic problems [39, 47]. The most important definitions and conditions of structural identifiability for general nonlinear systems were presented in [110] in a very clear way. Further developments in the field include the identifiability conditions of rational function state-space models [115] and the possible effect of special initial conditions on identifiability [134].

Both the articles [102] and [165] realized the weaknesses of the conventional estimation algorithms, and provided improved methods for the estimation of HH models. Lee et.al. [102] proposed a new numerical approach to interpret voltage clamp experiments. As one of the main results of this article, it is stated, that all channel parameters can be determined from a single appropriate voltage step.

The aim of this chapter is to carry out a rigorous identifiability analysis in a simple case of the HH model class under voltage clamp measurement conditions in order to verify or falsify the above results related to parameter estimation of HH models.

3.2 Hodgkin-Huxley type mathematical modeling of membrane dynamics and ion channels

Hodgkin-Huxley (HH) models, which stand for the most widely used model class in computational neuroscience, are nonlinear electric circuit models, composed of parallel voltage dependent (and possibly voltage independent) conductances, which refer to various type membrane currents.

The basic modelling assumptions of the HH model, which are based on the kinetic description of the behavior of multiple voltage-dependent subunits [70], are evident and well formulated from the physical perspective. In contrast, if we analyze the model from the point of view of system theory, as a nonlinear state-space model (a system of nonlinear ordinary differential equations, ODE's), several interesting questions arise, related not only to the bifurcation structure of the model [78, 55], but also to the identifiability properties of the system class [110].

The general HH model is based on the description of ionic currents in the following form:

$$I_i = g_i m_i^{p_{mi}} h_i^{p_{hi}} (V - E_i) \tag{3.1}$$

where I_i is the current of the i-th channel, m_i and h_i are the corresponding activation and inactivation variables on the powers p_{mi} and p_{hi}, which correspond to the number

DOI:10.15774/PPKE.ITK.2010.005

of independent subunits of the voltage channel protein. V is the membrane voltage and E_i is the reversal potential of the corresponding ion.

The dynamics of the activation and inactivation variables are described by

$$\frac{dm_i}{dt} = (m_{i\infty}(V) - m_i)/\tau_{mi}(V), \quad \frac{dh_i}{dt} = (h_{i\infty}(V) - h_i)/\tau_{hi}(V) \tag{3.2}$$

where $m_{i\infty}(V)$ and $h_{i\infty}(V)$ denote the voltage dependent steady state values of activation and inactivation variables, and $\tau_{mi}(V)$ and $\tau_{hi}(V)$ denote the voltage dependent time constants.

In general, two basic measurement protocols are used for parameter estimation of neuronal models: the *voltage clamp protocol*, when the voltage is fixed and the transmembrane currents are measured, and the *current clamp protocol*, in which case an arbitrary value of injected current to the cell is fixed. In the case of current clamp, the time evolution of the voltage can be calculated as a function of the membrane currents

$$\frac{dV}{dt} = -\frac{1}{C}(\sum_i I_i) \tag{3.3}$$

where in addition to the above detailed ionic currents with voltage dependent conductance, constant conductance leak type currents can also be taken into account.

In the case of voltage clamp, where the voltage is held constant, the only remaining differential variables are the activation and inactivation variables.

In the following, we analyze the identifiability properties of the most simple HH model, a single ion channel, under the assumptions of first order activation and inactivation dynamics and voltage clamp measurement protocol.

3.2.1 A simple ion channel model

We consider a simple hypothetical ion channel with one activation (m) and one inactivation variable (h). The current, which is the measured variable under voltage clamp circumstances, is simply described by

$$I = gmh(V - E) \tag{3.4}$$

where V is the voltage, g is the maximal conductance, and E is the reversal potential of the corresponding ion. Both m and h are differential variables described by the equations

$$\frac{dm}{dt} = \frac{m_\infty(V) - m}{\tau_m(V)} \tag{3.5}$$

$$m_\infty(V) = \left(1 + exp\left(\frac{V_{1/2m} - V}{k_m}\right)\right)^{-1}, \quad k_m > 0 \tag{3.6}$$

$$\frac{1}{\tau_m(V)} = \left(c_{bm} + c_{am} exp\left(-\frac{(V_{Maxm} - V)^2}{\sigma_m^2}\right)\right)^{-1} \tag{3.7}$$

DOI:10.15774/PPKE.ITK.2010.005

$$\frac{dh}{dt} = \frac{h_\infty(V) - h}{\tau_h} \tag{3.8}$$

$$h_\infty(V) = \left(1 + exp\left(\frac{V_{1/2h} - V}{k_h}\right)\right)^{-1}, \quad k_h < 0 \tag{3.9}$$

$$\frac{1}{\tau_h(V)} = \left(c_{bh} + c_{ah} exp\left(-\frac{(V_{Maxh} - V)^2}{\sigma_h^2}\right)\right)^{-1} \tag{3.10}$$

where $V_{1/2m}$, k_m, $V_{1/2h}$, and k_h are the parameters of the Boltzmann functions which describe the steady state activation and inactivation values. c_{bm}, c_{am}, V_{Maxm}, σ_m, c_{bh}, c_{ah}, V_{Maxh} and σ_h denote the parameters of Gauss-functions which describe the voltage dependent time-constants.

We have to note that the approximation of the steady state values with Boltzmann functions is not always valid, at it is described in [165]. However in the rest of this chapter we assume that this consideration holds. It can be said that in the literature the use of Boltzmann-type sigmoid functions is widespread for the description of steady-state values, but not exclusive (see e.g. [93]).

The description of the voltage dependent time constants in the literature is more diverse. In fact, the variability of time constant curves corresponding to various rate constant functions is described in [165]. In this study we will use standard Gauss functions, parameterized by c_{bm}, c_{am}, V_{Maxm}, σ_m, c_{bh}, c_{ah}, V_{Maxh} and σ_h.

3.2.2 Voltage step protocol

An important version of the voltage clamp method is when the voltage, which is in this case the manipulable input (u) of the system, is held piecewise constant ($V(t) = u(t) = V_0$ for $t_k \leq t < t_{k+1}$, $k = 1, \ldots, N$). During each interval, the values of m_∞, h_∞, τ_m and τ_h can be considered as time-invariant parameters in addition to g and E. This implies that the non-polynomial nonlinearities of Boltzmann and Gauss functions (Eqs. (3.6), (3.7) and (3.9), (3.10)) are naturally eliminated from the equations, and the model will fall into the class of polynomial systems, which makes the application of effective computer algebra based software tools (e.g. DAISY [11]) possible for identifiability testing.

Under this circumstances will denote the voltage independent nature of the above parameters shortly by supressing the V argument, i.e. $m_\infty(V) = m_\infty$, $\tau_m(V) = \tau_m$, $h_\infty(V) = h_\infty$ and $\tau_h(V) = \tau_h$, with $V = V_0$.

In this case, Eqs. (3.4-3.10) are simplified as follows:

$$I = gmh(V_0 - E) = gmh(u - E) \tag{3.11}$$

$$y = I, \quad u = V_0 = const.$$
$$\frac{dm}{dt} = \frac{m_\infty - m}{\tau_m}, \quad \frac{dh}{dt} = \frac{h_\infty - h}{\tau_h} \tag{3.12}$$

where the model parameters are $g, E, m_\infty, \tau_m, h_\infty$ and τ_h.

DOI:10.15774/PPKE.ITK.2010.005

3.3 Structural identifiability notions and tools

In the following we will give a short formal definition of structural identifiability, and provide a sufficient condition of this concept. In general let us consider the following class of models

$$\begin{aligned} \dot{x} &= f(x,u,\theta), \quad x(0) = x_0 \\ y &= h(x,u,\theta) \end{aligned} \tag{3.13}$$

where $x \in \mathbb{R}^n$ is the state vector, $y \in \mathbb{R}^m$ is the output, $u \in \mathbb{R}^k$ is the input, and $\theta \in \mathbb{R}^d$ denotes the parameter vector. We assume that the functions f and h are polynomial in the variables x, u and θ. We remark that majority of nonlinear state-space models with smooth right-hand sides can also be embedded into the above polynomial model form (3.13) on the price of increasing the state space dimension [68].

3.3.1 Global structural identifiability analysis using differential algebra

Shortly speaking, *global structural identifiability* means that

$$y(t|\theta') \equiv y(t|\theta'') \Rightarrow \theta' = \theta'' \tag{3.14}$$

where

$$y(t|\theta) = h(x(t,\theta), u(t), \theta) \tag{3.15}$$

and $x(t,\theta)$ denotes the solution of (3.13) with parameter vector θ. This means that if the system outputs are identical, then the underlying parameters are the same: this is a model property, e.g. the property of (3.13).

The following notations, definitions and conditions are mostly taken from [110]. Let us denote a differential polynomial $F(u, \dot{u}, \ldots, y, \dot{y}, \ldots)$ by $F(u, y; p)$ where $p = \frac{d}{dt}$.

The structure (3.13) is *globally identifiable* if and only if by differentiating, adding, scaling and multiplying the equations the model can be rearranged to the parameter-by-parameter linear regression form:

$$P_i(u,y;p)\theta_i - Q_i(u,y;p) = 0 \quad i = 1, \ldots, d \tag{3.16}$$

It is visible from (3.16) that θ_i can be expressed as

$$\theta_i = \frac{Q_i(u,y;p)}{P_i(u,y;p)} \quad i = 1, \ldots, d \tag{3.17}$$

if P_is are non-degenerate. The non-degenerate condition can be fostered by ensuring that the inputs excite the system dynamics sufficiently so that the parameter vector can be determined in a numerically well-conditioned way.

DOI:10.15774/PPKE.ITK.2010.005

3.4 Structural identifiability of ion channel models

In this section the identifiability properties of the ion channel model defined in 3.2.2 are analyzed.

3.4.1 Elimination of differential variables from the ion channel model under voltage step conditions

The identifiability analysis requires to eliminate the differential (state) variables m and h from the model Eqs. (3.11)-(3.12) and then to find the parameter groups that can be determined from the resulting equations. The first step towards the input-output description described by Eq. (3.16) is to algebraically eliminate those differential variables from the model (3.11)-(3.12) that are not identical to the output y. This means that both m and h have to be eliminated in this case. Firstly, the time-derivative of the output is computed as

$$\dot{y} = \dot{I} = g(u-E)(\dot{m}h + m\dot{h}) = g(u-E)(\frac{m_\infty - m}{\tau_m}h + m\frac{h_\infty - h}{\tau_h}) \tag{3.18}$$

The above equation can be rearranged to

$$\begin{aligned} \dot{y}\tau_m\tau_h &= g(u-E)((m_\infty - m)\tau_h h + m(h_\infty - h)\tau_m) \\ &= g(u-E)(m_\infty\tau_h h + m h_\infty\tau_m) - y(\tau_m + \tau_h) \end{aligned} \tag{3.19}$$

If we further take the time-derivative of Eq. (3.19) we get the expression

$$\tau_m\tau_h\ddot{y} = g(u-E)((h_\infty - h)m_\infty + (m_\infty - m)h_\infty) - \dot{y}(\tau_m + \tau_h) \tag{3.20}$$

Let us rearrange Eqs. (3.19) and (3.20)

$$\begin{aligned} \frac{\tau_m\tau_h\dot{y} + y(\tau_m + \tau_h)}{g(u-E)} &= h_\infty\tau_m m + m_\infty\tau_h h \\ 2m_\infty h_\infty - \frac{\tau_m\tau_h\ddot{y} + \dot{y}(\tau_m + \tau_h)}{g(u-E)} &= h_\infty m + m_\infty h \end{aligned}$$

which is a set of linear equations in the variables m and h, therefore they can be expressed as:

$$m = \frac{-\tau_m\tau_h^2\ddot{y} - \dot{y}(2\tau_m + \tau_h)\tau_h - (\tau_m + \tau_h)y + 2g(u-E)m_\infty h_\infty\tau_h}{h_\infty g(u-E)(\tau_h - \tau_m)} \tag{3.21}$$

$$h = \frac{\tau_m^2\tau_h\ddot{y} + \dot{y}(\tau_m + 2\tau_h)\tau_m + (\tau_m + \tau_h)y - 2g(u-E)m_\infty h_\infty\tau_m}{m_\infty g(u-E)(\tau_h - \tau_m)} \tag{3.22}$$

The above explicit expressions for m and h show that the system is *algebraically observable* [39, 11] in this case.

DOI:10.15774/PPKE.ITK.2010.005

3.4.2 Identifiability of g, m_∞ and h_∞

The next step in the identifiability analysis would be to substitute Eqs. (3.21) and (3.22) into the model equations (3.11-3.12) and try to express the parameters in the form of Eq. (3.16). However, this step produces so lengthy expressions, that we will rely on computer algebra programs.

In this subsection we analyze the case when it is assumed that only the parameters g,m_∞ and h_∞ are unknown. We use the differential algebra software DAISY for identifiability analysis of the model [11]. The code used for the analysis can be found in Appendix E.

At first, the results of the analysis show that the model is algebraically observable, which is in good agreement with our results regarding the elimination of differential variables (see Eq. (3.21) and (3.22)).

At second, according to the identifiability results of the analysis, the parameters g, m_∞ and h_∞ are not independent, namely no identifiable pair of the three can be chosen. This results seems trivial in the case of steady state, when $m = m_\infty$ and $h = h_\infty$, because in this case only the product of the three parameters appears as output in $y = I = gmh(V - E)$. But the dependence also holds during the transient period.

In the following, we present an interesting example illustrating non-identifiability when the parameters of the system are different, but the outputs of the two systems are identical.

Example for non-identifiability at constant input voltage

In this subsection we present two cases of the model (3.11-3.12) that have different parameters but provide the same output in the case of a constant input voltage. The key issue for this counterexample is the modification of the initial values of the state variables.

In general, in the case of constant voltage, the trajectory of the state-space variables can be expressed as:

$$m = m_\infty + (m(0) - m_\infty)exp\,(-t/\tau_m) \qquad h = h_\infty + (h(0) - h_\infty)exp\,(-t/\tau_h) \quad (3.23)$$

The current, which is the output (y) from the point of view of systems theory, can be described in this case by Eq. (3.24) below

$$\begin{aligned} I(t) &= y(t) = gmh(V - E)m \\ &= g(m_\infty + (m_0 - m_\infty)exp\,(-t/\tau_m))(h_\infty + (h_0 - h_\infty)exp\,(-t/\tau_h))(V - E) \end{aligned} \quad (3.24)$$

Now, let us scale the model parameters with a positive scalar λ as follows: $m^*_\infty = \lambda \cdot m_\infty$, and $g^* = g/\lambda$. Furthermore, let us choose the initial values of the state variables as $m^*(0) = \lambda \cdot m(0)$, $h^*(0) = h(0)$. The output of the modified model is

DOI:10.15774/PPKE.ITK.2010.005

then

$$\begin{aligned} y^*(t) &= g^*(V-E)m^*h^* \\ &= (V-E)g^*(m^*_\infty + (m^*(0)-m^*_\infty)e^{-p_1 t})(h_\infty + (h^*(0)-h_\infty)e^{-p_3 t}) \\ &= (V-E)\frac{g}{\lambda}(\lambda m_\infty + (\lambda m(0)-\lambda m_\infty)e^{-t/\tau_m})(h_\infty + (h(0)-h_\infty)e^{-t/\tau_h}) \\ &= y(t) \end{aligned} \tag{3.25}$$

from which it is clear, that the scaled model generates exactly the same output as the original one. The circumstances of the above case are not very likely to hold in the case of a standard voltage clamp protocol, where the voltage is held at an other constant value (the holding potential V_{hold}) before the voltage step. The holding potential determines the initial values of the differential variables: $m(0) = m(0) = m_\infty(V_{hold})$ and $h(0) = h(0) = h_\infty(V_{hold})$). However, the scenario is not impossible, as we will show below.

Example for non-identifiability in the case of a single voltage step

Using two fictitious neurons, we will now show that the measurable current responses of a voltage step during voltage clamp measurement can be identical in the case of different parameters. In this case, we relax the former assumption that the input voltage is constant during the experiment. This means that we will use the original non-polynomial ion channel model given by Eqs. (3.4)-(3.10).

Let us suppose that both neurons to be compared here inhibit only one ion channel, and the activation and inactivation characteristics of the first neuron are described by

$$\begin{aligned} m_\infty(V) &= \left(1 + exp\left(\frac{V_{1/2m} - V}{k_m}\right)\right)^{-1} \\ h_\infty(V) &= \left(1 + exp\left(\frac{V_{1/2h} - V}{k_h}\right)\right)^{-1} \end{aligned} \tag{3.26}$$

The parameter values for the two neurons can be found in Table 3.1. The other parameters in the case of both neurons were the following

$$\begin{aligned} &h_\infty = 0.75,\ V_{Maxm} = -78mV,\ \sigma_m = 34,\ c_{am} = 8.7ms, \\ &c_{bm} = 0.8ms,\ E = -93mV,\ V_{Maxh} = -23mV \\ &\sigma_h = 24,\ c_{ah} = 6.9ms,\ c_{bh} = 9ms. \end{aligned} \tag{3.27}$$

Table 3.1: Parameters of the two neurons

No	$V_{1/2m}$	k_m	$V_{1/2h}$	k_h	g
1	-31.932 mV	13.033	-44.354 mV	-5.139	67 nS
2	-41.056 mV	10.555	-44.354 mV	-5.139	44.67 nS

DOI:10.15774/PPKE.ITK.2010.005

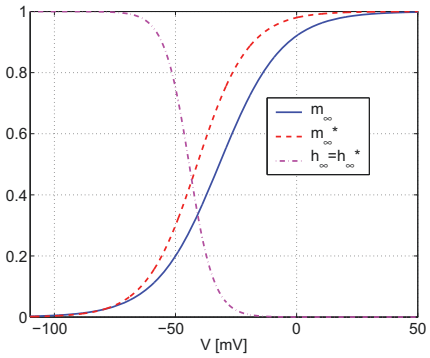

Figure 3.1: Voltage dependencies of the steady activation and inactivation state functions m_∞, m^*_∞ and h^*_∞=h^*_∞

As it is shown in Fig. 3.1, the value of m_∞ is 0.35 at -40mV and it is 0.20 at -50mV. At the same time, the value of m^*_∞ of the second neuron is 0.525 at -40mV and 0.30 at -50mV. The inactivation curve corresponding to h_∞ was the same in both cases. We applied a holding potential of -40 mV and a voltage step to -50 mV at t=100ms.

The comparison of trajectories of activation and inactivation variables and the output are depicted in Fig. 3.2. The figure clearly shows that the outputs are identical in the two cases, although the parameters of the two models are different.

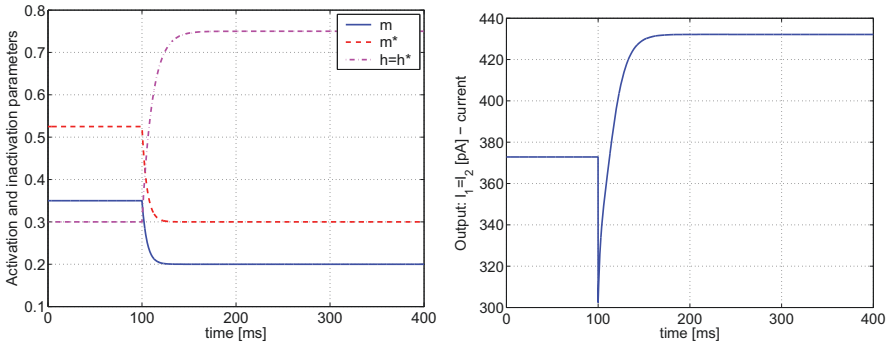

Figure 3.2: The activation and inactivation variables, and the output during the voltage step in the case of neuron 1 and 2. The upper index * refers to the activation and inactivation variables of neuron 2. The measured output current traces are identical in both cases.

Discussion

The article [102] implicitly realized this problem of interdependence between the activation/inactivation variables and the conductance, and they proposed a method to estimate the parameter g in which they assume that the voltage step is sufficiently large to ensure $m_\infty = 1$ (in addition this assumption may also imply $h_\infty = 0$). This

DOI:10.15774/PPKE.ITK.2010.005

method can be an appropriate solution for the estimation of g, but similarly to the proposed case the interdependence can also appear between m_∞ and h_∞.

Furthermore, the above investigated case serves also as an example of a voltage clamp trace where no local maximum (peak current) appears (see Fig. 3.2), which implies that method proposed in [102] can not be used without modification.

The above results imply that for the design of a parameter estimation method we have to take into account the possibility that the parameters m_∞, h_∞ and g can not be determined uniquely from a single voltage step. We have to admit that these special parametrizations which were used for the counterexamples are not very likely in the case of real neurons (these parameter sets probably form a set of measure 0 in the parameter space), but noise, deviations from the ideal Boltzmann functions and possible wrong guess of the powers of the activation and inactivation variables can further complicate the situation.

3.4.3 Identifiability of τ_m and τ_h

In the case of the voltage step protocol, the input (u=V) and the parameters m_∞, h_∞, τ_m and τ_h in Eq.(3.12) are constant. When we further assume that the m_∞, h_∞, g and other parameters of the model are known, the only unknown parameters are τ_m and τ_h.

The differential algebra based computer analysis shows, that the system is locally identifiable in this case. This means that both voltage dependent time constants can be estimated at each voltage value, if the other parameters are known. This fact will be important later in the proposed parameter estimation method.

DOI:10.15774/PPKE.ITK.2010.005

3.5 Proposed parameter estimation algorithm for one HH type channel model under voltage clamp measurement conditions

In this section we propose a parameter estimation method based on the results of the identifiability analysis. The main idea of the method is based on the decomposition of the parameter estimation problem into two consequtive steps

1. estimation of conductance, activation and inactivation parameters from the steady-state current values of multiple voltage clamp traces,

2. estimation of the voltage dependent time constants based on the entire current response.

3.5.1 Estimation of conductance and activation parameters

As we have demonstrated in the previous section, there is a possible (but we have to confess that not probable) scenario when the parameters g, m_∞ and h_∞ may not be identified independently. We can avoid this problem by using multiple voltage steps, and the prior knowledge that the voltage dependence of the steady state values of activation and inactivation functions are described by Boltzmann-functions (see Eqs. (3.6) and (3.9)). However, as it is described in [165], the Boltzmann functions are only approximations of the steady state curves.

This implies that we proceed from the local estimation problem of g, m_∞ and h_∞ to the global estimation of g, $V_{1/2m}$, k_m, $V_{1/2h}$ and k_h, which parameters uniquely determine the values of m_∞ and h_∞ at each particular voltage step value. The assumption of the accessability of multiple voltage steps is absolutely realistic, and we can ensure the application of the information content of every single measured voltage trace this way, which implies further benefits form the point of view of noise reduction.

Furthermore, the numerical method proposed in [102] is based on the determination of the time and value of the maximal current during the voltage step measurement, but a local maxima does not necessary appear in every case (see Fig. 3.2).

According to these observations, our aim is to propose a method for parameter estimation, which ensures a reliable solution to the widest set of possible parameter values, and is numerically feasible at the same time.

In the first step of the method we will analyze only the steady state currents in the case of multiple voltage values. In this case the equation

$$I = g m_\infty h_\infty (V - E)$$

holds. The state variables will be equal to their steady state values, no dynamics appear. Implicitly, in this case we can only estimate g, $V_{1/2m}$, k_m, $V_{1/2h}$ and k_h from the (steady state) current at several voltage values, τ_m and τ_h do not appear in the equations. Of course, in the case of real measurements we can only access the

DOI:10.15774/PPKE.ITK.2010.005

approximate values of steady state currents, but we now assume that the voltage step is long enough to provide the necessary values.

In this case, the estimation problem will result in an algebraic solvability problem of a system of nonlinear equations. If we suppose n measurements at distinct voltage values, we get the following system of nonlinear equations. Assume that the values of the (steady-state) currents (I_i) in the case of multiple voltage values (V_i) are known. and these are equal to

$$I_i = gm_{\infty i}h_{\infty i}(V_i - E) \quad for \;\; i = 1 \; to \; n \tag{3.28}$$

where n is the number of traces, and where

$$m_{\infty i} = \left(1 + exp\left(\frac{V_{1/2m} - V_i}{k_m}\right)\right)^{-1} \qquad h_{\infty i} = \left(1 + exp\left(\frac{V_{1/2h} - V_i}{k_h}\right)\right)^{-1} \tag{3.29}$$

The unknown variables to be determined are g, $V_{1/2m}$, k_m, $V_{1/2h}$ and k_h. Furthermore we know that $k_m > 0$ and $k_h < 0$. As we have five parameters to estimate, at least 5 measurements are needed for the estimation.

Parameter estimation algorithm for g, $V_{1/2m}$, k_m, $V_{1/2h}$, k_h

In the case of more than 5 measurements, a least squares (LS) estimation procedure is possible. With this, we can use an optimization-based reformulation of the problem. Let us define the following objective function:

$$W_1(\hat{\theta})_{VC} = \sum_{i=1}^{n}(I_i - \hat{g}\hat{m}_{\infty}\hat{h}_{\infty}(V_i - E))^2 \tag{3.30}$$

where

$$\hat{m}_{\infty i} = \left(1 + exp\left(\frac{\hat{V}_{1/2m} - V_i}{\hat{k}_m}\right)\right)^{-1} \qquad \hat{h}_{\infty i} = \left(1 + exp\left(\frac{\hat{V}_{1/2h} - V_i}{\hat{k}_h}\right)\right)^{-1} \tag{3.31}$$

where $\hat{\theta}$ denotes the parameter vector of the objective function, including estimated parameter values $\hat{g}$, $\hat{V}_{1/2m}$, $\hat{k}_m$, $\hat{V}_{1/2h}$ and $\hat{k}_h$. The vector containing the real values of the parameters (the vector to be determined) is

$$\theta = arg \; min_{\hat{\theta}} W_1(\hat{\theta})_{VC}$$

For the optimization process we used the efficient, gradient-free Nelder-Mead simplex algorithm [123] to minimize the error.

Convergence properties of the Nelder-Mead simplex method for the estimation problem of g, $V_{1/2m}$, k_m, $V_{1/2h}$ and k_h

We analyzed the convergence of the optimization in the case of the parameters with the values $g = 67 \; nS$, $V_{1/2m} = -31.93 \; mV$, $K_m = 13.03$, $V_{1/2h} = -44.35 \; mV$ and $k_h = -5.14$.

DOI:10.15774/PPKE.ITK.2010.005

Simulation results showed that the convergence of the algorithm to the global optimum ($W_1(\theta)_{VC} = 0$) strongly depends on the number of voltage values (n). In the case of $n = 5$ voltage values, the algorithm can easily stuck in local minima, close to or far from the global solution, depending on the initial values of the parameters, and the values of the voltage steps. If we add further voltage values, the convexity properties of the problem seem to improve. The convergence properties of the algorithm may depend further on the exact values of the voltage steps.

The results show, that measurement data of steady state currents at multiple values makes the estimation of the parameters g, $V_{1/2m}$, k_m, $V_{1/2h}$, k_h possible with the proposed optimization method, if we assume an appropriate ($\pm 25\%$) initial guess of the parameters. Simulation experiments show that the number of the required voltage steps (n) is at least twice as much as the number of parameters to estimate (in this case 10). More voltage values, of course, may ensure the convergence to the global optimum, even in the case of worse initial guess of parameters, however $n > 12 - 14$ values are not very realistic. Furthermore we showed that the result of the estimation method can be sensitive to the distribution of the voltage values in the voltage range. The choice in which the voltage values equidistantly cover almost the entire range of activation and inactivation functions seems promising.

The proposed method is strongly based on steady-state currents, and as a consequence, it works only if there is a voltage interval present, in which both the steady state activation and inactivation variables are practically not equal to 0. If the intersection interval is narrow, a reasonable consideration would be to arrange the voltage steps in a way which provides high density of voltage values in the intersection interval. In this case the values of the steady state currents will be significantly lower, and convergence properties of the method can significantly deteriorated by measurement noise. However, without noise, the proposed method applied with 10 voltage steps ranging equidistantly from -80 to -8 mV successfully converged to the nominal parameters for e.g. in the case of activation/inactivation characteristics depicted in Fig. 3.3. Compared to other cases where the intersection is closer to the inflexion points, a one order higher number of iterations (few thousand evaluations) was needed to find the nominal parameters.

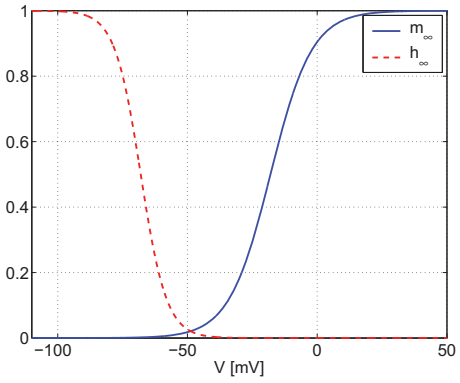

Figure 3.3: Activation and inactivation curves (m_∞ and h_∞), with narrow intersection (V-type curves)

DOI:10.15774/PPKE.ITK.2010.005

The nominal parameters (corresponding to Fig. 3.3) and the initial values for the optimization (±50%) are detailed in the Table 3.2.

Table 3.2: Nominal and initial parameters in the case of V-type characteristics

	g	$V_{1/2m}$	k_m	$V_{1/2h}$	k_h
Nominal	67	-18	8	-68	-5
Initial	83.75	-27	12	-102	-2.5

Discussion

Possible generalizations of the problem can be the addition of further ion channels of the same or different type, and the inclusion of different powers of activation and inactivation variables in the current equations. From an optimization point of view the inclusion of powers of activation and inactivation variables will lead to a mixed-integer nonlinear programming problem.

We have to note that the basic Nelder-Mead simplex algorithm does not handle constrains on the parameter values. In contrast, we have explicit constraints on the maximal conductance and the slope factor of the Boltzmann functions in our case, namely $g > 0$, $k_m > 0$ and $k_h < 0$. According to the simulation experiences, the simplex based optimization usually does not result in parameter values which violate these constraints. But if they do, one can easily identify the non correctness of the values, drop the result and start the optimization process from a different point in the parameter space.

A further alternative can be the usage of the freely available Asynchronous Parallel Pattern Search (APPS) algorithm [72], which can handle these linear constraints of the parameters, and can be easily parallelized. Moreover, the method can effectively handle noisy objective functions.

The optimization does not require high computational power due to the static nature of the problem. The optimization process took 10-15 s on a typical dual-core desktop PC.

3.5.2 Estimation of voltage dependent time constants

After the estimation of g and the parameters of the Boltzmann functions, our next task is to determine the time constants at the particular voltages defined by the applied voltage steps. In this case the global estimation of c_{bm}, c_{am}, V_{Maxm}, σ_m, c_{bh}, c_{ah}, V_{Maxh} and σ_h is also possible, but it is not needed, because the results of the identifiability analysis have shown that at a particular voltage value τ_m and τ_h are identifiable. On the other hand, if we perform a series of local estimations of τ_m and τ_h, we have to estimate only 2 parameters at the same time instead of 8. Thereafter, one can fit any kind of function (not only gaussian) on these time

DOI:10.15774/PPKE.ITK.2010.005

constants corresponding to the particular voltage values, which may also reduce the number of parameters in the resulting model.

According to the results of the previous sections, we assume that the values of g, $V_{1/2m}$, k_m, $V_{1/2h}$, k_h are known, and the parameters $\tau_m(V)$ and $\tau_h(V)$ at different voltages are left to estimate. For the identification of $\tau_m(V_i)$ and $\tau_h(V_i)$ at a certain voltage we can either use the method proposed in [102] considering the time constants as unknown parameters if a local maxima is present, or, similarly to the method described in [165], we can simply perform the minimization of the following objective function:

$$W_2(\hat{\theta})_{VC} = \frac{1}{N}\|I^m_{tot} - I^s_{tot}(\theta)\|_2 \tag{3.32}$$

where $\hat{\theta}$ is the parameter vector (including $\hat{\tau}_m(V_i)$ and $\hat{\tau}_h(V_i)$), N is the number of data points in the measurement record, and I^m_{out} and I^s_{out} denote the measured and model computed (simulated) total output current (as a discrete time sequence) and $\|.\|_2$ is the 2-norm. The state trajectories can be determined either by explicit by solving the differential equations (see Eq. 3.24) or by simulation.

Convergence properties of the Nelder-Mead simplex method for the time constants estimation problem

In this subsection we analyze the performance of the Nelder-Mead simplex method in case of minimizing the objective function described in Eq. (3.32). We perform this estimation for every voltage step ($i = 1, ..., n$). The optimization procedure can provide convergence to local minima also in this case. This problem can be handled via starting the optimization process from different initial parameter values, and neglecting the parameter values which result in a high value of the objective function.

The convergence to the global optimum (i.e. to the nominal parameters) depends on the value of the voltage steps, but in this case also on the holding potential. The holding potential had no role in the case of the estimation of g, $V_{1/2m}$, k_m, $V_{1/2h}$, k_h, because we only analyzed the values of the steady state currents. Now the input data of the parameter estimation process is the whole current trace, and the initial values of the activation and inactivation variables, which are determined by the holding potential (V_{hold}), have high impact on the result. The comparison of the results in the case of several voltage step protocols is depicted in Fig. 3.4. The parameters of the particular voltage protocols are described in Table 3.3, while the interpretation of protocol parameters is depicted in Fig. 3.5.

Discussion

According to the simulation results, the reason for the significant deviances of the inactivation time constant in the low voltage ranges is, that the holding potential and the value of the voltage step defined only a small change in the steady state value of the inactivation variable (see the relevant values in the range of -90 - -60 in Fig. 3.1). If we apply a holding potential value that differs more from the value of the voltage step (for example -20 mV as in the case of estimation 3), we get more reliable results in the lower voltage ranges.

DOI:10.15774/PPKE.ITK.2010.005

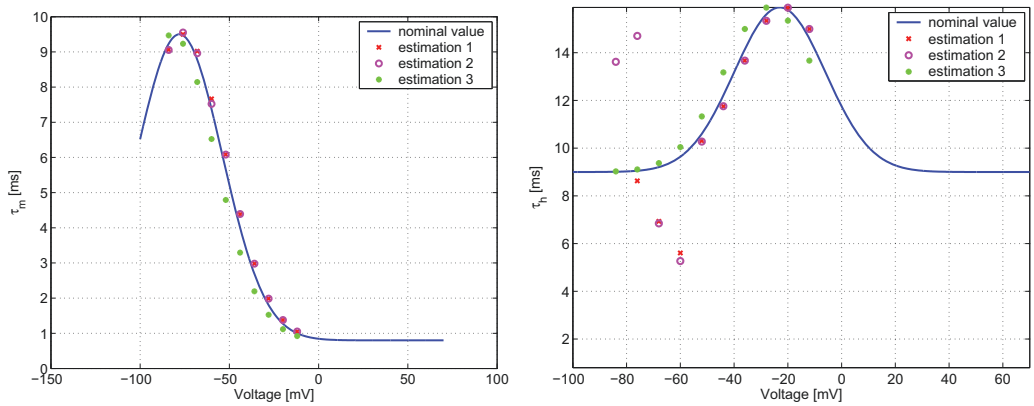

Figure 3.4: Results of the parameter estimation process for $\tau_m(V_i)$ and $\tau_h(V_i)$ at various voltage step protocols

Table 3.3: Different voltage step protocols for the estimation of τ_m and τ_h

	estimation 1	estimation 2	estimation 3
V_{hold} [mV]	-92	-68	-20
V_{base} [mV]	-94	-94	-88
$interval$ [mV]	8	8	8
$step_{num}$	10	10	10

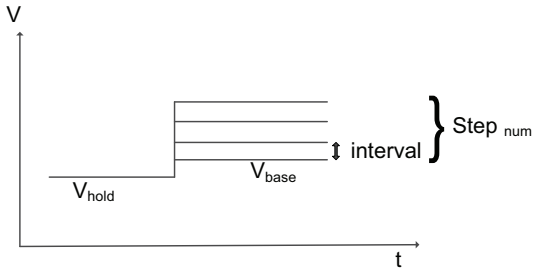

Figure 3.5: Interpretation of VC protocol parameters V_{hold}, V_{base}, $interval$ and $step_{num}$

In general it can be said, that the results are more reliable if the difference of the holding potential and the voltage step is large enough. This implies that if it is possible, it is worth to complete the voltage step protocol with both a lower, and a higher holding potential.

In addition, as it has been noted in section 3.5.2, if peak current occurs in the corresponding trace and the activation, inactivation and conductance parameters have been determined, the method proposed in [102] can be used to efficiently determine the time constants at particular voltage values. In this case the preliminary

DOI:10.15774/PPKE.ITK.2010.005

knowledge of m_∞ and h_∞ can further enhance the effectiveness of the algorithm proposed by Lee et. al [102].

Regarding the computational needs of this optimization problem, the estimation of τ_m and τ_h, it can be said, that in spite of the fact that the optimization is dynamic in this case, thanks to the low number of simultaneously estimated parameters (2 in this case), the running times are of similar order to the ones proposed in 3.5.1 by estimating g, $V_{1/2m}$, k_m, $V_{1/2h}$ and k_h.

3.6 Conclusions and future work

The identifiability properties of a simple HH type ion channel under voltage clamp measurement conditions have been analyzed in this chapter. It is shown that at constant voltage the parameters g m_∞ and h_∞ are interdependent. Based on the identifiability results, we have shown that in the case of a single voltage step, all these parameters may be theoretically impossible to determine at the same time.

We can circumvent this problem by using multiple voltage steps, and by utilizing the prior knowledge that the voltage dependence of the steady state values of activation and inactivation functions are described by Boltzmann-functions.

Furthermore, a parameter estimation method is proposed, which is based on the decomposition of the identification problem. The first step includes the estimation of the maximal conductance value and the activation/inactivation parameters from the values of steady state currents obtained from multiple voltage step traces. The second step of the parameter estimation problem focuses on the parameters of the voltage dependent time constants, and is also formulated as an optimization problem.

The analysis of the parameter estimation method showed that the following considerations have to be taken into account if we wish to use the proposed results for the design of voltage clamp protocols:

1. The voltage steps should be long enough to ensure that the activation and inactivation variables are able to (at least approximately) reach their steady state values.

2. At least 10 voltage steps are required for the safe estimation of the investigated 5 parameters corresponding to the activation, inactivation curves and conductance values.

3. To provide a reliable estimation of the time constants in the wide voltage range, the measurements have to be completed both with a higher and a lower holding potential.

One of the future perspectives is the generalization of the identifiability results and the parameter estimation process in two possible ways to get closer to the realistic cases. First, ion channel models can be considered, where the activation and inactivation variables appear at higher powers, and second, models with multiple types of ionic conductances can be analyzed, where the current of variable channels appear additively in the output equation. In addition, the identifiability analysis of

DOI:10.15774/PPKE.ITK.2010.005

the kinetic description of HH models (see e.g. [165]) would be a sound sequel of the work described in this chapter.

DOI:10.15774/PPKE.ITK.2010.005

Chapter 4

Hodgkin-Huxley modelling and parameter estimation of GNRH neuronal electrophysiology

In this chapter a simple, one compartment Hodgkin-Huxley type electrophysiological model of GnRH neurons is presented, that is able to reasonably reproduce the voltage clamp (VC) traces, and the most important qualitative features in the current clamp (CC) traces, such as *baseline potential*, *depolarization amplitudes*, *sub-baseline hyperpolarization* phenomenon and *average firing frequency* in response to excitatory current observed in GnRH neurons originating from hypothalamic slices.

The parameters of the model are estimated using averaged VC traces of multiple GnRH neurons, and characteristic values of measured current clamp traces. Regarding the resulting parameter values, in most of the cases a good agreement with literature data was found. The simplicity of the model allows its future integration as a building block into composite models that describe a few connected GNRH neurons.

Modification of model parameters makes the model capable of *bursting*, the effects of various parameters to burst length are analyzed.

4.1 The significance of GnRH neurons

As it is described in section 9.2, of Appendix A, central control of reproduction in vertebrates is governed by a neuronal pulse generator that controls the activity of hypothalamic neuroendocrine cells secreting Gonadotropin-releasing hormone (GnRH). The pulsatile release of GnRH, which is closely associated with concurrent increases in multiunit electrical activity in the mediobasal hypothalamus [87, 88, 164, 166, 28], is driven by the intrinsic activity of GnRH neurons, characterized by bursts and prolonged episodes of repetitive action potentials correlated with oscillatory increases in intracellular Ca^{2+} [29, 30].

In close relation with this, several in vitro experiments have shown that changes in cytosolic Ca^{2+} concentration determine the secretory pattern of GnRH [141], underlining that Ca^{2+} plays a central role in the signal transduction processes that lead to exocytosis. Furthermore, GnRH secretion from perifused GT1 and hypothalamic

DOI:10.15774/PPKE.ITK.2010.005

cells is reduced by L-type Ca^{2+} channel inhibitors and augmented by activation of voltage-gated Ca^{2+} channels [97].

The models of GnRH pulse generator, which can be found in the literature nowadays, use very simple generalized neuron models and networks. Furthermore, they are neither based on the known membrane properties of GnRH neurons, nor are able to describe the effect of gonadal hormones [21]. Nevertheless, these investigations can provide novel results about pulsatility and synchronization [54, 84].

As it has been stated, to increase the clinical relevance of neuroendocrine models, one has to use sub-models based on as up-to-date biological information as available. In the field of computational neuroendocrinology, in addition to GnRH related topics, good examples of this approach are the articles of Komendantov et al. [93] and Roper et al. [132], which address magnocellular neurosecretory cells.

The general aim of this chapter is to *construct a simple dynamic model of a GnRH neuron* that reproduces some of its characteristic properties (see section 4.2) and *the parameters of which can be determined from measurements*. This work is intended to be the first step of a bottom-up method towards the main purpose of building a hierarchical model of the GnRH pulse generator which also describes the effect of hormones secreted by the ovary, and is able to capture the main qualitative features of GnRH release in different phases of the ovarian cycle.

4.1.1 General electrophysiology and modelling of GnRH neurons

Sim et al. [138] have classified GnRH neurons in intact female adult mice as belonging to four distinct types. Herbison et al. [67] have characterized the basic membrane properties of GnRH neurons. As mentioned in the article [67], none of the GnRH neuron types seems to express specific electrophysiological 'fingerprint' in terms of the types of the expressed ion channels. However several recordings have demonstrated significant heterogeneity in the basic membrane properties of GnRH neurons [139, 142] which points to functional heterogeneity. Furthermore, the dynamics of GnRH neurons are affected by peripherial hormones including estradiol (E_2) [35, 118, 43, 66, 26, 121] and progesterone (P_4) [79, 23].

Based mainly on data collected from GT1 cells, which are basically GnRH neurons immortalized via targeted tumorigenesis, a couple of mathematical models [101, 155, 46, 103] have been proposed to explain some of the observed experimental results. These models focus mainly on the autocrine regulation by GnRH through adenylyl cyclase and calcium coupled pathways [65], which may contribute to burst formation [46]. The model described in [103] analyzes the control of bursting by calcium dependent potassium currents: small conductance (SK) currents described in [108], and a slow UCL-current.

However, the firing pattern of GT1 cells and that of the models published in these articles is qualitatively different compared to GFP-tagged GnRH neurons originating from hypothalamic slices. The depolarization, hyperpolarization amplitudes and the spontaneous firing frequency are much lower in the case of GT1 cells (compare e.g. the data published in [153, 154, 101, 155] and [138, 27, 35]). This implies that while these models can be appropriate for analyzing the mechanism of action cor-

DOI:10.15774/PPKE.ITK.2010.005

responding to GnRH and various drugs which act through Ca^{2+} coupled pathways, they may be inadequate when the aim is to describe the in vivo behavior of GnRH neurons and the GnRH pulse generator network. Furthermore these models do not include the A-type potassium current, which is shown to be present in GnRH neurons [100, 30, 138, 19, 67] and is affected by the ovarian hormone estradiol [35, 43], and thus may be a key regulator of neuronal activity during the ovarian cycle.

In order to fulfill the aim of electrophysiological model development, GFP-based whole-cell patch clamp recordings were carried out on mouse GnRH neurons (which were available by courtesy of S. Moenter, Univ. of Virginia, Charlottesville, VA, USA). The measurements were performed by Imre Farkas in the Laboratory of Endocrine Neurobiology, Institute of Experimental Medicine of the Hungarian Academy of Sciences. In the present work the obtained data are used to identify a Hodgkin-Huxley type conductance-based model [71] of membrane dynamics. The elements of the model (ionic conductances of specific types of ionic channels) are designed using literature data.

The outline of this chapter is as follows. In section 4.2 the required properties of the model are specified, in section 4.3 the measurement methods, mathematical modelling and parameter estimation are described. Section 4.4 summarizes the simulation results of the model. Conclusions are drawn in 4.5. The appendix D describes the details of the parameter estimation process.

4.2 Model specification

In this section the desired features of the model are defined, and the intended use of the model is explained.

4.2.1 Characteristic features to be described by the model

The above mentioned experimental observations indicate important characteristic features of GnRH neurons, which should be reproduced by the model. In particular, the following features are to be described by our model.

1. The model should qualitatively reproduce the typical *VC (voltage clamp) traces* of GnRH neurons originating from hypothalamic slices.

2. The model should be able to reproduce the shape of action potentials observed in GnRH neurons originating from hypothalamic slices. For details see the later detailed experimental results and for example the data published in [138, 27, 35], in particular *the high depolarization amplitudes and the characteristic sub-baseline hyperpolarization after the action potentials (APs).*

3. The model should exhibit similar *excitability properties* to the cells observed during the measurement process. This means that the same current injection which proved to be able to evoke APs during measurement should have the same effect on the model.

DOI:10.15774/PPKE.ITK.2010.005

4. The model should be capable of *bursting*. Bursting properties of this neuroendocrine cell have been described in several articles corresponding to GnRH neurons originating from hypothalamic slices [98, 142, 26] as well as in the case of GT1 cells [154, 24]. Based on the above articles, the duration of bursts in GnRH neurons have been found to range between 1 and 40 s with an average frequency about 10 Hz.

4.2.2 Intended use of the model

Several mathematical models can be found which aim at describing the hormone levels during the menstrual cycle [16, 57, 62, 61, 129]. The GnRH pulse generator in these models is taken into account (if it is taken into account at all) in a rather simplified way. A more detailed, neurophysiologically relevant model of the GnRH pulse generator network, would surely improve the significance of such models.

The model to be developed should be able to reproduce the dynamic properties of GnRH neurons relevant from the point of view of the female neuroendocrine cycle. Furthermore it should be used as an element of a neural network that responds to the ovarian hormone levels, and the excitation delivered by neighboring anatomical areas. A further intended aim of this network model will be to analyze the synchronization phenomena [38] between GnRH neurons.

4.3 Materials and Methods

The structure of the applied mathematical model together with the measurement results is briefly described in this section. The details of the measurement conditions can be found in Appendix D (section 12).

4.3.1 Mathematical model

The suggested model framework of single cell models

The model framework is proposed for a single compartment. The developed single compartment model can serve as a good basis for possible later research focusing on multicompartmental modelling.

Although the modelling of intracellular Ca^{2+} levels can unravel interesting interactions [64], at this first stage of model development we do not include the changes of intracellular Ca^{2+} concentration and calcium dependent currents in the model and, as a consequence, we assume a constant reversal potential of Ca^{2+}. This simplification can be accepted as long as we do not wish to take into account Ca^{2+} dependent currents and exocytosis, and the model provides reasonable results. In addition, possible model simulation results corresponding to intracellular Ca^{2+} levels could only be validated with Ca^{2+} imaging, which was not available during the measurements.

DOI:10.15774/PPKE.ITK.2010.005

Elements of the model

The elements of the model are presented in terms of ionic channels that are taken into account.

1. The presence of tetrodotoxin-sensitive *Na^+ currents* has been experimentally confirmed in the case of GT1 cells [19] and embryonic GnRH neurons [100]. Adult GnRH neurons were found to fire Na^+ dependent action potentials [138]. The sodium current in the model will be denoted by I_{Na}. We suppose third order activation and second order inactivation dynamics.

2. The presence of *A-type K^+ transient or rapidly activating/ inactivating conductance* has been described in the case of GT1 cells [19, 30], in embryonic cultures [100], and in GnRH neurons originating from mice [138, 67]. This current will be denoted by I_A in the model. This type of potassium current is quite widely studied in the literature even in the case of GnRH neurons [35], and on hypothalamic neurons in general [159, 112]. These results provide useful initial values for the parameters of this current. Furthermore, literature data indicated that the ovarian hormone estradiol modulates this current in mice GnRH neurons [35] and also in GT1 cells [43].

3. A voltage gated *delayed outward rectifier K^+ channel* can be assumed, which contributes to the more slowly activating, sustained component of the outward K^+ current (I_K) - see [100, 30, 138, 19, 67].

4. A *non-inactivating M-type K^+ current* (I_M) is also taken into account, which is considered a key modulator of neuronal activity in GnRH cells [172].

   As stated before, the main perspective of this modeling procedure is the description of GnRH release. Based on the results that underline the importance of calcium oscillations corresponding to hormone release [141, 97], we take into account 3 types of Ca^{2+} conductance to be able to describe the qualitatively different components of the calcium current.

   Furthermore, according to the results of Beurrier et al. [13], the interplay of different calcium currents can contribute to periodic bursting behavior which can be of high importance regarding neuroendocrine functions.

5. *Low voltage activated (LVA) T-type* Ca^{2+} conductance, which is activated in earlier phases of depolarization (I_T), has been described in the case of rat [80] and mouse GnRH neurons [67], as well as in GT1 cells [153]. The paper [175] proves that the expression of the T type calcium channels is estradiol dependent in hypothalamic GnRH neurons. As a result, during the preovulatory LH surge a much altered calcium conductance of the GnRH neurons will contribute to their action potential burst formation.

DOI:10.15774/PPKE.ITK.2010.005

6. Furthermore, based on the results of Watanabe et al. [160] related to GT1-7 cells, and in vitro experiments [80, 125], we assume a *high voltage gated (HVA) Ca^{2+} channel* representing *R and N type conductances* (I_R)

7. In addition, a *HVA long-lasting current (L-type) Ca^{2+} channel* is modelled (I_L) - see the articles [97, 125] for in vitro results and [153] for GT1 measurements.

8. Lastly, two *leakage currents* corresponding to *sodium* (I_{leakNa}) and *potassium* (I_{leakK}) with constant conductance are taken into account.

Several other ionic currents have been shown to appear in GnRH neurons, for example the $I_{Q/H}$ current [138], Ca^{2+} activated potassium currents [27, 46], which are not considered in the model. The reason for this is that the further (especially Ca^{2+} dependent) currents would significantly increase the model complexity, which would lead to a significantly harder solvability of the parameter estimation problem. Furthermore these currents turned out to be nonessential for the reproduction of the features determined in section 4.2.1. After a simple model has been identified it can easily be extended with the currents omitted in the first step of the modelling process.

Model Equations

The **equivalent electric circuit** of a one-compartment GnRH neuron model with all the above conductances is shown in Fig, 4.1.

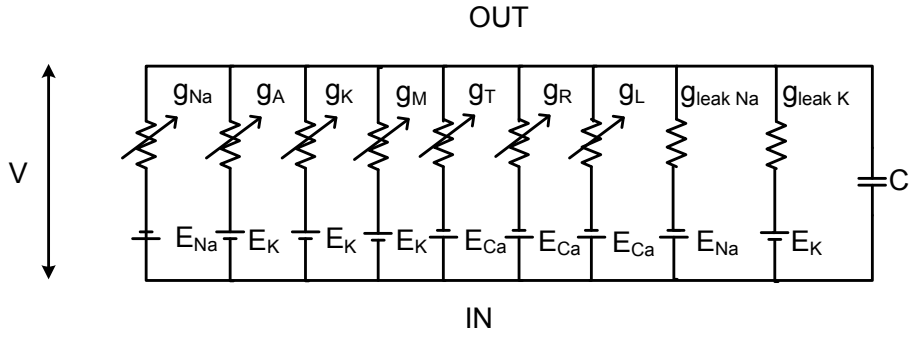

Figure 4.1: Parallel conductance model, with conductances representing different ion channels in voltage dependent and independent manner. g_{Na} denotes the sodium conductance, g_A, g_K and g_M denote the A-type, delayed rectifier and M-type potassium conductances, g_T, g_R and g_L stand for the conductances related to T-type LVA and the R and L-type HVA calcium currents, g_{leakNa} and g_{leakK} correspond to the voltage independent leakage currents.

The HH type model depicted in Fig, 4.1 can be described by the following equa-

DOI:10.15774/PPKE.ITK.2010.005

tions:

$$\frac{dV}{dt} = -\frac{1}{C}(I_{Na} + I_A + I_K + I_M + I_T + I_R + I_L + I_{leakNa} + I_{leakK}) + \frac{1}{C}I_{ex} \quad (4.1)$$

$$\frac{dm_i}{dt} = (m_{i\infty} - m_i)/\tau_{mi}, \quad \frac{dh_i}{dt} = (h_{i\infty} - h_i)/\tau_{hi} \quad (4.2)$$

where V is the the membrane voltage, C is the membrane capacitance, I_{Na} denotes the sodium current, I_A, I_K and I_M denote the A-type, delayed rectifier and M-type potassium currents, I_T, I_R and I_L stand for the T-type LVA and the R and L-type HVA calcium currents, I_{leakNa} and I_{leakK} for the leakage currents. The m_i and h_i variables are the activation and inactivation variables of the corresponding currents. $m_{i\infty}, h_{i\infty}$ and $\tau_{mi/hi}$ denote the steady-state activation and inactivation functions, and the voltage dependent time constants of activation and inactivation variables, which are nonlinear Boltzmann and Gauss -like functions of the membrane potential:

$$a_{\infty i} = \frac{1}{1 + e^{\frac{V_{1/2_{ai}} - V}{K_{ai}}}}$$

$$a \in \{m, h\}, \qquad i \in \{Na, A, K, M, T, R, L\}, \; K_{mi} > 0, K_{hi} < 0 \;\; \forall i$$

$$\tau_{ai} = C_{base_{ai}} + C_{amp_{ai}} \, e^{\frac{-(V_{max_{ai}} - V)^2}{\sigma_{ai}^2}} \quad (4.3)$$

The M-type current has only activation dynamics.

Finally, I_{ex} refers to the external injected current. The currents of ionic channels are given by

$$\begin{aligned} I_{Na} &= \bar{g}_{Na} m_{Na}^3 h_{Na}^2 (V - E_{Na}), \quad I_A = \bar{g}_A m_A^2 h_A^2 (V - E_K) \\ I_K &= \bar{g}_K m_K h_K (V - E_K), \quad I_M = \bar{g}_M m_K (V - E_K) \\ I_T &= \bar{g}_T m_T h_T (V - E_{Ca}), \quad I_R = \bar{g}_R m_R^2 h_R (V - E_{Ca}) \\ I_L &= \bar{g}_L m_L^2 h_L (V - E_{Ca}) \\ I_{leakNa} &= \bar{g}_{leakNa} (V - E_{Na}), \quad I_{leakK} = \bar{g}_{leakK} (V - E_K) \end{aligned} \quad (4.4)$$

where the E_{Na}, E_K, E_{Ca} denote the reversal potentials of the corresponding ions.

4.3.2 Measurement results

Overall 5 cells have been investigated by performing voltage clamp (VC) and current clamp (CC) measurements.

Voltage clamp

VC traces without prepulse have been recorded in the case of all cells, and voltage clamp recordings with prepulse have been completed in the case of one cell (No. 2). Some typical traces of the averaged VC results are depicted in Fig. 4.2. A more exhaustive depiction of averaged VC traces can be found in the results section (4.4.1), where they are compared with model simulation results.

DOI:10.15774/PPKE.ITK.2010.005

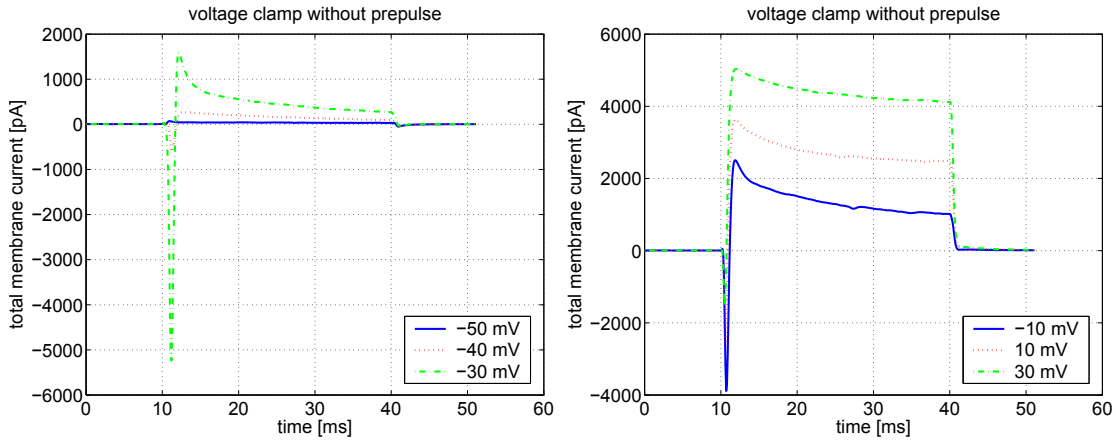

Figure 4.2: Measured voltage clamp (VC) traces without prepulse averaged for 5 cells in the lower and higher voltage ranges. The holding potential was -70 mV, the voltage step was applied from 10 to 40 ms.

In Fig. 4.2 it can be seen, that as the value of the clamping voltage step increases, the amplitude of the inward current decreases distinctly. This can be either related to the inactivation of sodium current, or rather to the overlapping of sodium and fast potassium currents, which are more active at higher voltages. As it can be seen in Fig. 4.2, the inward current related to sodium current appears suddenly in the range of -20, -40 mV - which indicates a steep slope in the activation dynamics of the sodium current. Furthermore the fast decrease after the positive local maxima suggests fast inactivation dynamics of the A-type potassium current and higher powers of the inactivation variable corresponding to this conductance.

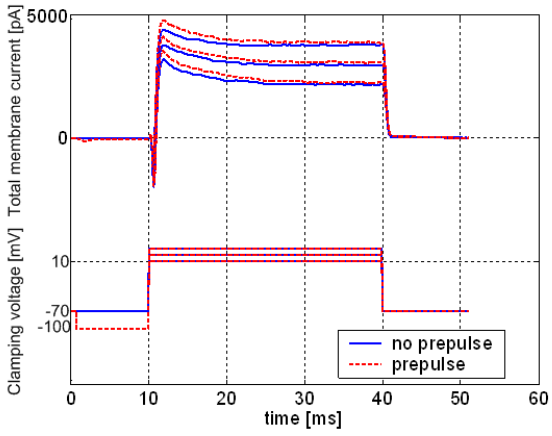

Figure 4.3: Comparison of VC traces (step to 10 20 30mV from -70 mV) without and with prepulse in the case of cell No.2. The prepulse facilitates the recovery from inactivation in the case of the fast A-type potassium current, and also influences slower currents. Down: Voltage clamp waveforms

DOI:10.15774/PPKE.ITK.2010.005

Fig. 4.3 clearly indicates that the application of prepulse facilitates the recovery of the inactivation variable of the fast A-type current and increases it's amplitude. It is worth to observe that the application of prepulse also moderately affects the sustained component of the outward current. Since measurement data of several cells were available, but VC traces with prepulse were not recorded in all of the cases, the averaged VC traces without prepulse were used as basis for parameter estimation procedure. Voltage clamp traces with prepulse were used to validate the resulting model, by comparison of the measured and simulated effects of prepulse to VC traces.

Current clamp

Regarding the current clamp (CC) measurements, various amplitude depolarizing injected current steps were needed to elevate APs. The 30 pA traces of the cells are depicted in Fig. 4.4.

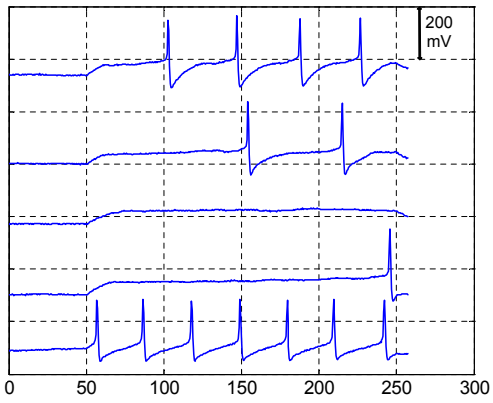

Figure 4.4: The 30 pA current clamp (CC) traces of the cells 1-5 (from up to down). The resting potential values of the cells were: -71, -69.2, -73, -79, and -53 mV.

4.3.3 Parameter estimation of the GnRH neuronal model

The parameter estimation problem of neuronal models is a widely studied area in neuroscience literature. The diversity of models, however, implies a broad range of approaches and solutions that are sometimes difficult to apply for other type of neurons or estimation tasks.

In addition, regarding membrane properties, GnRH neurons form a heterogenous population [138], which implies that cells with different functionality may be described by models with significantly different parameters.

The basic articles, which describe the parameter estimation of Hodgkin-Huxley type models have been published by Tabak et al. [145] and Willms et al. [165]. The article of Lee et al. [102] analyzes the effect of simplifying assumptions on the results of parameter estimation, and provides a promising problem-reformulation

DOI:10.15774/PPKE.ITK.2010.005

based numerical method in the case of VC measurements. Haufler et al. [63] describe a synchronization-based method based on CC measurements. The very interesting paper of Tien et al. [148] focuses on bursting neural models and uses a geometric approach. The paper [74] provides a statistical method for the parameter estimation of multicompartmental models. Despite the above valuable work, however, there is a lack of mathematically and algorithmically well founded parameter estimation method for neuronal models, that is able to take into account both the qualitative and quantitative aspects of measured data.

The method proposed in section 3.5 can not be used in this case. The primary reason for this is, that the solvability properties of the algebraic equations described in Section 3.5.1 significantly deteriorate with such an increase in the number of ionic channels. At second, the available voltage steps in the measurement results are not long enough to provide reasonable values of steady-state currents.

The basic membrane dynamics-model is considered to be acceptable, if it approximates available measurement data qualitatively and quantitatively well. This observation is used later on to formulate an appropriate objective function for the parameter estimation. Furthermore we require that the model parameters reproduce values known from the literature in a satisfactory manner.

In the following we describe the parameter estimation process in the case of our model.

The **estimated parameters** were the membrane capacitance C in (4.1), the maximal conductances $\bar{g}_i$ where $i \in \{Na, A, K, M, T, R, L, leakNa, leakK\}$, in Eqs (4.4), and the activation/inactivation parameters $V_{1/2_{ai}}, K_{ai}, C_{base_{ai}}, C_{amp_{ai}}, \sigma_{ai}, V_{max_{ai}}$ in (4.3). This, all together, means 88 parameters.

The algorithmic part of the parameter estimation procedure minimizes an objective function that is a function of the parameters to be estimated, i.e. an optimization-based estimation procedure is used [72]. A multistep recursive parameter estimation approach has been applied that combines standard optimization based steps with physical qualitative considerations. The objective functions and the algorithm for parameter estimation can be found in section 13.1 of Appendix E.

It is important to note, however, that the algorithmic parameter estimation method had to be completed with heuristic elements, that are based on the prior qualitative knowledge on the system. The main aim of these steps was to avoid local minimum points of the objective functions and to reproduce those qualitative features of the model behavior, which inhibit significant physiological importance, and, according to our observations, can not be captured well by the numerical optimization methods. These features were the sharp action potentials and partially the significant hyperpolarizations after the APs.

The parameter estimation was carried out using the data averaged for all the 5 cells. The voltage clamp traces could be interpreted without any problem, and the 2-norm based optimization could be applied for the averaged traces. To increase the validity of the model, our approach was to take both voltage and current clamp traces into account during parameter estimation. Current clamp (CC) traces in this case were taken into account in the way, that the model should have had similar firing properties as the average cell population - see Fig. 4.3. This meant, that the average number of APs, and the average depolarization and hyperpolarization values

DOI:10.15774/PPKE.ITK.2010.005

of the recorded CC traces in response to 30pA excitatory current were compared to model simulation. The value of 30pA was chosen, because this CC trace was available in the case of all the cells, and in response to this current 4 of the 5 cells fired action potentials.

Initial values for the optimization

Before applying the optimization algorithm, intuitive rough-tuning of the activation/inactivation parameters (parameters of the Boltzmann and Gauss functions) and conductance values was performed to capture some important features of the neural behavior. This way we achieved that the model qualitatively matched the VC traces in the whole analyzed voltage range. In addition, the sign of the currents, the appearance and approximate time of local maximum in the simulations matched measurement results, too. Furthermore, the proper choice of initial parameter values ensured that model is able to fire action potentials in response to exciting current about 30 pA.

This preparation proved to be necessary for convergence to an acceptable optimum. This initialization step demands significant knowledge of the model and of the measured data, but can not be avoided because the model has a very complex bifurcation structure and therefore can undergo large sudden qualitative changes in its response to identical input by changing slightly the parameters. This suggests a very small attracting region in the parameter space around the optimum.

The above laborious rough tuning procedure was mainly based on qualitative considerations. In addition to the assumptions which provided an acceptable reproduction of the VC traces in wide voltage range (especially at low voltage values), the intuitive initialization of activation parameters was based on decomposition of the CC trace. The considered parts of the CC trace are shown in Fig 4.5. From different parts of the CC trace, the initial values of different parameters were roughly estimated as follows.

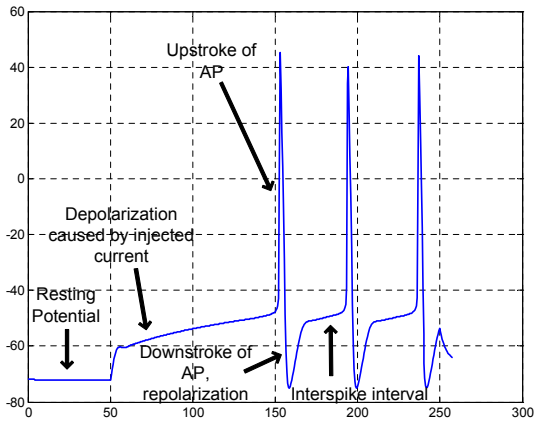

Figure 4.5: Membrane potential during CC (30 pA) - model simulation. The number and shape of APs show good agreement with measurement results.

DOI:10.15774/PPKE.ITK.2010.005

1. Our simulation studies show that the *resting potential* is mainly determined by the potassium and the low threshold Ca (g_T) conductances, their steady-state parameters (m_∞, h_∞) and the leak conductances.

2. *Injected current-induced depolarization* is dominantly influenced by the 3 potassium currents, the T-type calcium current, and in minor part by the leak currents.

3. *Upstroke of AP* is influenced by Na and R and L-type Ca currents.

4. *Downstroke of AP* and hyperpolarization is determined mainly by K^+ currents, especially by the recovery of A-type current from inactivation.

5. Finally the *interspike intervals* are influenced by delayed rectifier and M-type potassium currents, low threshold T-type calcium and partially by A-type potassium and leak currents.

The determination of suitable initial values was decomposed into two phases. First, the activation parameters were chosen based on intuitive tuning of literature data, then the maximal channel conductances were determined from VC and CC data.

4.4 Results and Discussion

As a result of an iterative process of heuristic and numerical optimization steps, a parameter set was found, which was able to provide a good fit of VC traces, and produced the observed and desired firing properties defined in 4.2.1 at the same time. Reproduction of both voltage and current clamp traces by neuronal models is not prevalent in literature. The estimated model parameters can be found in Appendix D (section 13.3.1).

An other set of parameter values described in 13.3.2 was used to reproduce bursting and analyze some of the bursting properties of the model. Bursting is detailed in subsection 4.4.3.

If we compare the results with literature data, we can make the following observations.

- The activation and inactivation curves of the A-type K^+ current in the model show reasonable agreement with the results published by [35]. Furthermore, the voltage-dependence characteristics of the activation time constant of τ_{mA} of I_A in higher voltage ranges (above 0 mV) are in good agreement with the results of Luther et al. [112] regarding hypothalamic cells. In the lower voltage ranges the activation time constant published in [112] exceeds the one of the model by 1-4 ms. The inactivation time constants of the model show significant difference (20-30 ms) in the lower voltage ranges (about -40 mV) compared to this work.

- The activation and inactivation curves of R-type Ca^{2+} current are in good agreement with the results of Kato et al. [80]. The amplitude of Ca^{2+} currents

DOI:10.15774/PPKE.ITK.2010.005

in the case of VC simulations is similar compared to measurement results of the article [80].

- The characteristics of the T-type LVA Ca^{2+} current are in good agreement with the results of [146].

4.4.1 Voltage clamp results

In Fig. 4.6 the comparison of the averaged VC traces and the model simulations can be seen. The holding potential was -70 mV.

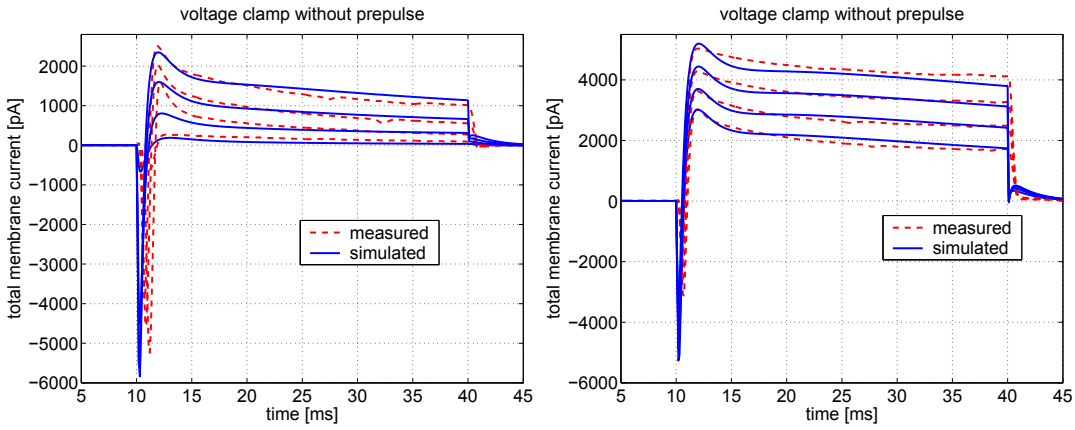

Figure 4.6: Measured and simulated VC traces corresponding to voltage steps of -40 -30 -20 and -10 mV and to voltage steps of 0 10 and 20 mV.

As it can be seen in Fig. 4.6, the model performs better in the medium and high voltage ranges. The steady-state and pre-steady state currents are well fit, and the dynamics of the transient currents are quite reasonably captured in the case of approximately half of the traces. Furthermore, in some cases, after the end of the voltage step, at 40 ms, significant tail currents appear in the simulations, which are not confirmed by measurement results.

Effect of prepulse

Because VC measurements with prepulse were not available for all of the cells, the prepulse VC data were not used for the parameter estimation process. Instead, these measurements were used for model validation. In Fig. 4.7, where the prepulse response of the model is depicted, it can be seen that the effect of prepulse on the model, is qualitatively the same as observed in the case of cell 2 depicted in Fig 4.3: it moderately enhances the recovery of the A-type current, and in general it increases the amplitude of the outward K^+ current. Furthermore the quantitative degree of the increase is approximately the same as observed in measurements.

DOI:10.15774/PPKE.ITK.2010.005

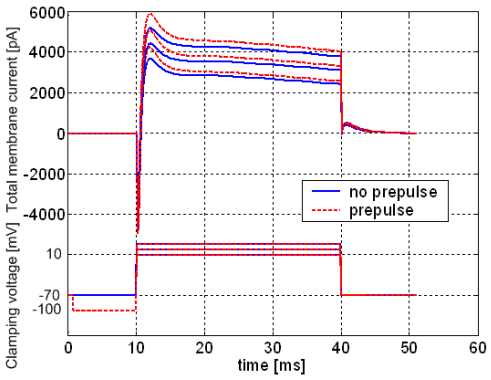

Figure 4.7: Simulated VC traces with and without prepulse in the case of 10, 20, 30 mV voltage steps. Down: voltage clamp waveforms.

4.4.2 Current clamp results

It should be noted that the model parameters were estimated using both VC and CC traces, while CC measurements were only available for one current step value (30 pA). The simulated CC trace in response to a 30 pA current step is depicted in Fig. 4.5. In contrast to the VC traces where the simulated responses were compared to the average measured responses, in the case of CC only the characteristic features of the measured and simulated CC traces were compared. The characteristic values (number of APs, depolarization and hyperpolarization values) of the simulated CC trace are compared with the average values corresponding to the measured CC traces (depicted in Fig. 4.4) in Table 1.

Table 4.1: Average characteristic values of measured and simulated CC traces, in response to 30 pA: resting potential (RP) in mV, number of APs (APs), depolarization value (DP) in mV, hyperpolarization value (HP) in mV.

	RP	APs	DP	HP
measured	-69.05	2.8	43.25	-86.75
simulated	-72.1	3	42.93	-75.03

The results show that the model can reasonably capture the excitability properties of the GnRH neuron in this case of injected current. The resting potential, the number of APs, the average depolarization amplitude, and the average time between the APs in the simulation results show also good agreement with measurement data.

On the other hand, while the model reproduces the characteristic sub-baseline hyperpolarization, it can not describe the hyperpolarization amplitudes well. The reason for this may be the lack of Ca^{2+} activated K^+ channels, however it is stated in [155] that $[Ca^{2+}]_i$ levels reached during spontaneous AP firing are not sufficient to activate large and small conductance Ca^{2+}-activated K^+ channels. In the case

DOI:10.15774/PPKE.ITK.2010.005

of bursting these channels could possibly improve the description of sub baseline hyperpolarization.

The simulations also showed, that hyperpolarization is determined dominantly by the delayed rectifier K-type and non-inactivating M-type K^+ currents, and by the recovery of A-type K^+ current from inactivation. Furthermore the deactivation and inactivation of high voltage activated Ca^{2+} currents, as well as that of the Na^+ current turned out to be essential for the sub-baseline hyperpolarization. The higher powers of the activation variables of fast Ca^{2+} currents - similar to the model published by Fletcher et al. [46] - facilitates this fast deactivation.

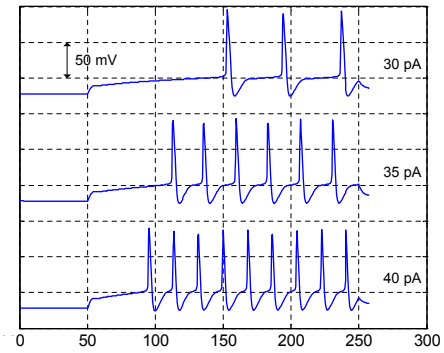

Figure 4.8: Simulated CC traces in the case of various amplitude injected currents. The current injection starts at 50 ms and ends at 250 ms. The model reproduces the increase in firing frequency in response to the increase in injected current. The resting potential is about -72mV.

Furthermore, as one increases the injected current in the simulations, the firing frequency increases (see Fig. 4.8), as it could be observed in CC measurements.

4.4.3 Bursting properties of the model

As it is described in [29, 30, 103], bursts and prolonged episodes of repetitive action potentials contribute to oscillatory increases in intracellular Ca^{2+}, which determine the secretory pattern of GnRH [141]. According to [153] and [156], which describe results corresponding to cultured cells, the burst formation ability of GnRH neurons is relevant also in the case of individual cells, not connected in a neuronal network.

Several results support the hypothesis, that bursts in GnRH neurons are connected with depolarizing afterpotentials (DAPs) [98]. The results of Chu et al. [27] show that these slow DAPs are connected with TTX dependent sodium conductances.

As it has been described in section 4.2.1, our aim was to create a model which is able to describe bursting. The resting potential of the basic model, which showed no bursting properties, was about -70 mV as depicted in Fig. 4.5. As described by Suter et al. [142], the average resting potential of GnRH neurons that generated bursts was about -60 mV. This data served as a basic guideline in the task of parameter

DOI:10.15774/PPKE.ITK.2010.005

modification to achieve bursting. The basic parameter set of the bursting model is described in Tables 13.3 and 13.4 in section 13.3.2 of Appendix D. In the simulations a 2 ms wide 100 pA pulse was applied at 50 ms to evoke bursting. The simulation result of the basic bursting model is depicted as the first trace in Fig. 4.10.

Furthermore we have to note, that the average firing frequency in the burst simulations ranged from 33 to 40 Hz, which is higher compared to the burst frequency described in [142] and [98]. In general it can be stated that the bursting of the model is quite sensitive to parametric changes, and bursting can be easily terminated or turned into a continual firing pattern.

Dependence on T-type Ca^{2+} current

The sodium conductance of the model is not able to reproduce 400-600 ms DAPs as described in [98] according to the observed simulation results. However, the T-type Ca^{2+} current in the model, which inhibits slow deactivation features, and interacts with the A-type current during after-hyperpolarization, can produce short depolarizing oscillations following the APs, which can serve as basis for bursting.

Reducing the maximal conductance of this current can cause the abrupt termination of bursting, as depicted in Fig. 4.9. These simulation results indicate that the model predicts a possible mechanism of bursting, which is based on T-type Ca^{2+} currents. This hypothesis of course requires further experiments for validation.

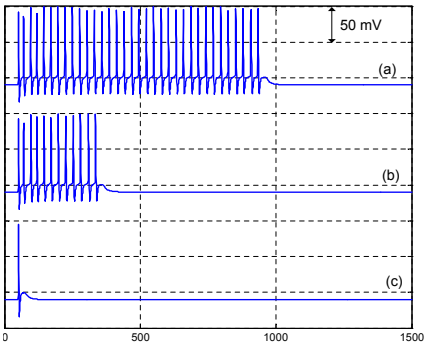

Figure 4.9: Reducing the T-type Ca^{2+} current ($\bar{g}_T$ = 10.79 nS) leads to the shortening of burst length (b) compared to basic burst simulation (a) ($\bar{g}_T$ = 10.8 nS). Further reduction of $\bar{g}_T$ (10.2 nS) leads to the termination of bursting (c). The depolarizing wave after the AP can still be observed in this case. The baseline potential was about -60 mV

Influence of the Ca^{2+} currents on the length of burst

Model simulations show that not only T-type, but other Ca^{2+} currents influence the bursting behavior. If we decrease the R-type Ca^{2+} conductance of the model by 0.02 nS, the length of the burst decreases (compared to the first trace of Fig. 4.9),

DOI:10.15774/PPKE.ITK.2010.005

as it can be seen in the first trace in Figure 4.10. Increasing this conductance (by 0.01 nS) implies an opposite effect, as depicted in the second trace of Fig. 4.10.

The L-type Ca^{2+} conductance affects bursting in the opposite way. If the conductance is decreased the length of the burst increases, and vice versa.

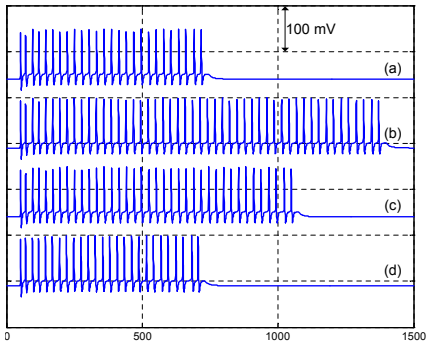

Figure 4.10: The R-type Ca^{2+} conductance enhances the burst length: (a) $\bar{g}_R = 10.83nS$, (b) $\bar{g}_R = 10.86nS$. The L-type conductance shows an opposite effect: If the conductance is decreased ($\bar{g}_L = 13nS$), the burst length increases (c), and if the conductance is increased ($\bar{g}_L = 15nS$) , the burst length decreases (d).

The modulating effect of the L-type Ca^{2+} current in the model simulations is an interesting result, which can be the subject of further simulation and experimental studies.

Influence of the K^+ currents on the length of burst

Farkas et al. [43] analyzed the effect of estrogen in the case of GT1 cells, and found that estrogen modulates (increases) the expression of the Kv4.2 subunit, which contributes to the function of the A-type K^+ channels. This might be interpreted as an increase in the parameter $\bar{g}_A$. We can see in Fig. 4.11 that the maximal conductance of the fast A-type K^+ current is able to control the length of the bursts in the case of this parametrization. In the case of trace (a) , $\bar{g}_A$ was increased to $375.1nS$, which reduced the burst length, compared to the reference case shown in (a) of Fig. 4.9.

DeFazio et al. [35] described that estradiol strongly influences the excitability of GnRH neurons in the case of ovariectomized mice. This article also describes that estrogen significantly affects the inactivation characteristics of A-type K^+ current, by depolarizing the voltage at which the current inactivates. The activation curve is also affected but in a less serious fashion.

With the proposed model one is able to test whether the increased cell excitability (which should lead to increased bursting activity) can be caused by these effects of estrogen on activation curves of the A K^+ current. In trace (b) of Fig. 4.11 we can see, that shifting the activation curve of the A-type K^+ current to the left (by decreasing the $V_{1/2}$ parameter of the steady state curve by 0.02 mV) decreases the length of the burst. Trace (c) depicts that increasing the $V_{1/2}$ parameter of the

DOI:10.15774/PPKE.ITK.2010.005

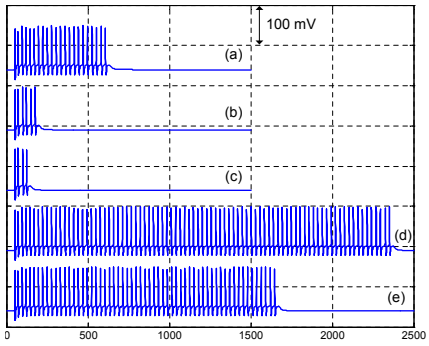

Figure 4.11: (a) increase of $\bar{g}_A$ from 375 to 375.1 nS reduces the burst length. (b) change of $V_{1/2}$ of m_∞ of the A-type current to -33.22 from -33.2 and increasing the $V_{1/2}$ parameter of h_∞ curve (c) from -61.5 mV to -61.47 mV acts in a similar fashion. (d) Decrease of $V_{1/2}$ of h_∞ of the A-type to -61.501 significantly increases the length of the burst. (e) Modulation by M-type current: The reduction of $\bar{g}_M$ from 4.7 mS to 4.69 mS increases burst length.

inactivation curve by 0.03 mV has similar effects. In contrast, decreasing the $V_{1/2}$ parameter of the inactivation curve of I_A can lead to significant increase in burst length (trace (d) in Fig. 4.11).

It is likely that the combination of multiple effects of estrogen is necessary to increase cell excitability, and this complex effect can not be captured by manipulating single parameters of the model. For example the results of Farkas et al. [43] indicate that estrogen also affects the K-type potassium current.

Finally, the effect of M-type K^+ current was analyzed. Decreasing the M-type conductance also increases burst length, as expected (see trace (e) in Fig. 4.11).

In fact, further in silico, in vitro and in vivo experiments are necessary for the reasonable description of estrogen effect on GnRH cell electrophysiology.

4.5 Conclusions and future work

As the first step of a bottom-up procedure to build a hierarchical model of the GnRH pulse generator, a simple one compartment Hodgkin-Huxley type electrophysiological model of the GnRH neuron was constructed. The parameters of the model were estimated using both VC and CC data originating from cells in hypothalamic slices. The initial values of parameter estimation were determined using literature data and qualitative biological knowledge. The parameter estimation process itself was carried out as a combination of algorithmic (APPS) and manual methods to reproduce the voltage clamp traces and firing pattern observed in the measurement data.

The resulting parameter set provides a good fit in terms of the qualitative features of neuronal behavior (resting potential, excitability, depolarization amplitudes, sub-baseline hyperpolarizations), and an acceptable numerical fit of VC measurement

DOI:10.15774/PPKE.ITK.2010.005

results. Further measurements are planned with specific channel blockers, that would help in further tuning or even re-parametrization of the model.

Applying parametric changes, which lead to the increase of baseline potential and enhance cell excitability, the model becomes capable of bursting. The properties of bursting behavior could be of high impact regarding physiological functions corresponding to hormone release. The bursts experienced in model simulations are dependent on Ca^{2+} currents, and are strongly affected by the parameters of the A-type K^+ current. Further experiments are necessary to test whether this type of bursting can really appear in GnRH neurons, or this phenomenon is an artificial in silico secondary product of the model.

The resulting model may be used as reference in the development of future models for the GnRH neuron. As soon as an appropriate Hodgkin-Huxley type model of membrane dynamics has been identified and validated, it will be completed with further elements influencing intracellular Ca^{2+} dynamics (models of intracellular compartments such as the endoplasmic reticulum, Ca buffers [136], and IP_3 signaling [173, 149]), which probably exert an important impact on hormone release.

Additionally, the model will be extended to take the complex effects of estradiol on the dynamics of membrane potential into account [26].

In addition to improve the one-cell model, a further aim is to describe the GnRH pulse generator network of the hypothalamus. The novel results of Campbell et al. regarding dendro-denritic bundling and shared synapses between GnRH neurons [22] may serve as a good basis for such work, providing information about the structure and possible interaction mechanisms between GnRH neurons.

DOI:10.15774/PPKE.ITK.2010.005

Chapter 5

Summary

In this chapter, the main results of the thesis are summarized.

ODE models of intracellular signaling pathways: rapid and slow transmission (Chapter 2)

A simplified dynamic model has been developed for the description of the dynamic behavior of G protein signaling, which takes into account the effect of slow (β-arrestin coupled) transmission, RGS mediated feedback regulation and ERK-phosphatase mediated feedback regulation. The parameters of the model have been determined via numerical optimization.

It has been shown, that the proposed reaction kinetic model of the system gives rise to an acceptable qualitative approximation of the G protein dependent and independent ERK activation dynamics that is in good agreement with the experimentally observed behavior.

Identifiability analysis of Hodgkin-Huxley type neuronal models (Chapter 3)

Identifiability properties of a single Hodgkin-Huxley type voltage dependent ion channel model have been analyzed under voltage clamp circumstances. With formal identifiability analysis, it was shown that even in the simplest case when only the conductance and the steady state activation and inactivation parameters are to be estimated, no identifiable pair from the three can be chosen.

In addition, a possible novel identification method was proposed, which is based on the decomposition of the parameter estimation problem in two parts. The first part includes the estimation of the maximal conductance value and the activation/inactivation parameters from the values of steady state currents obtained from multiple voltage step traces. The use of steady state currents allows the estimation of the first parameter group independently of the other parameters. This parameter estimation problem results in a system of nonlinear algebraic equations, which was solved as an optimization problem.

The second part of the parameter estimation problem focuses on the parameters of the voltage dependent time constants, and is also formulated as an optimization problem. The parameter estimation method is demonstrated on

DOI:10.15774/PPKE.ITK.2010.005

in silico data, and the optimization process was carried out using the Nelder-Mead simplex algorithm in both cases.

The results of the analysis were used to formulate explicit criteria for the design of voltage clamp protocols.

Hodgkin-Huxley modelling of GnRH neuronal electrophysiology (Chapter 4)

A simple, one compartment Hodgkin-Huxley type electrophysiological model of GnRH neurons has been presented, that is able to reasonably reproduce the voltage clamp traces, and the most important qualitative features in the current clamp traces in the same time. The corresponding qualitative features of the current clamp trace were baseline potential, depolarization amplitudes, sub-baseline hyperpolarization phenomenon and average firing frequency in response to excitatory current. These features were observed in GnRH neurons originating from hypothalamic slices.

The parameters of the model have been estimated using averaged VC traces of multiple GnRH neurons, and characteristic values of measured current clamp traces. Regarding the resulting parameter values, in most of the cases a good agreement with literature data was found.

Modification of model parameters makes the model capable of bursting, the effects of various parameters to burst length have been analyzed.

DOI:10.15774/PPKE.ITK.2010.005

Chapter 6

Possible application area of the results and future work

Because the results and conclusions of the described work are summarized at the end of each chapter in dedicated sections, this Chapter of the thesis reviews the results from the point of view of practical applicability, and describes some future perspectives of the work done.

6.1 Possible application area of the results

In several disorders of reproductive system (which can be caused for eg. by polycystic ovary syndrome [5], long lasting usage of hormonal contraceptives, etc.), the hormonal cycle is disturbed, or it can even disappear. In these cases, to restore fertility, one possibility is the administration of the key hormone GnRH, or it's analogues to the patient. However, the oral administration of such medicines implies a slow imbibition, which can lead to unwanted side effects. Continuous high concentrations of GnRH (decapeptide preparations) will inhibit menstrual cycle, no restoration of fertility occurs. After publication of a study that showed increased risk of ovarian cancer in women who used clomifene longer than 12 months, the Committee on Safety of medicines in the UK has recommended that women should not take clomifene for longer than six months. One possible solution to this problem may be the application of portable GnRH pumps (see the figure 6.1), which are able dose the medicines in a pulsatile way directly into the blood, achieving a time-concentration profile close to the physiological one [83, 82]. However, the optimal usage of these devices would require a feedback, which takes the dynamics of the drug effects into account. Models like the one provided in chapter 2, may help in the development and application of such devices.

In addition to the significance of arrestins and slow transmission in GnRH signaling, the importance of the slow transmission becomes evident nowdays in more and more fields of physiology and medicine. Nowadays health experts refer to diabetes mellitus as the disease of the future. According to the statistics of the World Health Organization (WHO) an increase of the adult diabetes population from 4% (in 2000, meaning 171 million people) to 5.4% (366 million worldwide) is predicted by the year

DOI:10.15774/PPKE.ITK.2010.005

Figure 6.1: patient wearing a GnRH pump

2030 [163]. Several new results point to the possibility, that β-arrestins play a central role in diabetes mellitus and insulin resistance [140, 130, 111]. Thus our results may be useful in the modelling and possible therapeutic design corresponding to this disorder.

As stated before, the neuronal model of GnRH electrophysiology presented in Chapter 4 is intended to be later used in hierarchical models describing the hypothalamic GnRH pulse generator structure. A physiologically relevant model of the GnRH pulse generator would significantly enhance the usefulness of mathematical models corresponding to the reproductive neuroendocrine cycle. In addition, such models can be applied in computational studies of neuronal interactions. A composite model of 2-3 neurons would be able to describe and study many kinds of interactions, including for example endocannabinoid signaling.

The parameter estimation method proposed in chapter 3 can be used in the synthesis and identification of neuronal models. Furthermore these results provide bases for the future design of voltage clamp protocols in electrophysiological measurements dedicated to computational modelling.

6.2 Future work

A further refinement possibility of the signaling model described in chapter 2 is to include regulation mechanisms of GRK's. In fact this model can be easily extended by reactions, which describe the ERK induced GRK activation, for example. The effect of such considerations in this model's dynamics could then be analyzed and compared to physiological activation patterns.

Furthermore, a typical qualitative dynamical behavior of the model structure could be validated by various tests. For example, if we find an acceptable agreement with physiological activation patterns, we could considerably decrease the concentration of several key elements in the mathematical model, and then analyze the

DOI:10.15774/PPKE.ITK.2010.005

activation pattern dynamics. Moreover, we can also validate these results obtained with the activation patterns on si-RNA treated cells, where the corresponding protein is eliminated from the system.

Regarding the identifiability results detailed in chapter 3, a sound sequel of the work would be the anlysis of a Kuo-Bean type voltage dependent ion channel model [99, 155], where, in contrast to Hodgkin-Huxley type ion channel models, the processes of activation and inactivation are not assumed to be independent, which is a more realistic consideration.

The resulting GnRH neuronal model described in chapter 4 may be used as reference in the development of future models for the GnRH neuron. As soon as an appropriate Hodgkin-Huxley type model of membrane dynamics has been identified and validated, it will be completed with further elements influencing intracellular Ca^{2+} dynamics (models of intracellular compartments such as the endoplasmic reticulum, Ca buffers [136], and IP_3 signaling [173, 149]), which probably exert an important impact on hormone release. These new elements basically require reaction kinetic models, which describe the effect of buffers in the cytosol and in the endoplasmic reticulum (ER) [136]. Furthermore, such a model could be completed with the description of G-protein related signaling events, which affect membrane dynamics, corresponding to preliminary results on the dynamics of G-protein signaling [34].

Additionally, the model will be extended to take the complex effects of estradiol on the dynamics of membrane potential into account [26].

DOI:10.15774/PPKE.ITK.2010.005

Chapter 7

Acknowledgements

The author would like to thank the cooperation, help and support to the following people and organizations: Prof. Katalin Hangos, Gábor Szederkényi, Prof. Tamás Roska, Erzsébet Németh, Csaba Fazekas, Prof. József Bokor, Tamás Péni, Gábor Rödönyi, Tamás Luspay and the members of the SCL, Prof. György M. Nagy, Prof. Zsolt Liposits, Imre Farkas, Erik Hrabovszky, Szabolcs Káli, Márk Oláh, Ibolya Bodnár, Prof. Péter Érdi, Jean-Martin Beaulieu, István Ábrahám, Szabolcs Káli, Zoltán Somogyvári, Krisztina Szanyiszló, Levente Kovács, Prof. Ákos Jobbágy, Prof. Zoltán Benyó, Prof. Béla Lantos, István Harmati, Prof. Péter Szolgay, Prof. András Falus, all teachers students and administrators of the Interdisciplinary Doctoral School, Prof. György Serény, András Simon, Barnabás Farkas, The Hungarian National Scientific Research Fund (OTKA K-68170, K-67625) and Ministry of Health (ETT T-177/2006) to NGM, my parents and my friends.

DOI:10.15774/PPKE.ITK.2010.005

Chapter 8

Publications and Citations related to the thesis

Journal papers

[P1] D. Csercsik, K.M. Hangos and G.M. Nagy, "A simple reaction kinetic model of rapid (G protein dependent) and slow (β-Arrestin dependent) transmission," *Journal of Theoretical Biology*, vol 255(7), pp. 119-128, 2008, doi:10.1016/j.jtbi.2008.07.032 IF: 2.454 (**Thesis 1**)

[P2] D. Csercsik, I. Farkas, G. Szederkényi, E, Hrabovszky, Zs. Liposits and K.M. Hangos, "Hodgkin-Huxley type modelling and parameter estimation of GnRH neurons," *BioSystems*, vol 100, pp. 198-207, 2010, doi:10.1016/j.biosystems.2010.03.004 IF: 1.477 (**Thesis 3**)

Conference papers

[P3] D. Csercsik, K.M. Hangos, Gy.M. Nagy "Reaction kinetic models of rapid (g-protein dependent) and slow (beta-arrestin dependent) transmission," *Conference Abstract: Proc. IBRO International Workshop on Complex Neural Networks,"From synaptic transmission to seeing the brain in action,"* 24-26 January Debrecen, Hungary, 2008. (**Thesis 1**)

[P4] D. Csercsik , G. Szederkényi., K.M. Hangos and I. Farkas: "Parameter Estimation of Hodgkin-Huxley model of GnRH neurons," *Proceedings of the 9th International Phd. workshop: Young Generation Viewpoint*, October 1 - 3, Izola, Slovenia, 2008. (**Thesis 3**)

[P5] D. Csercsik , G. Szederkényi., K.M. Hangos and I. Farkas: "Model Synthesis and Identification of a One-Compartment Hodgkin-Huxley Type GnRH Neuron Model," *Frontiers in Systems Neuroscience. Conference Abstract: 12th Meeting of the Hungarian Neuroscience Society.* doi: 10.3389/conf.neuro.01.2009.04.106 (**Thesis 3**)

[P6] D. Csercsik , G. Szederkényi., K.M. Hangos and I. Farkas: "Dynamical Modeling and Identification of a GnRH neuron," *MCBMS'09 7th IFAC sympo-*

DOI:10.15774/PPKE.ITK.2010.005

sium on Modelling and Control in Biomedical Systems, August 12-14, Aalborg, Danemark, 2009 (**Thesis 3**)

[P7] D. Csercsik , G. Szederkényi., K.M. Hangos and I. Farkas: "Model Synthesis and Identification of a Hodgkin-Huxley-Type GnRH neuron model," *ECC'09 European Control Conference*, August 23-26, Budapest, Hungary, 2009 (**Thesis 3**)

[P8] D. Csercsik , G. Szederkényi. and K.M. Hangos: "Identifiability of a Hodgkin-Huxley type ion channel under voltage step measurement conditions," *9th International Symposium on Dynamics and Control of Process Systems*, July 5-7, Leuven, Belgium, 2010 (**Thesis 2**)

Citations in Journals

[C1] T. Wilhelm, "The smallest chemical reaction system with bistability," *BMC Systems Biology*, vol 3(90), 2009, doi:10.1186/1752-0509-3-90 (**P1**)

DOI:10.15774/PPKE.ITK.2010.005

Chapter 9

Appendix A: The reproductive neuroendocrine system and the hypothalamus-pituitary axis

9.1 The female hormonal cycle in general

The system of ovarian and pituitary hormones regulates and maintains the menstrual cycle in adult women. Although cycles are usually between 25 and 30 days apart, a woman's normal cycle can range anywhere from 22-40 days long. The menstrual cycle can be divided into two phases: the follicular phase and the luteal phase separated by ovulation and menstruation. During the menstrual cycle, the anterior pituitary affected by Gonadotropine-releasing hormone (GnRH) secreted in the hypothalamus, secretes hormones in a pulsatile way to stimulate the growth and development of ovarian follicles: Follicle-stimulating hormone (FSH) and luteinizing hormone (LH).

Consequently, cells in the the ovaries secrete hormones which affect the secretion of pituitary hormones and GnRH: Estradiol (E_2), progesteron (P_4) and inhibin (Ih).

The simultaneous change of ovarian and pituitary hormone levels and the change of the affected tissues during the cycle is depicted in 9.1. Figures 9.2 and 9.3 are depicting some of the underlying interactions.

The detailed description of the ovarian interactions exceeds the possibilities of this study, but we have to mention some basic information to provide basis for a general insight to the whole system's structure. The elements of the hypothalamus-pituitary axis, which are more in the focus of this thesis are discussed below in 9.2.

9.1.1 Cell types of the ovary

Theca cells, which are influenced mainly by LH, secrete androgen hormone (testosterone). Following ovulation theca cells are forming the corpus luteum, and secrete progesteron. The aromatase enzyme of the **granulosa cells** is able to turn testosterone into estradiol. Furthermore the granulosa cells of ovarian follicles in mammals produce inhibin, which hormone together with estradiol regulates the oestrous cycle.

DOI:10.15774/PPKE.ITK.2010.005

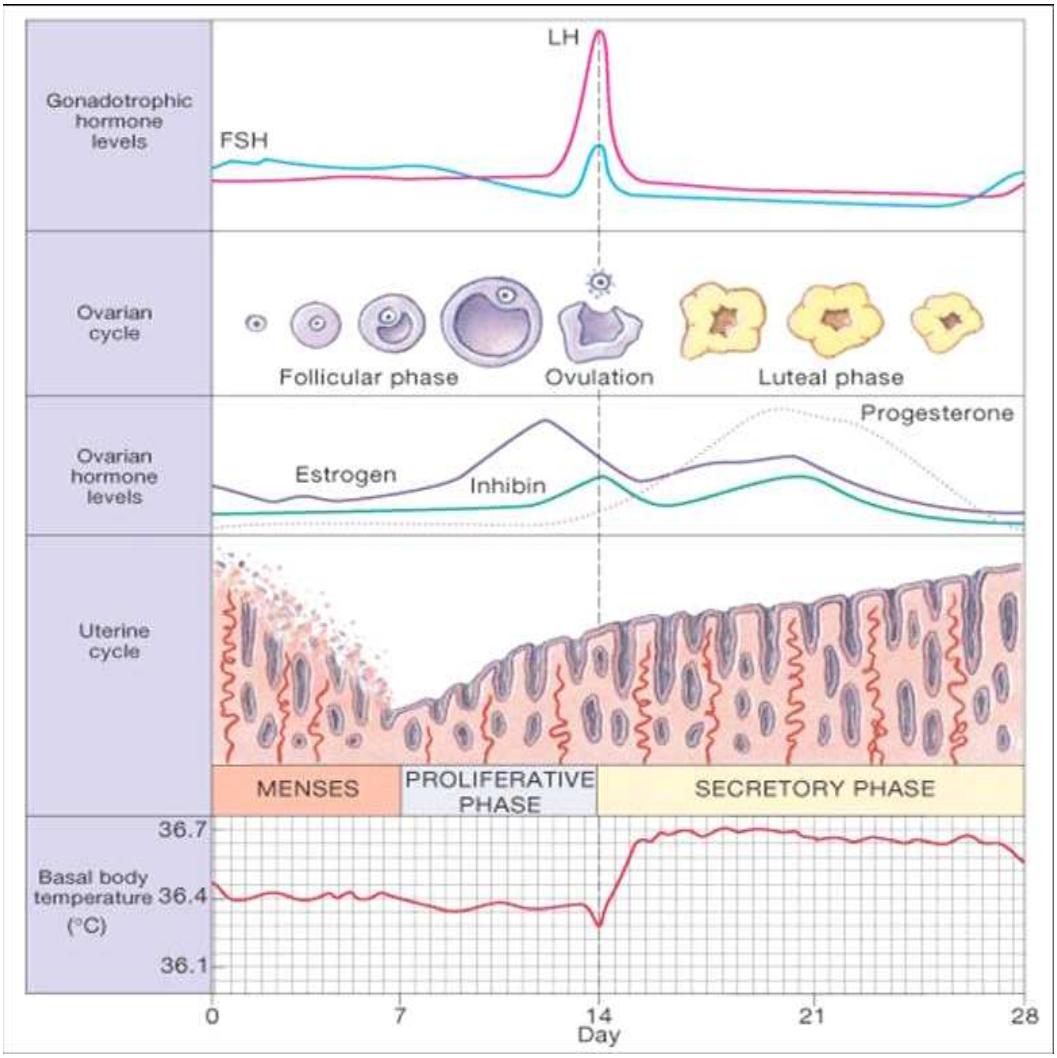

Figure 9.1: The hormonal and the menstrual cycle

9.1.2 Ovarian interactions

The physiological explanation for the interplay and effect of ovarian hormones has been formulated by Taya et al. in [147] as follows: Inhibin is a main inhibitor of FSH secretion, a chemical signal of the number of growing follicles in the ovary, and thus a key hormone in determining species-specific ovulation rates. On the other hand, oestradiol acts as a signal of follicular maturation in the ovary, and a signal determining the timing of the preovulatory LH surge.

In other words, the pituitary and ovarian hormones work together to release an ovum (egg) to be fertilized. An abrupt increase in LH in response to rapid, high amplitude GnRH pulses in the pituitary is required for ovulation of an egg from the ovaries marking the beginning of the luteal phase of the cycle.

Following ovulation, high levels of estrogen and progesterone secreted by the corpus luteum feedback to the hypothalamus and inhibit GnRH pulses and LH and FSH secretion.

DOI:10.15774/PPKE.ITK.2010.005

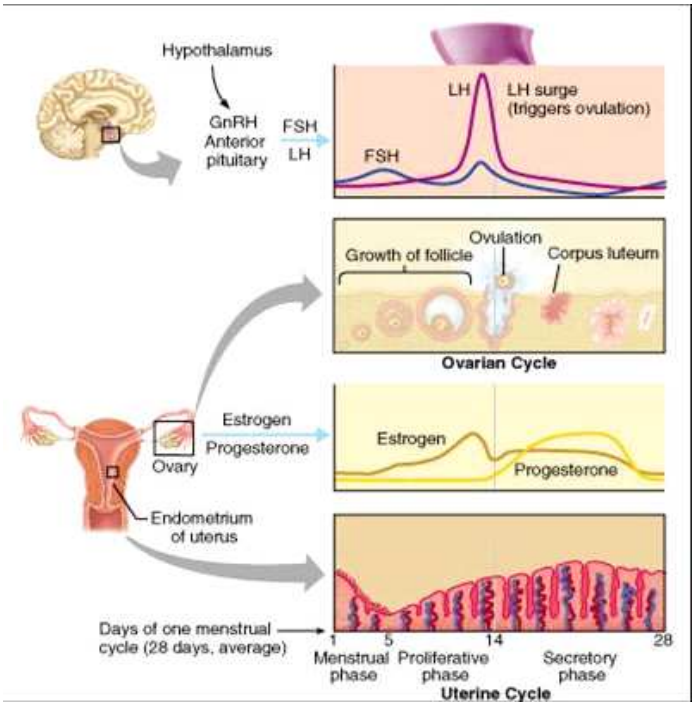

Figure 9.2: The sites of hormone synthesis and hormonal action

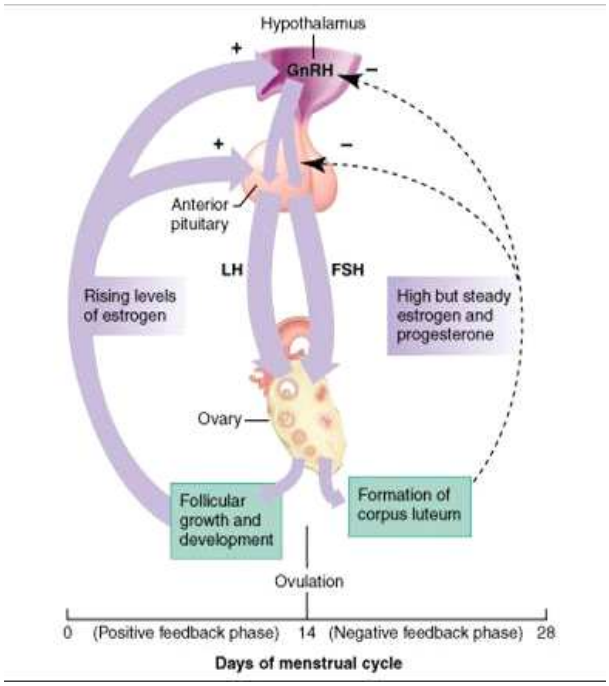

Figure 9.3: Some trans-tissue interactions

DOI:10.15774/PPKE.ITK.2010.005

If fertilization does not occur, the cycle is repeated: Corpus luteum atresia with the accompanying fall in the steroid hormones restarts the cycle, allowing the slow GnRH pulse frequency required for FSH release and recruitment of the next follicle [45].

Figure 9.4 taken from [131] briefly summarizes the ovarian interactions, and depicts the morphology of the ovary.

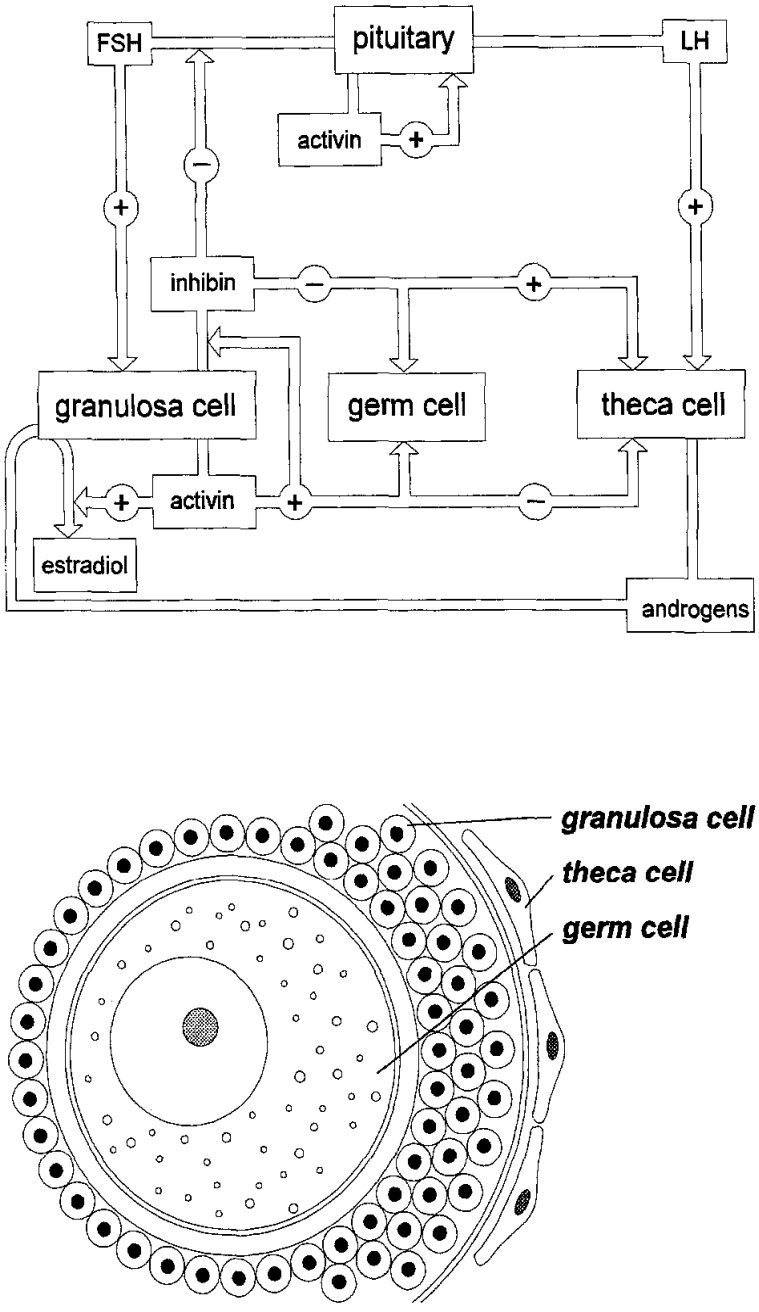

Figure 9.4: Summary of endocrine, paracrine, and autocrine actions in the ovary [131]

DOI:10.15774/PPKE.ITK.2010.005

9.2 The Hypothalamus-Pituitary axis

Gonadotropin releasing hormone (GnRH or LhRH) is the first key hormone of reproduction in vertebrates. In many species, three forms of GnRH and three cognate receptors have been described. GnRH I regulates the hypothalamo-pituitary axis, while GnRH II is thought to have a role as a neuromodulator affecting reproductive behaviour and GnRH III (salmon GnRH) functions only in teleost [120]. Although three cognate receptors have evolved, in man and several other species GnRH I and II interact with the type I GnRH receptor (GnRHR) [120], since the type II GnRHR is not expressed as a mature and functional receptor [126]. The human type II GnRHR gene is disrupted by a frameshift and premature stop codon, but remains transcriptionally active, and it is becoming increasingly apparent that a conventional type II GnRHR system is not present in man [120].

The neuroendocrine cells in the hypothalamus secrete GnRH in a pulsatile way, closely associated with concurrent increases in multiunit electrical activity in the mediobasal hypothalamus (MUA volleys) [166]. Neuroendocrine regulation of GnRH release in induced ovulators is described in [4].

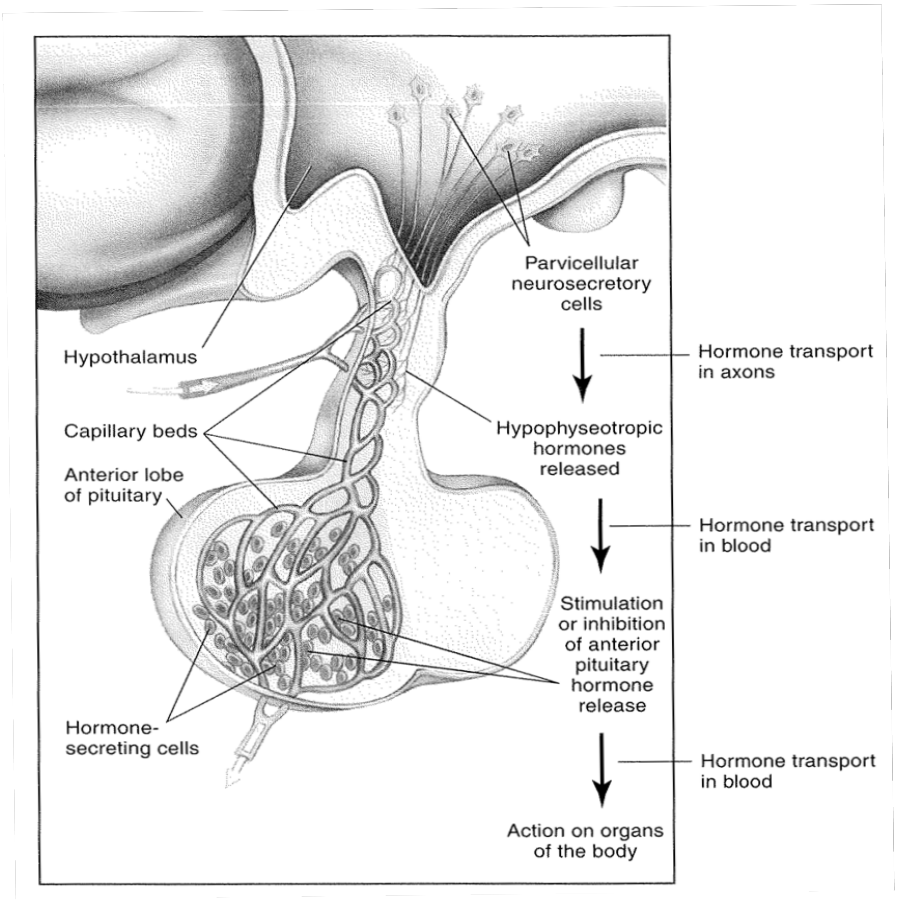

Figure 9.5: Figure from [6]: The hypothalamus and the pituitary and the corresponding neuroendocrine tissues

DOI:10.15774/PPKE.ITK.2010.005

A mathematical model describing the GnRH pulse generator is described in [21]. GnRH pulse frequency varies considerably over a normal menstrual cycle, the pulse intervals are on the scale of 8-240 minutes. GnRH achieves its effects at the pituitary gonadotropes by interaction with a heptahelical **G-protein coupled receptor** ($GPCR$) [135].

The gonadotropin cells in the adenohypophysis which are influenced also by peripherial hormones (E_2, P_4, Ih), responding to GnRH signals from the hypothalamus, synthetize and release the gonadotropin hormones, LH and FSH, which play important role in the growth and maturation of follicles. In particular, a sudden rise in LH serum concentration known as the LH surge triggers ovulation. Secretory rates of LH and FSH depend upon the frequency and the amplitude of GnRH pulses [164]. Gonadotropes represent only about 10% of pituitary cells and are divided into monohormonal cells (18% LH and 22% FSH cells) and 60% multihormonal (LH + FSH) cells.

The hormones LH and FSH are composed of three genes: A common element called α-subunit, and a $FSH\beta$ or a $LH\beta$ subunit. Many results detailed below provide basic for the hypothesis, that the control of the expression of these three genes is controlled separately: $FSH\beta$ is preferentially transcribed at slower GnRH pulses whereas $LH\beta$ and α preferentially transcribed at more rapid pulse frequencies.

A pulsatile pattern of GnRH stimulation is essential for normal secretion of luteinizing hormone (LH), while both continuous and fast-frequency GnRH stimulation result in a paradoxical decrease in gonadotrope responsiveness known as desensitization.

9.2.1 The gonadotropin-inhibitory system

In 2006 a new pituitary-related mechanism was identified by Kriegsfeld et al [96, 95]. An RFamide (Arg-Phe-NH_2) peptid that inhibits gonadotropin release was identified, named gonadotropin-inhibitory hormone (GnIH). Their results have shown, that *in vivo* GnIH administration rapidly inhibits LH secretion. Additionally GnIH neurons form close appositions with GnRH cells, suggesting direct means of GnRH modulation. Furthermore GnIH cells express estrogen receptor-α and exhibit roboust immediate early gene expression after gonadal hormone stimulation.

9.2.2 The effect of the ovary on pituitary

The ovary produces E_2, P_4 and Ih, which influence the pituitary's synthesis and release of the gonadotropin hormones during the various stages of the cycle. Basal gonadotrophin secretion during the normal menstrual cycle is predominantly under a negative ovarian effect. It is suggested that in contrast to FSH, the secretion of LH in response to GnRH is controlled by different ovarian mechanisms during the two phases of the menstrual cycle [2].

9.2.3 The effect of gonadal steroids on gonadotropin cells

Estradiol - E_2

DOI:10.15774/PPKE.ITK.2010.005

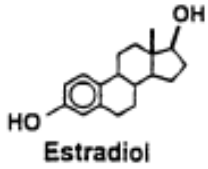

Estradiol

It has been assumed that the increase in secretion of estradiol that occurs following the demise of the corpus luteum is responsible for the events leading to the ovulatory surge of gonadotropins. The increase in media concentrations of LH as response to E_2 are not surprising in light of the fact that there is an estrogen response element (ERE) upstream of the coding region in the rat LHβ-subunit gene, and that this element confers positive regulation of the gene [137]. Furthermore, estradiol suppresses phosphorylation of cyclic adenosine 3*,5*-monophosphate (cAMP) response element binding protein (CREB) in the Pituitary [41].

Effects of E_2 on GnRHR and on Hypothalamus

Estradiol increases synthesis and insertion of GnRH receptors (GnRHR) into the membranes of gonadotropes. This is a relatively rapid response with the increase in number of membrane receptors occurring in 4-6 h in sheep [56]. However, Nett et al. reported that concentrations of mRNA for GnRH receptor increase prior to an increase in circulating concentrations of estradiol [124].

Furthermore, estradiol appears to stimulate a sustained secretion of GnRH from the hypothalamus that is initiated 12-15 h after administration of estradiol, several hours after the increase in GnRH receptors on gonadotropes [118]. Thus, in inducing a pre-ovulatory surge of gonadotropins, estradiol first increases sensitivity of the pituitary gland to GnRH and once gonadotropes are maximally sensitized, it then causes a dramatic increase in the amount of GnRH being released into the hypophyseal portal circulation to stimulate the massive release of LH needed to induce ovulation.

The duration of the increased secretion of GnRH induced by estradiol supersedes the duration of LH surge.

Thus, it has been speculated that the surge is terminated either because the pituitary gland becomes insensitive to the continued stimulation by GnRH, or because it becomes depleted of releasable stores of LH, or both. In this regard, Nett et al. have shown that approximately 75% of the LH contained in the pituitary gland of ewes is released during an ovulatory surge. Moreover, by the end of the massive increase in LH secretion during the ovulatory surge, there is a decrease in the number of GnRH receptors in the pituitary gland of ewes [150], which, as mentioned before, occurs well before the end of the increased secretion of GnRH. Thus, it appears that the termination of the LH surge is strongly affected by the combination of down-regulation of GnRH receptors and depletion of releasable stores of LH [124]. The effects of other gonadal steroids are described later.

DOI:10.15774/PPKE.ITK.2010.005

The effects of estradiol on the gonadotropin-inhibitory system is described above in 9.2.1.

Progesterone - P_4

In vivo progesterone decreases the frequency of GnRH pulses secreted into the hypothalamic- hypophyseal portal circulation [79].

Furthermore, progesterone decreases numbers of receptors for GnRH and amounts of mRNA encoding for the GnRH receptor in cultured ovine anterior pituitary cells [170]. We infer from these data that progesterone can act directly on the pituitary gland to influence responsiveness to GnRH. Moreover, Nett et al. were unable to stimulate an increase in number of GnRH receptors in the anterior pituitary by administering estradiol to ewes during the luteal phase of the estrous cycle. This implies that progesterone can block the positive effect of estradiol on GnRH receptor gene expression [150].

The fact that concentrations of mRNA for GnRH receptor increase prior to an increase in circulating concentrations of estradiol [150] lead some to hypothesize that a decrease in concentrations of progesterone may be important for initiating events that lead to the pre-ovulatory increase in sensitivity of the pituitary gland to GnRH. To support this supposition, there have been several publications indicating that progesterone is a negative regulator of the GnRH receptor gene in farm animals [33, 20, 150].

Expression of the GnRH receptor gene and numbers of GnRH receptors in the pituitary gland are lowest during the luteal phase of the estrous cycle when concentrations of progesterone are elevated [20].

Inhibin

Two forms of inhibin (A and B) are expressed in the ovaries of most species examined, including pig, human, monkey, rat, and mouse. Both inhibin (Ih) and estradiol (E_2) use separate and distinct mechanisms to decrease production of FSH 60%-80% while increasing receptors for GnRH (GnRHR) 400%-600% in ovine pituitary cultures [53].

Evidences for an endocrine role for ovarian inhibin in suppressing pituitary FSH secretion are summarized in [86].

A highly sensitive two-site assay format for inhibin B was developed and applied to the measurement of serum inhibin B during the human menstrual cycle [58]. In contrast to inhibin A levels which were lowest during the early follicular phase and maximal during the mid-luteal phase, serum inhibin B levels were relatively high during the early follicular phase but remained very low throughout the luteal phase. These intriguing observations suggest that the two different inhibin forms have different physiological roles during the menstrual cycle.

In fact, although administration of exogenous inhibin can suppress circulating FSH in nonhuman primates, passive immunoneutralization studies have been unable to show a rise in plasma FSH following administration of inhibin antisera during either the luteal or the follicular phase of the menstrual cycle [48, 49].

DOI:10.15774/PPKE.ITK.2010.005

Activins

Activins are homomeric or heteromeric dimers of inhibin B subunits and are produced by a wide variety of tissues including the pituitary gland, specifically by gonadotropes. Activins stimulate synthesis of FSH by a direct action on pituitary gonadotropes [116]. Once synthesized, FSH appears to be secreted constituitively by gonadotropes.

It appears that the mechanism by which estradiol inhibits synthesis and secretion of FSH in cultured pituitary cells is by inhibiting production of activin β_B (the form of activin produced by the pituitary gland).

Follistatin

Follistatin, also produced by the pituitary gland, is an activin-binding protein and may decrease FSH synthesis by sequestering activin [117]. In fact, as described by Nett et al. in [150], in the case of E_2 treatment the mRNA concentration of follistatin did not change.

DOI:10.15774/PPKE.ITK.2010.005

Chapter 10

Appendix B: Simulation results of the basic G protein signaling model

10.1 Simulation Results of the basic model

The simulations were performed to test the response to a stimulus at $t = 0$, and analyze the qualitative system response as function of the rate constants. The stimulus was simulated using an additive term in the differential equation related to the ligand, which described the replacement of the ligand at the cell's surface from its environment. Furthermore, constant maximal relative ligand concentration (being equal to 1) of the environment was assumed. The simulation time was chosen to be 20 minutes. The input of the system is depicted in Fig. 10.1.

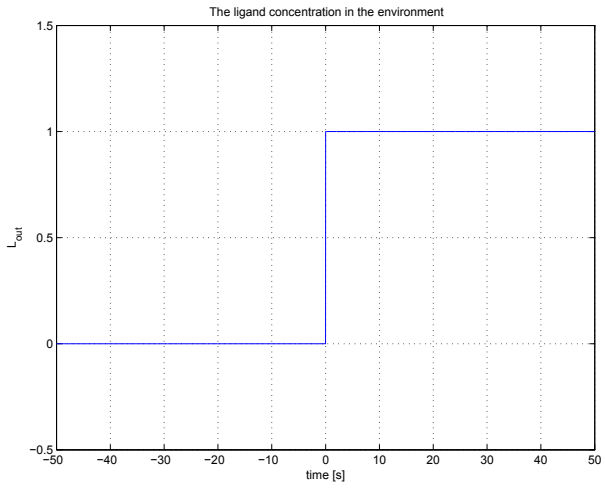

Figure 10.1: The ligand concentration in the environment

The initial states of the system were chosen in all cases to correspond to an inactive cell that is, no ligand was bound on any receptor, and all $G\alpha$ subunit was bound to ligand-free receptors in the form of $R(G\alpha - GDP)$.

Four parameter sets were used to study the qualitative model's behavior in the case of various rate constants. The parameters of the sets are collected in Table

DOI:10.15774/PPKE.ITK.2010.005

Table 10.1: Parameter sets for the basic model structure

Parameter	Set 1 Basic	Set 2	Set 3	Set 4
k_1^+	40	2	40	40
k_1^-	40	2	40	40
k_2^+	30	1	30	30
k_2^-	0	0	0	0
k_3^+	0.005	0.005	0.2	2
k_3^-	0	0	0	0
k_4^+	0.4	0.4	0.4	0.4
k_4^-	0.4	0.4	0.4	0.4
k_5^+	1	1	1	1
k_5^-	0	0	0	0

10.1.

In all cases of the simulation the initial state was assumed as total inactivity in the cell. This means that no ligand bound receptors, no active $G\alpha$, etc. were present.

The system response with the **basic parameter set 1** is depicted in Fig. 10.2. It is seen that the ligand concentration on the cell surface drops suddenly at the beginning of the transient, because the free $G\alpha - GDP$-bound receptors associate with the ligand. Later the ligand concentration returns to the value of 1, due to the supply from the environment.

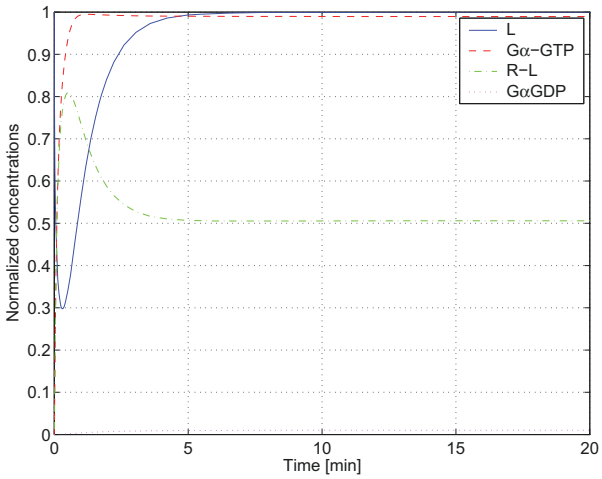

Figure 10.2: The system response with parameter set 1

The $G\alpha - GTP$ activates fast in this case, and its concentration is stabilized at a constant value. The explanation for this and for the constant low concentration of $G\alpha - GDP$ is that the dephosphorylated free $G\alpha$ can always find a free receptor to re-associate with, and the $G\alpha - GDP$-bound receptor is activated again by the

DOI:10.15774/PPKE.ITK.2010.005

ligand, which is present in a large extent. This way the $G\alpha$ subunit is quickly reactivated.

The k_1, k_2 and k_3 parameters can be related to the speed of the association and the coordinates of the resulting steady-state.

With the **parameter set 2**, a slower association and activation dynamics corresponding to k_1^+ and k_2^+ is assumed.

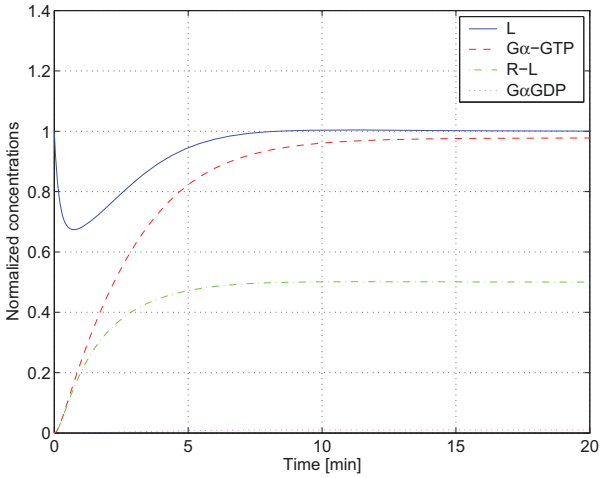

Figure 10.3: The system response with parameter set 2

As Figure 10.3 depicts, the ligand-receptor association and the G protein activation become slower, but the resulting steady-state is very similar to that of the basic case.

The effect of a faster deactivation rate (k_3^+) of G protein is analyzed with the **parameter set 3**.

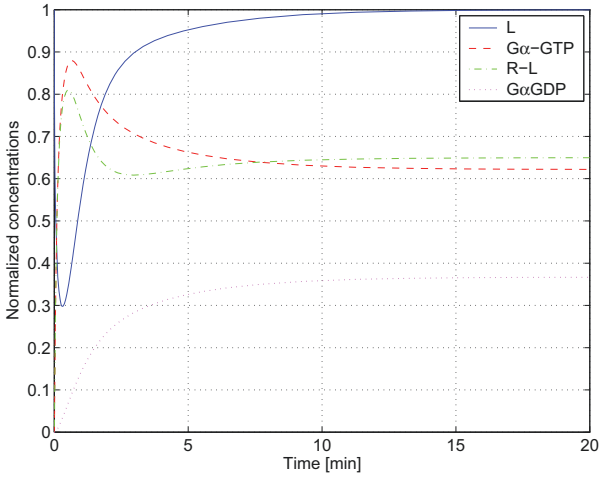

Figure 10.4: The system response with parameter set 3

The system response is seen in Figure 10.4, where the G protein activation shows a small overshoot, and it is stabilized at a lower concentration due to the faster deac-

DOI:10.15774/PPKE.ITK.2010.005

tivation rate. Furthermore we have to note that the further increase of the dephosphorylation rate k_3 implies even lower maxima of the G protein activation curve, and lower steady-state concentration. The $G\alpha - GDP$ concentration is strongly increased in this case.

If the deactivation rate (k_3^+) is further increased in **parameter set 4**, the overshoot becomes more dominant, but also the peak value of activated G protein concentration decreases (as it can be seen in figure 10.5), and a quasi steady-state is reached in 2 minutes, which is not a good qualitative approximation of the physiological behavior.

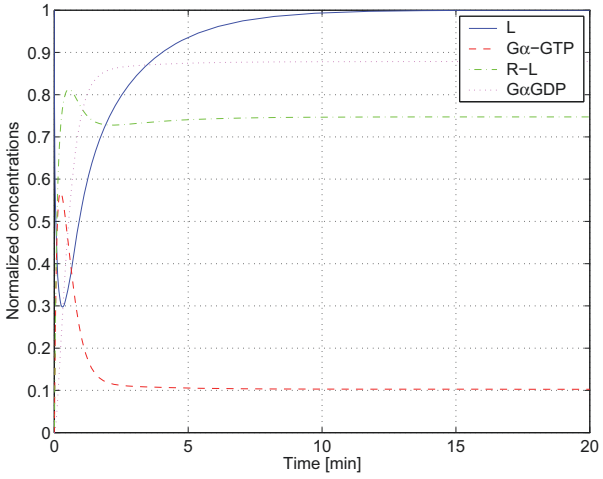

Figure 10.5: The system response with parameter set 4

10.1.1 Discussion

As a conclusion from the simulation results, we can conclude that the **basic model** without the inclusion of slow transmission and the regulation of signaling is able to describe the ligand-induced G protein activation in the cell, and it can be extended with G protein dependent signaling pathways. The ligand concentration on the cell surface (B) is affected by the ligand bounding of the receptors, and by the ligand concentration of the environment (the input - L_{env}). In this basic model the dephosphorylated $G\alpha - GDP$ can always find a free receptor, which induces its re-phosphorylation in the case of constant environmental ligand concentration. This process implies a stable steady-state of the system, in which the $G\alpha - GTP$ concentration remains at a significantly high constant level.

DOI:10.15774/PPKE.ITK.2010.005

Chapter 11

Appendix C: Sensitivity analysis of the extended G protein signaling model

11.1 Sensitivity Analysis

A simulation based sensitivity analysis of the extended model was carried out to analyze changes in the model output in response to parametric changes and changes in initial values.

11.1.1 Parameter sensitivity

In the first step, the change in the model response was analyzed in the case of 10% perturbation of model parameters (rate constants). The ERK activation curves, like the ones depicted in Figs. 2.5 (both pathways active) and 2.6 (G protein and β/Arrestin dependent pathways), were regarded as model responses. The change was measured as a quadratic error between the response (total phospho-ERK concentration trajectory) in the nominal case, and the response in the case with the perturbed parameter.

$$S = 1000 \int_0^{t_{final}} ([ERK_p^{tot}](t) - [\overline{ERK}_p^{tot}](t))^2 \quad dt$$

where the overline refers to the perturbation of a certain parameter. The multiplication with 1000 was used to normalize the resulting values. Furthermore, as it is described in 2.3.2, all curves were normalized with the maximum value of the nominal curve in the case of both pathways active. t_{final} was 60 min.

In the case of all parameters, the effect on all three model responses was analyzed. The three cases were the following

1. Both pathways active
2. Only G protein coupled transmission
3. Only β-Arrestin coupled transmission

DOI:10.15774/PPKE.ITK.2010.005

The parameter sensitivity analysis was carried out only for parameters with nonzero values. The results of the parameter sensitivity analysis are summarized in table 11.1.1.

Table 11.1: Parameter sensitivity of the model response

parameter	S (Both signaling pathways)	S (G-prot)	S (slow transmission)
k_1^+	$10^{-3}0.3582$	$10^{-3}0.2767$	$10^{-3}0.0875$
k_1^-	$10^{-4}0.6616$	$10^{-4}0.5127$	$10^{-4}0.1544$
k_2^+	$10^{-3}0.1720$	$10^{-3}0.1296$	$10^{-3}0.0462$
k_3^+	0.0144	0.0334	0.0004
k_4^+	0.0281	0.0916	0.1452
k_4^-	0.0120	0.0379	0.0625
k_5^+	0.0503	0.0929	0.0143
k_5^-	$10^{-4}0.9434$	$10^{-4}0.9208$	$10^{-4}0.1031$
k_6^+	0.4793	0.0176	0.9710
k_6^-	0.1970	0.0078	0.3881
k_7^+	0.7390	0.0004	1.2937
k_8^+	1.1905	0.0046	2.0506
k_9^+	0.1290	0.2924	0
k_9^-	0.0607	0.1390	0
k_{10}^+	0.1809	0.2595	0
k_{11}^+	1.5711	0	2.6568
k_{11}^-	0.3871	0	0.6505
k_{12}^+	0.6349	0	1.0339
k_{13}^+	0.0178	0.0417	0.0291
k_{13}^-	0.0050	0.0097	0.0075
k_{14}^+	0.0912	0.0672	0.0439
k_{15}^+	0.0269	0.1087	0.0001
k_{15}^-	0.0055	0.0225	0.0000
k_{16}^+	0.0065	0.0275	0.0000
k_{17}^+	3.2919	0.4954	3.7051
k_{19}^+	0.1937	0.0633	0.2704
k_{19}^-	0.0750	0.0287	0.1531
k_{20}^+	0.1157	0.0108	0.0646
k_{21}^+	10^{-3} 0.8096	$10^{-3}0.0039$	$10^{-3}0.5137$
k_{21}^-	0.0002	0.0004	0.0183
k_{22}^+	10^{-5} 0.0281	$10^{-5}0.0234$	$10^{-5}0.3128$

DOI:10.15774/PPKE.ITK.2010.005

Discussion

As described in 2.3.1, the model is not significantly sensitive to the parameters k_1^+, k_1^- and k_2^+. The explanation for this is, that the value of these rate constants is much higher (of order 2), compared to other parameters. This can be related to the assumption, that the speed of ligand-receptor interactions is significantly higher, than the other interactions taken into account. However, this implies, that in later development simplifications may be possible regarding these reactions.

The parameters to which the system showed also reduced sensitivity were in addition k_{21}^+, k_{21}^- and k_{22}^+. These parameters are related to the ERK autoregulation by ERK-phosphatase. This suggests, that in future studies, this mechanism has to be modelled in a different way, or it's explicit inclusion in the model may be neglected, and it's effect may be integrated in the spontaneous dephosphorylation rate of ERK (corresponding to k_{17}^+), which shows high sensitivity. The final parameter which shows reduced sensitivity is k_5^-, the backward rate of Gα GDP and Receptor reassociation.

In addition it can be seen from the results of the parameter sensitivity analysis, that the reactions, which correspond to the G protein coupled pathway (for eg. k_5^+), or regulation of G protein signaling (for eg. k_{13}^+) have much higher impact on G protein related response, and lower effect on slow transmission, and vice versa (see for eg. the rate constant k_8^+ corresponding to spontaneous dephosphorylation of the receptor-ligand complex, which inhibits slow transmission).

11.1.2 Sensitivity to initial values

At second, the change in the model response was analyzed in the case of 10% perturbation of nonzero initial values (specie concentrations). The change in the model response was measured as in the previous subsection (11.1.1). The results of the analysis are summarized in table 11.1.2.

Table 11.2: Sensitivity of the model response to initial values

specie	S (Both signaling pathways)	S (G-prot)	S (slow transmission)
L	0.0010	0.0007	0.0009
RGαGDP	2.8972	0.7606	2.8737
GRK	0.6477	0.0240	1.3105
ERK	3.3388	0.4169	3.6353
ERKP	0.3213	0.0724	0.4001

Discussion

As first, as we can see, it seems that the sensitivity of the model response to ligand concentration is surprisingly low. If we do further analysis, and perturb the ligand

DOI:10.15774/PPKE.ITK.2010.005

concentration more (about 50%), we may observe an increase of the numerical sensitivity value of about order 2. This points to a saturation type ultrasensitivity of the model corresponding to the concentration of the ligand.

The further rows of table 11.1.2 show, that the concentrations corresponding to the internal state of the system (RGαGDP, which corresponds to the receptor number, GRK which is necessary for the initiation of slow transmission) have quite significant impact on the model response. It is not surprising furthermore, that the model output is highly influenced by the initial concentration of ERK, which is the central element of the model and furthermore it corresponds directly to the output (ERK_p).

The initial concentration of ERK phosphatase (ERKP), which is responsible for the short-loop autoregulation has the lowest impact on model response among intracellular elements, which is in good agreement with the parameter sensitivity analysis described in the previous subsection 11.1.1.

DOI:10.15774/PPKE.ITK.2010.005

Chapter 12

Appendix D: GnRH electrophysiology

12.1 Obtaining and preparing samples

Brains of 60-90 days old male mice were used for obtaining GnRH neurons for measurements. The mouse was decapitated, and the brain was rapidly removed and placed in ice-cold artificial cerebrospinal fluid (ACSF) oxygenated with 95% O_2-5% CO_2 mixture. Brains were blocked and glued to the chilled stage of a Leica VT1000s vibratome, and 250-micrometer-thick coronal slices containing the medial septum through to the preoptic area were cut. The slices were then incubated at room temperature for 1 hour in oxygenated ACSF consisting of (in mM): 135 NaCl, 3.5 KCl, 26 $NaHCO_3$, 10 D-glucose, 1.25 NaH_2PO_4, 1.2 $MgSO_4$, 2.5 $CaCl_2$., pH 7.3.

12.2 Whole-cell recording of GnRH neurons

Slices were transferred to the recording chamber, held submerged, and continuously superfused with oxygenized ACSF. All recordings were made at 33°C.

In order to visualize GnRH neurons in the brain slices, GnRH-enhanced green fluorescent protein (GnRH-GFP) transgenic mice (kind gift by Dr. Suzanne Moenter) were chosen in which the GnRH promoter drives selective GFP expression in the majority of GnRH neurons. GnRH-GFP neurons were identified in the acute brain slices by their green fluorescence, typical fusiform shape and apparent topographic location in the preoptic area and medial septum.

The electrodes were filled with intracellular solution (in mM): 140 KCl, 10 HEPES, 5 EGTA, 0.1 $CaCl_2$, 4 MgATP, 0.4 NaATP, pH 7.3 with NaOH. Resistance of patch electrodes was 2-3 MΩ. Holding potential was -70 mV, near the average resting potential of the GnRH cells. Pipette offset potential, series resistance and capacitance were compensated before recording.

The protocol for voltage clamp (VC) recordings was the following: twelve voltage steps were applied starting from the holding potential. The first step was -40mV and the subsequent steps were increased by 10 mV. Duration of the steps was 30 ms, starting at 10 ms. During the voltage clamp measurements with prepulse, a -100

DOI:10.15774/PPKE.ITK.2010.005

mV prepulse was applied just preceding the voltage steps (from 0.8 to 10 ms) with a duration of 9.2 ms.

The protocol for current clamp (CC) recordings to activate action potentials (APs) was: the holding current was 0 pA. First the resting potential was measured then current step of 10 pA for 200 ms was applied to the cells. If the 10 pA current failed to evoke APs, it was elevated by 10 pA steps till it induced 3-4 APs.

DOI:10.15774/PPKE.ITK.2010.005

Chapter 13

Appendix E: Parameter estimation details and model parameters of the GnRH neuronal model

13.1 Objective functions

In this section, the objective functions used for parameter estimation can be found.

13.1.1 Voltage clamp (VC) measurements without prepulse

The manipulated external input to the system was the clamping voltage V_{clamp}. Square signals of different amplitudes were used as inputs. The parameters of the voltage steps were the following: The holding potential was -70mV, and voltage steps of -40 to 60 mV were simulated with duration of 30 ms starting at 10 ms of the simulation, and simulation results were compared to measurement data. The results of lower voltage step measurements (-50 and -60 mV) were not taken into account because of the very low signal/noise ratio. The measured output was the total output membrane current:

$$I_{tot} = I_{Na} + I_A + I_K + I_M + I_T + I_R + I_L + I_{leakNa} + I_{leakK} \tag{13.1}$$

The objective function of the estimation in VC case was the standard two-norm of the difference between the measured and simulated output currents for the three measurements, i.e.

$$W(\theta)_{VC} = \frac{1}{Nn} \sum_{i=1}^{n} w_i \| I^m_{tot,i} - I^s_{tot,i} \|_2 \tag{13.2}$$

where θ is the estimated parameter vector, and $I^m_{out,i}$ and $I^s_{out,i}$ denote the measured and model computed (simulated) total output current (as a discrete time sequence) for the ith measurement, respectively. Furthermore, w_i is the weight of the ith measurement N is the number of data points in the measurement record and n is the number of traces. The weights w_i corresponding to different voltage steps were set higher in the case of lower value voltage steps. The reason for this lies in the observation that although the signal-noise ratio is lower in the case of these traces, at

DOI:10.15774/PPKE.ITK.2010.005

physiological behavior the membrane voltage rarely reaches high values (only during AP-s). Therefore w_i was set proportional to the maximum value of the ith trace. The sampling time of the VC measurements was 0.1 ms.

13.1.2 Current Clamp (CC)

The manipulated external input to the system was the excitation current I_{ex}. The holding current was 0 pA. A square signal of 30 pA of amplitude with duration of 200 ms starting at 50 ms was used as input. The measured output was the membrane voltage V.

The main aim in this case was to capture the qualitative features of the CC trace. In general the weights of the objective functions were determined from the different amplitudes of signals.

Three of such qualitative features are examined: the number of the APs, the depolarization and hyperpolarization amplitudes.

The functions to be minimized in this case take the following form:

- The first component penalizes the difference between the number of action potentials in the simulated and in the measured case:

$$W(\theta)_{CC1} = w_n |n^m_{AP} - n^s_{AP}| \tag{13.3}$$

  where n^m_{AP} and n^s_{AP} denote the number of APs in the measured and simulated case, $w_n = 10$

- The second component is based on the maximum values of the APs:

$$W(\theta)_{CC2} = \frac{w_{max}}{n_{AP}} \sum_{i}^{n_{AP}} |max(AP^m_i) - max(AP^s_i)| \tag{13.4}$$

  $max(AP^m_i)$ and $max(AP^s_i)$ denote the maximum value of the corresponding AP in the measured and simulated case, $w_{max} = 0.5$.

- The last component is based on the minimum values of the traces in order to capture the hyperpolarization phenomenon:

$$W(\theta)_{CC3} = w_{min} |min(CC^m) - min(CC^s)| \tag{13.5}$$

  where CC^m and CC^s denote the CC traces in the measured and simulated case, $w_{min} = 0.5$.

The overall value of the objective function is calculated as the sum of VC and CC objective functions, i.e.

$$W(\theta) = \sum_i W(\theta)_{CCi} + W(\theta)_{VC} \qquad i = 1, 2, 3 \tag{13.6}$$

The sampling time of the CC measurements was 0.5 ms. The model was fitted to average data of 5 cells. This meant the explicit averaging of VC traces and the averaging of characteristic features of CC traces.

DOI:10.15774/PPKE.ITK.2010.005

13.2 Numerical optimization algorithm

The basic Parallel Pattern Search (PPS) algorithm [91] is very simple, its main steps are the following (where W denotes the objective function to be minimized):
Initialization:

- Set the iteration counter $k = 0$.
- Select a set of search directions $\mathcal{D} = \{d_1, \ldots, d_p\}$.
- Select a step-length control parameter Δ_0.
- Select a stopping tolerance tol.
- Select a starting point x_0 and evaluate $W(x_0)$.

Iteration:

1. Compute $x_k + \Delta_k d_i$ and evaluate $W(x_k + \Delta_k d_i)$, for $i = 1, \ldots, p$ concurrently.
2. Determine x_+ and $W(x_+)$ such that $f(x_+) = \min\{W(x_k + \Delta_k d_i), i = 1, \ldots, p\}$.
3. If $W(x_+) < W(x_k)$, then $x_k \leftarrow x_+$ and $W(x_k) \leftarrow W(x_+)$. Else $\Delta_k \leftarrow \frac{1}{2}\Delta_k$.
4. If $\Delta_k > tol$, $k \leftarrow k + 1$, go to Step 1. Else, exit.

As described by Kolda et al. [91], the APPS algorithm is an asynchronous extension of the PPS method that efficiently handles situations when the individual objective function evaluations may take significantly different time intervals and therefore it is very suitable to be implemented in a parallel or grid environment. Furthermore, recent implementations of the APPS method handle bound and linear constraints on the parameters. The global convergence of APPS under standard assumptions is also proved in [92].

13.3 Model parameters

13.3.1 Parameters of the basic model

Parameters of the basic model, resulting from the fit to VC traces and average values of CC traces, are described in the following tables.

The reversal potentials (see Eq. (4.4)) were determined based on the ionic concentrations of the intra and extracellular solutions used during recording, and literature data. The estimated reversal potentials are:

$$E_{Na} = 100\ mV, \quad E_K = -94\ mV, \qquad E_{Ca} = 80\ mV$$

DOI:10.15774/PPKE.ITK.2010.005

Table 13.1: Estimated capacitance and conductance values

C	$\bar{g}_{Na}$	$\bar{g}_A$	$\bar{g}_K$	$\bar{g}_M$
7	170	170	67	7.7

$\bar{g}_T$	$\bar{g}_R$	$\bar{g}_L$	$\bar{g}_{leakNa}$	$\bar{g}_{leakK}$
3.2	10.5	10.4	0.06	0.12

where [C]=pF, [g]=nS

Table 13.2: Estimated activation and inactivation parameters

variable	$V_{1/2}$	K	V_{max}	σ	C_{amp}	C_{base}
m_{Na}	-38.2	4.5	-43	45	0.04	0.09
h_{Na}	-45	-4	-78	19	25	0.7
m_A	-36.2	10.9	-58	18	0.7	0.9
h_A	-63.5	-6.9	-100	32	24.4	3.4
m_K	-7.2	12.8	-25	40	0.9	2.0
h_K	-67.2	-8	-39	55	-90	103
m_M	-31.4	6.9	25	28	3.1	2.2
m_T	-47	5.5	-22	32	2.2	2.5
h_T	-78	-6.5	-53	22	3.8	4.1
m_R	-4	10.6	20	30	0	0.4
h_R	-37	-11.5	-47	26	22	17
m_L	-2	10.5	26	33	2.3	0.5
h_L	-34	-11.5	-35	49	65	80

where $[V_{1/2}]$=mV, $[V_{max}]$=mV, $[C_{amp}]$=ms, $[C_{base}]$=ms

13.3.2 Parameters of the bursting model

The parameters of the bursting model are described in the following tables. The parameters different from the basic model are emphasized with bold typeface.

DOI:10.15774/PPKE.ITK.2010.005

Table 13.3: Modified (in bold) capacitance and conductance values

C	$\bar{g}_{Na}$	$\bar{g}_A$	$\bar{g}_K$	$\bar{g}_M$
7	**190**	**375**	**57**	**4.7**

$\bar{g}_T$	$\bar{g}_R$	$\bar{g}_L$	$\bar{g}_{leakNa}$	$\bar{g}_{leakK}$
10.8	**10.85**	**13.4**	**0.08**	0.12

where [C]=pF, [g]=nS

Table 13.4: Modified (in bold) activation and inactivation parameters

variable	$V_{1/2}$	K	V_{max}	σ	C_{amp}	C_{base}
m_{Na}	-38.2	**4.51**	-43	45	0.04	0.09
h_{Na}	-45	-4	-78	19	**20**	0.7
m_A	**-32.2**	10.9	**-65**	**23**	**1.7**	0.9
h_A	**-61.5**	-6.9	-100	**19**	**10**	**5.4**
m_K	**-6.5**	12.8	-25	40	0.9	2.0
h_K	**-68.2**	-8	-39	55	-90	103
m_M	**-29.2**	**6.2**	25	28	3.1	2.2
m_T	**-45**	**7.5**	**-42**	32	**3.1**	**3.9**
h_T	**-73**	**-5.5**	**-44**	22	**4.8**	**4.4**
m_R	-4	10.6	-	-	0	0.4
h_R	-37	-11.5	-47	26	22	17
m_L	**-6**	**12**	26	33	2.3	0.5
h_L	-34	-11.5	-35	49	65	80

where [$V_{1/2}$]=mV, [V_{max}]=mV, [C_{amp}]=ms, [C_{base}]=ms

DOI:10.15774/PPKE.ITK.2010.005

Bibliography

[1] J. A. Adams, G. M. Omann, and J. J. Linderman. A mathematical model for ligand/receptor/G-protein dynamics and acrin polimerization in human neutrophils. *Journal of Theoretical Biology*, 193:543–560, 1998.

[2] E. Alexandris, S. Milingos, G. Kollios, K. Seferiadis, D. Lolis, and I.E. Messinis. Changes in gonadotrophin response to gonadotrophin releasing hormone in normal women following bilateral ovariectomy. *Clinical Endocrinology*, 47(6):721–6, 1997.

[3] I. Aradi and P. Érdi. Computational neuropharmacology: dynamical approaches in drug discovery. *Trends in Pharmacological Sciences*, 27:240–243, 2006.

[4] J. Bakker and M.J. Baum. Neuroendocrine regulation of GnRH release in induced ovulators. *Frontiers in Neuroendocrinology*, 21:220–262, 2000.

[5] N. Bayram, M. van Wely, and F. van der Veen. Pulsatile gonadotrophin releasing hormone for ovulation induction in subfertility associated with polycystic ovary syndrome. *Cochrane Database Syst Rev*, 1, 2004.

[6] M.F. Bear, P.W. Connors, and M.A. Paradiso. *Neuroscience: Exploring the Brain.* Wiliams & Wilkins, Baltimore, 1996.

[7] J. M. Beaulieu, R. R. Gainetdinov, and M. G. Caron. The Akt-GSK-3 signaling cascade in the actions of dopamine. *Trends in Pharmacological Sciences*, 28:166–172, 2007.

[8] J. M. Beaulieu, T. D. Sotinkova, S. Marion, R. J. Lefkowitz, R. R. Gainetdinov, and M. G. Caron. An Akt/β-Arrestin 2/PP2A signaling complex mediates dopaminergic neurotransmission and behavior. *Cell*, 122:261–273, 2005.

[9] J. M. Beaulieu, T. D. Sotinkova, W. D. Yao, L. Kockeritz, J. R. Woodgett, R.R. Gainetdinov, and M .G. Caron. Lithium antagonizes dopamine-dependent behaviors mediated by an AKT/glycogen synthase kinase 3 signaling cascade. *Proceedings of the National Academy of Sciences of the USA*, 101:5099–5114, 2004.

[10] J.M. Beaulieu, S. Marion, R.M. Rodriguiz, I.O. Medvedev, T.D. Sotnikova, V. Ghisi, W.C. Wetsel, R.J. Lefkowitz, R.R. Gainetdinov, and M.G. Caron. A β-arrestin 2 signaling complex mediates lithium action on behavior. *Cell*, 132:125–136, 2008.

[11] G. Bellu, M.P. Saccomani, S. Audoly, and L. D'Angio. DAISY: A new software tool to test global identifiability of biological and physiological systems. *Computer Methods and Programs in Biomedicine*, 88:52–61, 2007.

[12] N. Ben-Jonathan and R. Hnasko. Dopamine as a prolactin (PRL) inhibitor. *Endocrine Revievs*, 22:724–263, 2001.

DOI:10.15774/PPKE.ITK.2010.005

[13] C. Beurrier, P. Congar, B. Bioulac, and C. Hammond. Subthalamic nucleus neurons switch from single-spike activity to burst-firing mode. *The Journal of Neuroscience*, 19:599–609, 1999.

[14] U. S. Bhalla and R. Iyengar. Emergent properties of networks of biological signaling pathways. *Science*, 283:381–387, 1999.

[15] U. S. Bhalla, P.T. Ram, and R. Iyengar. MAP kinase phosphatase as a locus of flexibility in a mitogen-activated protein kinase signaling network. *Science*, 297:1018–1023, 2002.

[16] R.J. Bogumil, M. Ferin, J. Rootenberg, L. Speroff, and R.L. vande Wiele. Mathematical studies of the human menstrual cycle. i. formulation of a mathematical model. *Journal of Clinical Endocrinology and Metabolism*, 35:126–143, 1972.

[17] F. Boogerd, F.J. Bruggeman, JH.S. Hofmeyr, and H.V. Westerhoff. *Systems Biology: Philosophical Foundations*. Elsevier, Radarweg 29, PO Box 211, 1000 AE, Amsterdam, The Netherlands, 2007.

[18] L.J. Borg-Graham, C. Monier, and Y. Fregnac. Visual input evokes transient and strong shunting inhibition in visual cortical neurons. *Nature*, 393:369–373, 1998.

[19] M.M. Bosama. Ion channel properties and episodic activity in isolated immortalized gonadotropin-releasing hormone (GnRH) neurons. *Journal of Membrane Biology*, 136:85–96, 1993.

[20] J. Brooks and A.S. McNeilly. Regulation of gonadotropin-releasing hormone receptor mRNA expression in the sheep. *Journal of Endocrinology*, 143:175–82, 1994.

[21] D. Brown, A.E. Herbison, J.E. Robinson, R.W. Marrs, and G. Leng. Modelling the lutenizing hormone-releasing hormone pulse generator. *Neuroscience*, 63:869–879, 1994.

[22] R. Campbell, G. Gaidamaka, S.K. Han, and A.E. Herbison. Dendro-denritic bundling and shared synapses between gonadotropin-releasing hormone neurons. *Proceedings of the National Academy of Sciences of the USA*, 106:10835–10840, 2009.

[23] N. Chabbert-Buffet, D.C. Skinnerb, A. Caratyb, and P. Boucharda. Neuroendocrine effects of progesterone. *Steroids*, 65:613–620, 2000.

[24] A.C. Charles and T.G. Hales. Mechanisms of spontaneous calcium oscillations and action potentials in immortalized hypothalamic (GT1-7) neurons. *Journal of Neurophysiology*, 73:56–64, 1995.

[25] C. Y. Chen, Y. Cordeaux, and S. J. Hill. Modelling of signalling via g-protein coupled receptors: Pathway-dependent agonist potency and efficacy. *Bulletin of Mathematical Biology*, 65:933–958, 2003.

[26] Z. Chu, Josefa Andrade, M.A. Shupnik, and S.M. Moenter. Differential regulation of gonadotropin-releasing hormone neuron activity and membrane properties by acutely applied estradiol: Dependence on dose and estrogen receptor subtype. *Journal of Neuroscience*, 29:5616–5627, 2009.

DOI:10.15774/PPKE.ITK.2010.005

[27] Z. Chu and S.M. Moenter. Physiologic regulation of a tetrodotoxin-sensitive sodium influx that mediates a slow afterdepolarization potential in gonadotropin-releasing hormone neurons: possible implications for the central regulation of fertility. *Journal of Neuroscience*, 26:11961–73, 2006.

[28] P.M. Conn and M.E. Freeman. *Neuroendocrinology in Physiology and Medicine*. Humana Press, 999 Riverview Drive Suite 208 Totowa New Jersey 07512, 2000.

[29] J.L. Constantin and A.C. Charles. Spontaneous action potentials initiate rhythmic intercellular calcium waves in immortalized hypothalamic (GT1-1) neurons. *Journal of Neurophysiology*, 82:429–435, 1999.

[30] J.L. Constantin and A.C. Charles. Modulation of Ca^{2+} signaling by K^+ channels in a hypothalamic neuronal cell line (GT-1). *Journal of Neurophysiology*, 85:295–304, 2001.

[31] G. Craciun and M. Feinberg. Multiple equilibria in complex chemical reaction networks: II The species-reaction graph. *Siam Journal of Applied Mathematics*, 66:1321–1338, 2006.

[32] G. Craciun and M. Feinberg. Understanding bistability in complex enzyme-driven reaction networks. *Proceedings of the National Academy of Sciences of the United States of America*, 103:8697–8702, 2006.

[33] M.E. Crowder and T.M. Nett. Changes in the concentration of hypophyseal receptors for gonadotropin-releasing hormone associated with the preovulatory surge of luteinizing hormone in ewes. *Endocrinology*, 114:134–9, 1984.

[34] D. Csercsik, K.M. Hangos, and G.M. Nagy. A simple reaction kinetic model of rapid (G protein dependent) and slow (β-Arrestin dependent) transmission. *Journal of Theoretical biology*, 255:119–128, 2008.

[35] R.A. DeFazio and S.M. Moenter. Estradiol feedback alters potassium currents and firing properties of gonadotropin- releasing hormone neurons. *Molecular Endocrinology*, 16:2255–2265, 2002.

[36] K. A. DeFea, Z. D. Vaughn, E. M. O'Bryan, D. Nishijima, O. Dery, and N. W. Bunett. The proliferative and antiapoptotic effects of substance P are facilitated by formation of a beta-arrestin-dependent scaffolding complex. *Proceedings of the National Academy of Sciences of the USA*, 98:11086–91, 2000.

[37] S. M. DeWire, S. Ahn, R. J. Lefkowitz, and S. K.Shenoy. β-Arrestins and cell signaling. *Annual Reviews of Physiology*, 69:483–510, 2007.

[38] A. Di Garbo, M. Barbi, and S. Chillemi. The synchronization properties of a network of inhibitory interneurons depend on the biophysical model. *Biosystems*, 88:216–227, 2007.

[39] S. Diop and M. Fliess. On nonlinear observability. In *First European Control Conference, ECC'91*, page 152, Grenoble, 1991.

[40] H. G. Dohlman, J. Song, D. M. Apanovitch, P. R. DiBello, and K. M. Gillen. Regulation of G protein signalling in yeast. *Seminars in Cell and Developmental Biology*, 9:135–141, 1998.

DOI:10.15774/PPKE.ITK.2010.005

[41] R.W. Duan, J.L. Shin, and J. Larry Jameson. Estradiol suppresses phosphorylation of cyclic adenosine 3',5'-monophosphate response element binding protein (CREB) in the pituitary. *Molecular Endocrinology*, 13:1338–1352, 1999.

[42] P. Érdi. *Complexity Explained*. Springer, ISBN-13 978-3-540-35777-3 DOI 10.1007/978-3-540-35778-0, 2008.

[43] I. Farkas, P. Varju, and Zs. Liposits. Estrogen modulates potassium currents and expression of the Kv4.2 subunit in GT1-7 cells. *Neurochemistry International*, 50:619–627, 2007.

[44] M. Feinberg. On chemical kinetics of a certain class. *Archive for Rational Mechanics and Analysis*, 46:1–41, 2004.

[45] H.A. Ferris and M.A. Shupnik. Mechanisms for pulsatile regulation of the gonadotropin. *Biology of Reproduction*, 74:993–8, 2006.

[46] P.A. Fletcher and Y.X. Li. An integrated model of electrical spiking, bursting, and calcium oscillations in GnRH neurons. *Biophysical Journal*, 96:4514–4524, 2009.

[47] M. Fliess and S. T. Glad. An algebraic approach to linear and nonlinear control. In H. L. Treutelman and J. C. Willeuis, editors, *Essays on control: Perspectives in the theory and its applications*, pages 223–267. Birkhauser, Boston, 1993.

[48] H.M. Fraser and S.F. Lunn. Does inhibin have an endocrine function during the menstrual cycle? *Trends in Endocrinology and Metabolism*, 4:187–194, 1993.

[49] H.M. Fraser and C.G. Tsonis. Manipulation of inhibin during the luteal-follicular phase transition of the primate menstrual cycle fails to affect FSH secretion. *Journal of Endocrinology*, 142:181–186, 1994.

[50] N.J. Freedman and R.J. Lefkowitz. Desensitization of G protein-coupled receptors. *Recent Progress in Hormone Research*, 51:319–351, 1996.

[51] M. E. Freeman, B. Kanyicska, A. Lerant, and G. Nagy. Prolactin: Structure, function and regulation of secretion. *Physiological Reviews*, 80:1523–1631, 2000.

[52] S. Galandrin, G. Oligny-Longpre, and M. Bouvier. The evasive nature of drug efficacy: implications for drug discovery. *Trends in Pharmacological Sciences*, 28:423–430, 2007.

[53] B.R. Ghosh, J.C. WU, B.D. Strahl, G.V. Child, and W.L. Miller. Inhibin and estradiol alter gonadotropes differentially in ovine pituitary cultures: Changing gonadotrope numbers and calcium responses to gonadotropin-releasing hormone. *Endocrinology*, 137(11):5144–5154, 1996.

[54] J.D. Gordan, B.J. Attardi, and D.W. Pfaff. Mathematical exploration of pulsatility in cultured gonadotropin-releasing hormone neurons. *Neuroendocrinology*, 67:2–17, 1998.

[55] W. Govaerts and B. Sautois. Bifurcation software in Matlab with applications in neuronal modeling. *Computer Methods and Programs in Biomedicine*, 77:141–153, 2005.

DOI:10.15774/PPKE.ITK.2010.005

[56] D.W. Gregg, M.C. Allen, and T.M. Nett. Estradiol-induced increase in number of GnRH receptors in cultured ovine pituitary cells. *Biology of Reproduction*, 43:1032–6, 1990.

[57] R. Grigolienė and D. Švitra. The mathematical model of the female menstrual cycle and its modifications. *Informatica*, 11:411–420, 2000.

[58] N. Groome, P. Illingworth, M. O'Brian, R. Pai, F.E. Rodger, J. Mather, and A. McNeilly. Measurement of dimeric inhibin-b throughout the human menstrual cycle. *Journal of Endocrinology and Metabolism*, 81:1401–1405, 1996.

[59] J. S. Gutkind. Cell growth control by G protein-coupled receptors: from signal transduction to signal integration. *Oncogene*, 17:1331–1342, 1998.

[60] J.S. Gutkind. The pathways connecting G protein-coupled receptors to the nucleus through divergent mitogen-activated protein kinase cascades. *Journal of Biological Chemistry*, 273:1839–1842, 1998.

[61] L. Harris, P. M. Schlosser, and J. F. Selgrade. Multiple stable periodic solutions in a model for hormonal control of the menstrual cycle. *Bulletin of Mathematical Biology*, 65:157–173, 2006.

[62] L.A. Harris. *Differential equation models for the hormonal regulation of the menstrual cycle.* PhD thesis, North Carolina State University, www.lib.ncsu.edu/theses/available/etd-04222002-153727/unrestricted/etd.pdf., 2001.

[63] D. Haufler, F. Morin, J.C. Lacaille, and F.K. Skinner. Parameter estimation in single-compartment neuron models using a synchronization-based method. *Neurocomputing*, 70:1605–1610, 2007.

[64] A.D. Heilman and J. Quattrochi. Computational models of epileptiform activity in single neurons. *Biosystems*, 78:1–21, 2004.

[65] E.J.M. Helmreich and A. Bakardjieva. Hormonally stimulated adenylate cyclase: A membranous multicomponent system. *Biosystems*, 12:295–304, 1980.

[66] A.E. Herbison. Estrogen positive feedback to gonadotropin-releasing hormone (GnRH) neurons in the rodent: The case for the rostral periventricular area of the third ventricle (RP3V). *Brain Research Reviews*, 57(2):277–287, 2007.

[67] A.E. Herbison, J.R. Pape, S.X. Simonian, M.J. Skynner, and J.A. Sim. Molecular and cellular properties of GnRH neurons revealed through transgenics in mouse. *Molecular and Cellular Endocrinology*, 185:185–194, 2001.

[68] B. Hernández-Bermejo and V. Fairen. Lotka-volterra representation of general nonlinear systems. *Mathematical Biosciences*, 140:1–32, 1997.

[69] C. Hill, A. Goddard, J. Daevy, and G. Ladds. Investigating RGS proteins in yeast. *Cell & Developmental Biology*, 17:352–362, 2006.

[70] B. Hille. *Ion Channels of Excitable membranes.* Sinauer Associates Inc., ISBN 0-87893-321-2, 2001.

DOI:10.15774/PPKE.ITK.2010.005

[71] A.L. Hodgkin and A.F. Huxley. A quantitive description of membrane current and application to conduction and excitation in nerve. *Journal of Physiology*, 117:500–544, 1952.

[72] P.D. Hough, T.G. Kolda, and V.J. Torczon. Asynchronous parallel pattern search for nonlinear optimization. *SIAM Journal on Scientific Computing*, 23:134–156, 2002.

[73] C. Y. F. Huang and J. E. Ferrell Jr. Ultrasensitivity in the mitogen-activated protein kinase cascade. *Proceedings of the National Academy of Sciences of the USA*, 93:10078, 1996.

[74] Q.J.M. Huys, M.B. Ahrens, and L. Paninski. Efficient estimation of detailed single-neuron models. *Journal of Neurophysiology*, 96:872–890, 2006. doi:10.1152/jn.00079.2006.

[75] M. Ishii and Y. Kurachi. Physiological actions of regulators of G-protein signaling (RGS) proteins. *Life Sciences*, 74:163–171, 2003.

[76] E.M. Izhikevich. Neural excitatibility, spiking and bursting. *International Journal of Bifurcation and Chaos*, 10:1171–1266, 2000.

[77] E.M. Izhikevich. Simple model of spiking neurons. *IEEE Transactions on Neural Networks*, 14:1569–1572, 2003.

[78] E.M. Izhikevich. *Dynamical Systems in Neuroscience*. The MIT Press, 999 Riverview Drive Suite 208 Totowa New Jersey 07512, 2005.

[79] F.J. Karsch, J.T. Cummins, G.B. Thomas, and I.J. Clarke. Steroid feedback inhibition of pulsatile secretion of gonadotropin-releasing hormone in the ewe. *Biology of Reproduction*, 36:1207–18, 1987.

[80] M. Kato, K. Ui-Tei, M. Watanabe, and Y. Sakuma. Characterization of voltage-gated calcium currents in gonadotropin-releasing hormone neurons tagged with green fluorescent protein in rats. *Endocrinology*, 144:5118–5125, 2003.

[81] J.H. Kehrl and S. Sinnarajah. RGS2: a multifunctional regulator of G-protein signaling. *International Journal of Biochemistry & Cell Biology*, 32:432–438, 2001.

[82] E.J. Keogh, A. MacKellar, S.R. Mallal, A.G. Dunn, S.C. McColm, S.P. Somerville, T. Marshall, and J. Attikiouzel. Treatment of cryptorchdism with pulsatile luteinizing hormone releasing hormone. *Proceedings of the Annual Scientific Meeting of the R.A.C.P. (W.A), October 1981*, 1981.

[83] E.J. Keogh, S.R. Mallal, L. Cox, R. Pontifex, T.G. Marshall, and J. Attikiouzel. "Physiologic" administration of GnRH by a portable pump. *Proceedings of the 1980 Conference of the Australian Endocrine Society*, 1980.

[84] A. Khadra and Y.X. Li. A model for the pulsatile secretion of gonadotropin-releasing hormone from synchronized hypothalamic neurons. *Biophysical Journal*, 91:74–83, 2006.

[85] T. L. Kinzer-Ursem and J .J. Linderman. Both ligand- and cell-specific parameters control ligand agonism in a kinetic model of G protein coupled receptor signaling. *PLOS Computational Biology*, 3, 2008.

DOI:10.15774/PPKE.ITK.2010.005

[86] P.G. Knight. Roles of inhibins, activins, and follistatin in the female reproductive system. *Frontiers in Neuroendocrinology*, 17(4):476–509, 1996.

[87] E. Knobil. The neuroendocrine control of the menstrual cycle. *Hormone Research*, 36:53–88, 1980.

[88] E. Knobil. The hypothalamic gonadotropin hormonr releasing hormone (GnRH) pulse generator in the rhesus monkey and its neuroendocrine control. *Human Reproduction*, 3:29–31, 1988.

[89] M.R. Koelle. A new family of G-protein regulators - the RGS proteins. *Current Biology*, 9:143–147, 1997.

[90] W. Kolch, F. Calder, and D. Gilbert. When kinases meet mathematics: the systems biology of MAPK signalling. *FEBS Letters*, 579:1891–1895, 2005.

[91] T.G. Kolda. Revisiting asynchronous parallel pattern search for nonlinear optimization. *SIAM Journal of Optimization*, 16:563–586, 2005.

[92] T.G. Kolda and V.J. Torczon. On the convergence of asynchronous parallel pattern search. *SIAM Journal of Optimization*, 14:939–964, 2004.

[93] A.O. Komendantov, N.A. Trayanova, and J.G. Tasker. Somato-dendritic mechanisms underlying the electrophysiological properties of hypothalamic magnocellular neuroendocrine cells: A multicompartmental model study. *Journal of Computational Neuroscience*, 23:143–168, 2007. DOI 10.1007/s1-827-007-0024-z.

[94] D.C. Krauker, K.M Page, and S. Sealfon. Module dynamics of the GnRH signal transduction network. *Journal of Theoretical Biology*, 218:457–470, 2002.

[95] L.J. Kriegsfeld. Driving reproduction: RFamide peptides behind the wheel. *Hormones and Behavior*, 50(5):655–66, 2006.

[96] L.J. Kriegsfeld, D.F. Mei, G.E. Bentley, T. Ubuka, A.O. Mason nad K. Inoue, K. Ukena, K. Tsutsui, and R. Silver. Identification and characterization of a gonadotropin-inhibitory system in the brains of mammals. *Proceedings of the National Academy of Sciences of the USA*, 103:2410–2415, 2006.

[97] L.Z. Krsmanovic, S.S. Stojilkovic, F. Merelli, S.M. Dufour, M.A. Virmani, and K.J. Catt. Calcium signaling and episodic secretion of gonadotropin-releasing hormone in hypothalamic neurons. *Proceedings of the National Academy of Sciences of the USA*, 89:8462–8466, 1992.

[98] M.C. Kuehl-Kovarik, K.M.Partin, R.J. Handa, and F.E. Dudek. Spike-dependent depolarizing afterpotentials contribute to endogenous bursting in gonadotropin releasing hormone neurons. *Neuroscience*, 134:295–300, 2005.

[99] C.-C. Kuo and B.P. Bean. Na^+ channels must deactivate to recover from inactivation. *Neuron*, 12:819–829, 1994.

[100] K. Kusano, S. Fueshko, H. Gainer, and S. Wray. Electrical and synaptic properties of embryonic lutenizing hormone-releasing hormone neurons in explant cultures. *Proceedings of the National Academy of Sciences of the USA*, 92:3918–3992, 1995.

DOI:10.15774/PPKE.ITK.2010.005

[101] A.P. LeBeau, F. Van Goor, S.S. Stojilkovic, and A. Sherman. Modeling of membrane excitability in gonadotropin-releasing hormone-secreting hypothalamic neurons regulated by Ca^{2+}-mobilizing and adenylyl cyclase-coupled receptors. *The Journal of Neuroscience*, 20:9290–9297, 2000.

[102] J. Lee, B. Smaill, and N. Smith. Hodgkin-huxley type ion channel characterization: An improved method of voltage clamp experiment parameter estimation. *Journal of Theoretical Biology*, 242:123–134, 2006.

[103] K. Lee, W. Duan, J. Sneyd, and A.E. Herbison. Two slow calcium-activated afterhyperpolarization currents control burst firing dynamics in gonadotropin-releasing hormone neurons. *Journal of Neuroscience*, 30:6214–6224, 2010.

[104] R. J. Lefkowitz. Historical review: a brief history and personal reprospective of seven-transmembrane receptors. *Trends in Pharmacological Sciences*, 25:413–422, 2004.

[105] R. J. Lefkowitz and S.K. Shenoy. Transduction of receptor signals by beta-arrestins. *Science*, 308:512–517, 2005.

[106] G. Leng and D. J. MacGregor. Mathematical modelling in neuroendocrinology. *Journal of Neuroendocrinology*, 20:713–718, 2008.

[107] J. J. Linderman. Kinetic modeling approaches to understanding ligand efficacy. In T. Kenakin and J. A. Angus, editors, *The Pharmacology of Functional, Biochemical, and Recombinant Receptor Systems, Handbook of Experimental Pharmacology*, volume 148, pages 119–146. Springer-Verlag, 2000.

[108] X. Liu and A.E. Herbison. Small-conductance calcium-activated potassium channels control excitability and firing dynamics in gonadotropin-releasing hormone (GnRH) neurons. *Endocrinology*, 149:3598–3604, 2008.

[109] L. Ljung. *System Identification - Theory for the User*. Prentice Hall, Englewood Cliffs, N.J., 1987.

[110] L. Ljung and T. Glad. On global identifiability of arbitrary model parametrizations. *Automatica*, 30:265–276, 1994.

[111] B. Luan, J. Zhao, H. Wu, B. Duan, G. Shu, X. Wang, D. Li, W. Jia, J. Kang, and G. Pei. Deficiency of a β-arrestin-2 signal complex contributes to insulin resistance. *Nature*, 457:1146–1150, 2009.

[112] J.A. Luther and J.G. Tasker. Voltage-gated currents distinguish parvocellular from magnocellular neurones in the rat hypothalamic paraventricular nucleus. *Journal of Physiology*, 523:193–209, 2000.

[113] L. M. Luttrell, F. L. Roudabush, E. W. Choy, W. E. Miller, and M. E. Field. Activation and targeting of extracellular signal-regulated kinases by beta-arrestin scaffolds. *Proceedings of the National Academy of Sciences of the USA*, 98:2449–2454, 2001.

[114] L.M. Luttrell, Y. Daaka, and R.J. Lefkowitz. Regulation of tyrosine kinase cascades by G-protein-coupled receptors. *Current Opinion in Cell Biology*, 11:177–183, 1999.

DOI:10.15774/PPKE.ITK.2010.005

[115] G. Margaria, E. Riccomagno, M. J. Chappell, and H. P. Wynn. Differential algebra methods for the study of the structural identifiability of rational function state-space models in the biosciences. *Mathematical Biosciences*, 174:1–26, 2001.

[116] A.J. Mason, L.M. Berkemeier, C.H. Schmelzer, and R.H Schwall. Activin b: precursor sequences, genomic structure and in vitro activities. *Molecular Endocrinology*, 3:1352–8, 1989.

[117] J.P. Mather, P.E. Roberts, and L.A. Krummen. Follistatin modulates activin activity in a cell- and tissue-specific manner. *Endocrinology*, 132:2732–4, 1993.

[118] R.A. Maurer, K.E. Kim, W.E. Schoderbek, M.S. Robertson, and D.J. Glenn. Regulation of glycoprotein hormone alpha-subunit gene expression. *Recent Progress in Hormone Research*, 129:1175–82, 1999.

[119] P.L. Mellon, J.J. Windle, P.G. Goldsmith, C.A. Padula, J.L. Roberts, and R.I. Weiner. Immortalization of hypothalamic GnRH neurons by genetically targeted tumorigenesis. *Neuron*, 5:1–10, 1990.

[120] R.P. Millar, Z.L. Lu, A.J. Pawson, C.A. Flanagan, K. Morgan, and S.R. Maudsley. Gonadotropin-releasing hormone receptors. *Endocrine Reviews*, 25:235–275, 2004.

[121] I.M. Àbrahàm C.L. Jasoni N. Romanò, K. Lee and A.E. Herbison. Nonclassical estrogen modulation of presynaptic gaba terminals modulates calcium dynamics in gonadotropin-releasing hormone neurons. *Current Obstetrics and Gynaecology*, 149:5335–5344, 2008.

[122] K.L. Neitzel and J.R. Hepler. Cellular mechanisms that determine selective RGS protein regulation of G protein-coupled receptor signaling. *Seminars in Cell & Developmental Biology*, 17:383–389, 2006.

[123] J.A. Nelder and R. Mead. A simplex method for function minimization. *The Computer Journal*, 7:308–313, 1965.

[124] T.M. Nett, A.M. Turzillo, M. Baratta, and L.A. Rispoli. Pituitary effects of steroid hormones on secretion of follicle-stimulating hormone and luteinizing hormone. *Domestic Animal Endocrinology*, 23:33–42, 2002.

[125] C.S. Nunemaker, R.A. DeFazio, and S.M. Moenter. Calcium current subtypes in GnRH neurons. *Biology of Reproduction*, 69:1914–1922, 2003.

[126] A.J. Pawson, S. Maudsley, K. Morgan, L. Davidson, Z. Naor, and R.P. Millar. Inhibition of human type I gonadotropin-releasing hormone receptor (GnRHR) function by expression of a human type II GnRHR gene fragment. *Endocrinology*, 146:2639–2649, 2005.

[127] K.L. Pierce and R.J. Lefkowitz. Classical and new roles of β-arrestins in the regulation of G-protein-coupled receptors. *Nature Reviews Neuroscience*, 2:727–733, 2001.

[128] J. A. Pitcher, N. J. Freedman, and R. J. Lefkowitz. G protein-coupled receptor kinases. *Annuual Reviews of Biochemistry*, 67:653–692, 1998.

[129] I. Reinecke and P. Deuflhard. A complex mathematical model of the human menstrual cycle. *Journal of Theoretical Biology*, 247:303–330, 2007.

DOI:10.15774/PPKE.ITK.2010.005

[130] J.T. Rodgers and P. Puigserver. Insulin resistance: β-arrestin development. *Cell Research*, 19:275–276, 2009.

[131] L. Rombauts and D.L. Healy. Inhibins and activins in reproduction. *Current Obstetrics and Gynaecology*, 5(3):155–162, 1995.

[132] P. Roper, J. Callaway, T. Shevchenko, R. Teruyama, and W. Armstrong. AHP's, HAP's and DAP's: How potassium currents regulate the excitability of rat supraoptic neurones. *Journal of Computational Neuroscience*, 15:367–389, 2003.

[133] A. Roth and M. Häusser. Compartmental models of rat cerebellar purkinje cells based on simultaneous somatic and dendritic patch-clamp recordings. *Journal of Physiology*, 535:445–472, 2001.

[134] M. P. Saccomani, S. Audoly, and L. D'Angio. Parameter identifiability of nonlinear systems: the role of initial conditions. *Automatica*, 39:619–632, 2003.

[135] S.C. Sealfon, H. Weinstein, and R.P. Millar. Molecular mechanisms of ligand interaction with the gonadotropin-releasing hormone receptor. *Endocrine reviews*, 18(2):180–205, 1997.

[136] P.R. Shorten and D.J.N. Wall. A Hodgkin-Huxley model exhibiting bursting oscillations. *Bulletin of Mathematical Biology*, 62:695–715, 2000.

[137] M.A. Shupnik and B.A. Rosenzweig. Identification of an estrogen-responsive element in the rat LH beta gene. DNA-estrogen receptor interactions and functional analysis. *Journal of Biological Chemistry*, 266:17084–91, 1991.

[138] J.A. Sim, M.J. Skynner, and A.E. Herbison. Heterogeneity in the basic membrane properties of postnatal gonadotropin-releasing hormone neurons in the mouse. *The Journal of Neuroscience*, 21:1067–1075, 2001.

[139] D.J. Spergel, U Krüth, D.F. Hanley, R. Sprengel, and P.H. Seeburg. Gaba- and glutamate-activated channels in green fluorescent protein-tagged gonadotropin-releasing hormone neurons in transgenic mice. *The Journal of Neuroscience*, 19:2037–2050, 1999.

[140] J. St ockli and David E. James. Insulin action under arrestin. *Cell Metabolism*, 9:213–214, 2009.

[141] S.S. Stojilkovic, L.Z. Krsmanovic, D.J. Spergel, and K.J. Catt. GnRH neurons: intrinsic pulsatility and receptor-mediated regulation. *Trends in Endocrinology and Metabolism*, 5:201–209, 1994.

[142] K.J. Suter, J.P. Wuarin, B.N. Smith, F.E. Dudek, and S.M. Moenter. Whole-cell recordings from preoptic/hypothalamic slices reveal burst firing in gonadotropin-releasing hormone neurons identified with green fluorescent protein in transgenic mice. *Endocrinology*, 141:3731–3736, 2000.

[143] G .M. Omann T. A. Riccobene and J. J. Linderman. Modeling activation and desensitization of G-protein coupled receptors provides insight into ligand efficacy. *Journal of Theoretical Biology*, 200:207–222, 1999.

DOI:10.15774/PPKE.ITK.2010.005

[144] J. Tabak and L.E. Moore. Simulation and parameter estimation study of a simple neuronal model of rhythm generation: Role of NMDA and non-NMDA receptors. *Journal Computational Neuroscience*, 5:209–235, 1998.

[145] J. Tabak, C.R. Murphey, and L.E. Moore. Parameter estimation methods for single neuron models. *Journal of Computational Neuroscience*, 9:215–236, 2000.

[146] K. Talavera and B. Nilius. Biophysics and structure-function relationship of T-type Ca^{2+} channels. *Cell Calcium*, 40:97–114, 2006.

[147] K. Taya, H. Kaneko, T. Takedomi, H. Kishi, and G. Watanabe. Role of inhibin in the regulation of fsh secretion and folliculogenesis in cows. *Journal of Theoretical Biology*, 232:105–117, 2005.

[148] J.H. Tien and J. Guckenheimer. Parameter estimation for bursting neural models. *Journal of Computional Neuroscience*, 24:358–373, 2008.

[149] J.H. Tien, D. Lyles, and M.L. Zeeman. A potential role of modulating inositol 1,4,5-triphosphate receptor desenzitization and recovery rates in regulating ovulation. *Animal Reproduction Science*, 42(1-4):563–570, 1996.

[150] A.M. Turzillo, J.A. Clapper, G.E. Moss, and T.M. Nett. Regulation of ovine GnRH receptor gene expression by progesterone and estradiol. *Journal Reproduction and Fertility*, 113:251–6, 1998.

[151] J.J. Tyson, C.K. Chen, and B. Novák. Network dynamics and cell physiology. *Nature Reviews Molecular Cell Biology*, 2:908–916, 2001.

[152] J.J. Tyson, C.K. Chen, and B. Novák. Sniffers, buzzers, toggles and blinkers: dynamics of regulatory and signaling pathways in the cell. *Current Opinion in Cell Biology*, 14:221–231, 2003.

[153] F. Van Goor, L.Z. Krsmanovic, K.J. Catt, and S.S. Stojilkovic. Control of action potential-driven calcium influx in gt1 neurons by the activation status of sodium and calcium channels. *Molecular Endocrinology*, 13:587–603, 1999.

[154] F. Van Goor, L.Z. Krsmanovic, K.J. Catt, and S.S. Stojilkovic. Coordinate regulation of gonadotropin-releasing hormone neuronal firing patterns by cytosolic calcium and store depletion. *Proceedings of the National Academy of Sciences of the USA*, 96:4101–4106, 1999.

[155] F. Van Goor, A.P. LeBeau, L.Z. Krsmanovic, A. Sherman, K.J. Catt, and S.S. Stojilkovic. Amplitude-dependent spike-broadening and enhanced Ca^{2+} signaling in GnRH-secreting neurons. *Biophysical Journal*, 79:1310–1323, 2000.

[156] K. Wada, L. Hu, N. Mores, C.E. Navarro, H. Fuda, L.Z. Krsmanovic, and K.J. Catt. Serotonin (5-HT) receptor subtypes mediate specific modes of 5-HT-induced signaling and regulation of neurosecretion in gonadotropin-releasing hormone neurons. *Molecular Endocrinology*, 20:125–135, 2006.

[157] E. Walter. *Identification of State Space Models*. Springer, Berlin, 1982.

[158] E. Walter. *Identifiability of Parametric models*. Pergamon Press, Oxford, 1987.

DOI:10.15774/PPKE.ITK.2010.005

[159] D. Wang, C. Summers, P. Posner, and C.H. Gelband. A-Type K^+ current in neurons from neonatal rat hypothalamus and brain stem: Modulation by angiotensin II. *Journal of Neurophysiology*, 78:1021–1029, 1997.

[160] M. Watanabe, Y. Sakuma, and M. Kato. High expression of the R-type voltage-gated Ca^{2+} channel and its involvement in Ca^{2+}-dependent gonadotropin-releasing hormone release in GT1-7 cells. *Endocrinology*, 145:2375–2388, 2004.

[161] G. Weng, U.S. Bhalla, and R. Iyengar. Complexity in biological signaling systems. *Science*, 284:92–96, 1999.

[162] W.C. Wetsel, M.M. Valença, I. Merchenthaler, Zs. Liposits, F.J. Lópeza, R.I. Weiner, P.L. Mellon, and A.Negro-Villar. Intrinsic pulsatile secretory activity of immortalized luteinizing hormone-releasing hormone-secreting neurons. *Proc. Natl. Acad. Sci. USA*, 89:4149–4153, 1992.

[163] S. Wild, G. Roglic, A. Green, R. Sicree, and H. King. Global prevalence of diabetes - Estimates for the year 2000 and projections for 2030. *Diabetes Care*, 27:1047–1053, 2004.

[164] C.L. Williams, J.C Thalabard, K.T. O'Byrne, P.M. Grosser, M. Nishiara, J. Hotchkiss, and E. Knobil. Duration of phasic electrical activity of the hypothalamic gonadotropin-releasing hormone pulse generator and dynamics of luteinizing hormone pulses in the rhesus monkey. *Physiology/Pharmacology*, 87:8580–8582, 1990.

[165] A.R. Willms, D.J. Baro, R.M. Harris-Warrick, and J. Guckenheimer. An improved parameter estimation method for Hodgkin-Huxley models. *Journal of Computational Neuroscience*, 6:145–168, 1999.

[166] R.C. Wilson, J.S. Kesner, J.M. Kaufmann, T. Uemura, T. Akema, and E. Knobil. Central electrtophsysiological correlates of pulsatile lutenizing hormone secretion in the rhesus monkey. *Neuroendocrinology*, 39:256–260, 1984.

[167] P. J. Woolf, T. P. Kenakin, and J. J. Linderman. Uncovering biases in high throughput screens of G-protein coupled receptors. *Journal of Theoretical Biology*, 208:403–418, 2001.

[168] P. J. Woolf and J. J. Linderman. From the static to the dynamic: Three models of signal transduction in G-protein coupled receptors. In A. Christopoulos, editor, *Biomedical Applications of Computer Modeling*, pages 87–108. CRC Press, New York, 2000.

[169] P. J. Woolf, R. R. Neubig, and J. J. Linderman. Timing is everything: The role of kinetics in G protein activation. *Life Sciences*, 68:647–658, 2000.

[170] J.C. Wu, S.C. Sealfon, and W.L. Miller. Gonadal hormones and gonadotropin-releasing hormone (GnRH) alter messenger ribonucleic acid levels for GnRH receptors in sheep. *Endocrinology*, 134:1846–50, 1994.

[171] G. Xie and P.P. Palmer. How regulators of G protein signaling achieve selective regulation. *Journal of Molecular Biology*, 366:349–365, 2007.

[172] C. Xu, T.A. Roepke, C. Zhang, O.K. Ronnekleiv, and M.J. Kelly. Gonadotropin-releasing hormone (GnRH) activates the M-current in GnRH neurons: An autoregulatory negative feedback mechanism? *Endocrinology*, 149:2459–2466, 2007.

DOI:10.15774/PPKE.ITK.2010.005

[173] G.W. De Young and J. Keizer. A single-pool inositol 1,4,5-triphosphate-receptor-based model for agonist-stimulated oscillations in $[Ca^{2+}]$ concentration. *Proceedings of the National Academy of Sciences of the USA*, 89:9895–9899, 1992.

[174] N. Zerangue and L. Y. Jan. G-protein signaling: Fine-tuning signaling kinetics. *Current Biology*, 8:313–316, 1998.

[175] C. Zhang, M.A. Bosch, E.A. Rick, M.J. Kelly, and O.K. Rønnekleiv. 17β-estradiol regulation of T-type calcium channels in gonadotropin-releasing hormone neurons. *The Journal of Neuroscience*, 29:10552–10562, 2009.

[176] H. Zhong, S.M. Wade, P.J. Woolf, J.J. Linderman, M.J. Clark, J.R. Traynor, and R.R. Neubig. A spatial focusing model for G protein signals: RGS protein-mediated kinetic scaffolding. *Journal of Biological Chemistry*, 278:7278–7284, 2003.

[177] X. Zou, T. Peng, and Z. Pan. Modeling specificity in the yeast MAPK signaling networks. *Journal of Theoretical Biology*, 250:139–155, 2008.